

N 70 27942

N 70 27948

NASA TM X-53845

1969

**NASA TECHNICAL  
MEMORANDUM**

NASA TM X-53845

FACILITY FORM 802	N70 27942 (ACCESSION NUMBER)	N70 27948 (THRU)
	<del>99</del> 99 (PAGES)	1 (CODE)
	✓ (NASA CR OR TMX OR AD NUMBER)	24 (CATEGORY)

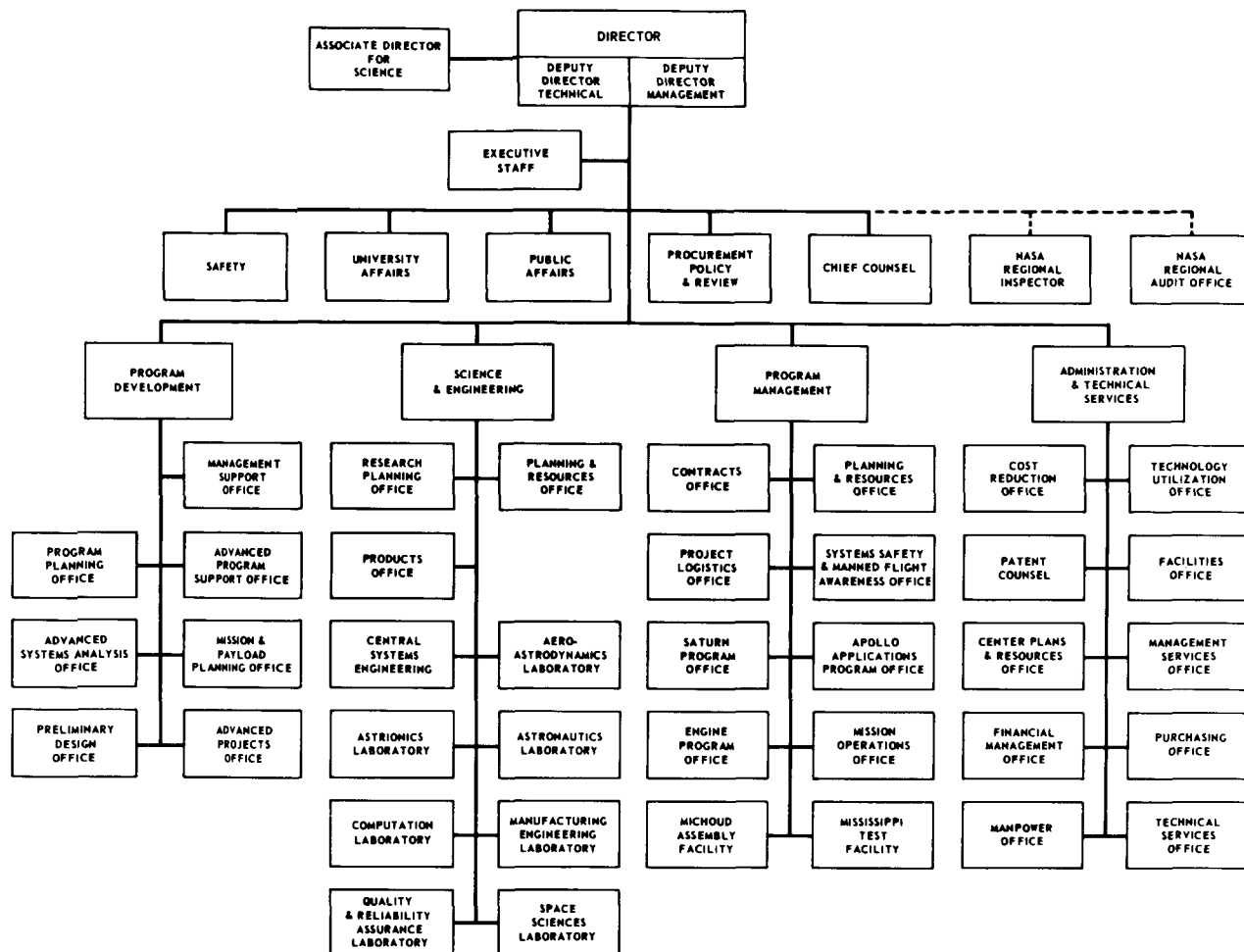
RADIATION PHYSICS RESEARCH AT MSFC

**RESEARCH ACHIEVEMENTS REVIEW  
VOLUME III                      REPORT NO. 7**

SCIENCE AND ENGINEERING DIRECTORATE  
GEORGE C. MARSHALL SPACE FLIGHT CENTER  
MARSHALL SPACE FLIGHT CENTER, ALABAMA

**CASE FILE  
COPY**

# GEORGE C. MARSHALL SPACE FLIGHT CENTER



## RESEARCH ACHIEVEMENTS REVIEWS COVER THE FOLLOWING FIELDS OF RESEARCH

- Radiation Physics
- Thermophysics
- Chemical Propulsion
- Cryogenic Technology
- Electronics
- Control Systems
- Materials
- Manufacturing
- Ground Testing
- Quality Assurance and Checkout
- Terrestrial and Space Environment
- Aerodynamics
- Instrumentation
- Power Systems
- Guidance Concepts
- Astrodynamics
- Advanced Tracking Systems
- Communication Systems
- Structures
- Mathematics and Computation
- Advanced Propulsion
- Lunar and Meteoroid Physics

NATIONAL AERONAUTICS AND SPACE ADMINISTRATION  
WASHINGTON, D. C.

**RESEARCH ACHIEVEMENTS REVIEW**  
**VOLUME III**                      **REPORT NO. 7**

RADIATION PHYSICS RESEARCH AT MSFC

SCIENCE AND ENGINEERING DIRECTORATE  
GEORGE C. MARSHALL SPACE FLIGHT CENTER  
MARSHALL SPACE FLIGHT CENTER, ALABAMA

1969

## PREFACE

In February, 1965, Dr. Ernst Stuhlinger, Director, Research Projects Laboratory ( now Space Sciences Laboratory ), initiated a series of Research Achievements Reviews which set forth those achievements accomplished by the laboratories of the Marshall Space Flight Center. Each review covered one or two fields of research in a form readily usable by specialists, systems engineers and program managers. The review of February 24, 1966, completed this series. Each review was documented in the "Research Achievements Review Series."

In March, 1966, a second series of Research Achievements Reviews was initiated. This second series emphasized research areas of greatest concentration of effort, of most rapid progress, or of most pertinent interest and was published as "Research Achievements Review Reports, Volume II." Volume II covered the reviews from March, 1966, through February, 1968.

This third series of Research Achievements Reviews was begun in March, 1968, and continues the concept introduced in the second series. Reviews of the third series are designated Volume III and will span the period from March, 1968, through February, 1970.

*The papers in this report were presented March 27, 1969.*

William G. Johnson  
Director  
Research Planning Office



# CONTENTS. . .

## A SUMMARY OF RESEARCH IN ELECTRON TRANSPORT AND BREMSSTRAHLUNG CROSS SECTIONS, RELATIVITY EXPERIMENTS, AND PLASMA SHIELDING

By Nat Edmonson

Page

BASIC RESEARCH IN ELECTRON TRANSPORT AND BREMSSTRAHLUNG CROSS SECTIONS . . . . .	1
RELATIVITY — ANALYSIS AND PROPOSED EXPERIMENTS. . . . .	4
PLASMA SHIELDING AGAINST SPACE RADIATIONS . . . . .	6
BIBLIOGRAPHY. . . . .	11

### LIST OF ILLUSTRATIONS

Figure	Title	Page
1.	Schematic of experimental arrangement. . . . .	2
2.	Comparison of computed and experimental transmission spectra for an aluminum target of thickness $\rho = 0.2$ for an incident kinetic energy of 2.5 MeV . . . . .	2
3.	Comparison of computed and experimental transmission spectra for an aluminum target of thickness $\rho = 0.4$ for an incident kinetic energy of 2.5 MeV . . . . .	2
4.	Comparison of computed and experimental transmission spectra for a gold target of thickness $\rho = 0.2$ for an incident kinetic energy of 2.5 MeV. . . . .	3
5.	Comparison of computed spectrum for a gold target of thickness $\rho = 0.4$ to an experimental spectrum for a gold target of thickness $\rho = 0.39$ for an incident kinetic energy of 2.5 MeV . . . . .	3
6.	Comparison of Monte Carlo calculated and experimentally derived transmitted energy distribution for aluminum targets . . . . .	4
7.	Schematic diagram of experimental equipment. . . . .	4
8.	Angular distribution of electrons emitted from a 2.515 gm/cm <sup>2</sup> thick gold target bombarded by 8.0 MeV electrons . . . . .	5
9.	Secondary electron spectra for data shown . . . . .	6
10.	Spectra of electrons emitted for an aluminum target . . . . .	6
11.	Bremsstrahlung cross sections as a function of photon angle. . . . .	7

## CONTENTS (Continued) . . .

	Page
12. Bremsstrahlung cross sections as a function of photon angle . . . . .	7
13. Electron bremsstrahlung cross sections. . . . .	8
14. Relativistic precessions of gyroscopes in a 804, 67-km (500-mile) polar orbit . . . . .	8
15. The atomic hydrogen maser . . . . .	8
16. Zeeman energy diagram for atomic hydrogen in the ground electronic state . . . . .	9
17. Schematic diagram of a space vehicle using a plasma radiation shield . . . . .	10
18. Section view of plasma radiation shield . . . . .	10
19. Schematic of toroidal electron plasma experiment . . . . .	11

## SUPERCONDUCTING MAGNETS FOR ACTIVE SHIELDING

	Page
By Eugene W. Urban . . . . .	13

### LIST OF TABLES

Table	Title	Page
1.	Applications of Superconductivity . . . . .	13
2.	Characteristics of Superconducting Magnet Systems . . . . .	14
3.	Three Exceptional Superconducting Magnets . . . . .	15
4.	Desirable Characteristics of a Shielding Magnet System . . . . .	16
5.	Superconductivity Research Studies . . . . .	17

### LIST OF ILLUSTRATIONS

Figure	Title	Page
1.	Superconducting magnet technology . . . . .	15
2.	Schematic of a flux jump experiment holder . . . . .	17

## REACTOR RADIATION SHIELDING

	Page
By Martin O. Burrell and Henry E. Stern . . . . .	19
REFERENCES . . . . .	23

### LIST OF TABLES

Table	Title	Page
1.	Shield Configurations . . . . .	20

### LIST OF ILLUSTRATIONS

Figure	Title	Page
1.	Gamma data comparison . . . . .	19
2.	Neutron data comparison . . . . .	20
3.	Gamma energy absorption coefficients . . . . .	21
4.	Neutron dose conversion factors . . . . .	21
5.	Experimental setup . . . . .	22
6.	Fast neutron data comparison . . . . .	22
7.	Gamma data comparison . . . . .	22
8.	General approximation of exhaust nozzle with cylinders . . . . .	23
9.	Secondary gamma dose rates at propellant tank top . . . . .	23

## RADIATION INDUCED OUTGASSING

By Raymond L. Gause	Page
SUMMARY . . . . .	25
INTRODUCTION . . . . .	25
RADIATION INDUCED OUTGASSING . . . . .	25
EXPERIMENTAL PROGRAM . . . . .	28
EXPERIMENTAL APPARATUS . . . . .	28
EXPERIMENTAL PROCEDURES . . . . .	28

## CONTENTS (Continued). . .

	Page
DATA ANALYSIS . . . . .	28
DISCUSSION OF EXPERIMENTAL RESULTS . . . . .	30
CONCLUSIONS AND RECOMMENDATIONS. . . . .	30
REFERENCES. . . . .	34

## LIST OF TABLES

Table	Title	Page
1.	Partial G-Values for Several Polymers . . . . .	31
2.	Radiation Induced Gas Yield (G) from Several Polymers. . . . .	32

## LIST OF ILLUSTRATIONS

Figure	Title	Page
1.	Compton scattering process . . . . .	26
2.	Absorption coefficient dependence on photon energy . . . . .	27
3.	Radiation induced outgassing mechanism for polyethylene . . . . .	27
4.	Vacuum irradiation chamber . . . . .	29
5.	Gamma irradiation source. . . . .	29
6.	Liquid hydrogen dewar before irradiation . . . . .	32
7.	Liquid hydrogen dewar after irradiation to $1 \times 10^{10}$ ergs-gm <sup>-1</sup> (C) . . . . .	33

## COSMIC RAY RESEARCH AND NUCLEAR INSTRUMENTATION DEVELOPMENT

By T. A. Parnell	Page
SUMMARY . . . . .	35
INTRODUCTION. . . . .	35
RESEARCH PROGRAM OF THE COSMIC RAY GROUP . . . . .	35
CONCLUSIONS . . . . .	41
REFERENCES. . . . .	42

## CONTENTS (Continued). . .

### LIST OF ILLUSTRATIONS

Figure	Title	Page
1.	Contours of proton flux over the South Atlantic at 670 km . . . . .	36
2.	Cross section of the detector system of the proton spectrometer . . . . .	37
3.	Prototype proton spectrometer with electronic analyzing circuits . . . . .	38
4.	Schematic of the detector system used by GSFC to detect and identify high energy cosmic rays . . . . .	38
5.	Theoretical pulse height distributions from an ideal proportional counter 5 cm thick for nuclei of $Z = 58$ and $Z = 59$ at 100 GeV total energy per particle. . . . .	40
6.	Results of Monte Carlo calculations considering that 10 000 identical particles of $Z = 58$ and $Z = 59$ penetrated a 10-layer proportional counter; the pulses from the 10 layers were averaged for each event. . . . .	40
7.	The cosmic ray air shower experimental arrangement . . . . .	41

## PROTON SENSITIVITY OF FILMS USED IN APOLLO TELESCOPE MOUNT SATELLITE MISSIONS

By Richard A. Potter	Page
SUMMARY . . . . .	43
INTRODUCTION. . . . .	43
FILM TEST PROCEDURES . . . . .	44
TEST RESULTS. . . . .	45

### LIST OF TABLES

Table	Title	Page
1.	Candidate Film Types . . . . .	46

## CONTENTS (Continued)...

### LIST OF ILLUSTRATIONS

Figure	Title	Page
1.	Plot of dose rate versus shield thickness .....	43
2.	Map indicating the South Atlantic Anomaly .....	44
3.	Flux versus time plot .....	45
4.	Curve of density versus exposure for Kodak spectroscopic film, type 103-0 .....	47
5.	Curve of density versus time in orbit for Kodak 103-0 film .....	48
6.	Density versus time in orbit for Panatomic-X film. ....	48
7.	Density versus time in orbit for Kodak SO-375 film .....	49
8.	Density versus dose, indicating the relative speeds of the candidate film types tested .....	49

## APPLICATIONS OF RADIATION PHYSICS RESEARCH

By Martin O. Burrell	Page
SUMMARY .....	51
INTRODUCTION .....	51
OAK RIDGE NATIONAL LABORATORY STUDY.....	51
COMPLEX GEOMETRY RESEARCH .....	53
REFERENCES.....	57

### LIST OF TABLES

Table	Title	Page
1.	GSFC X-Ray Telescope Experiment Number S-056 Panatomic-X Film .....	57

### LIST OF ILLUSTRATIONS

Figure	Title	Page
1.	Estimated neutron spectra in moon because of cosmic-ray bombardment.....	51
2.	Photon leakage spectrum from lunar surface.....	52

# CONTENTS (Concluded). . .

	Page
3. Neutron flux per unit energy versus energy at an atmospheric depth of 50 gm/cm <sup>2</sup> . . . . .	53
4. Neutron flux per unit energy versus energy at an atmospheric depth of 300 gm/cm <sup>2</sup> . . . . .	54
5. Rad dose versus depth in tissue for atmospheric depth of 36 gm/cm <sup>2</sup> ( $\approx$ 75 000 ft) . . . . .	55
6. Alpha-particle emission spectra from $\pi$ -capture in oxygen . . . . .	55
7. Centerline dose versus distance from base of cylinder with spherical cap . . . . .	55
8. Flow chart of radiation analysis . . . . .	56
9. Conceptual drawing of Apollo systems . . . . .	56
10. CPSM base line stowage . . . . .	57
11. Goddard H-Alpha camera and two detector points used in calculations . . . . .	57

# A SUMMARY OF RESEARCH IN ELECTRON TRANSPORT AND BREMSSTRAHLUNG CROSS SECTIONS, RELATIVITY EXPERIMENTS, AND PLASMA SHIELDING

By

Nat Edmonson

## BASIC RESEARCH IN ELECTRON TRANSPORT AND BREMSSTRAHLUNG CROSS SECTIONS

### Introduction

Basic research in electron transport and bremsstrahlung cross sections was motivated by the need for more precise knowledge about the interaction of electrons and other charged particles with materials used in the space research program. This research was begun several years ago and is now in its terminal stages. It has involved both theoretical and analytical investigations and has been performed in-house and by contract. Because MSFC lacked proper facilities for performing the experimental measurements, the experimental phases were performed under contract.

### Contracted Research

A contract with the National Bureau of Standards (NBS) of the Department of Commerce involves analytical studies of the penetration of electrons through matter. The contract is basically a stochastic or Monte Carlo study of the penetration of electrons through matter. The principal investigator for this contract is Dr. Martin J. Berger. The study has produced three computer programs as follows:

- Datatape — This program produces a data library that is stored on magnetic tape for use by Datapac-4. The library contains information of a general nature. For example, information is included about elastic scattering of electrons and positrons by atoms (Mott cross sections), bremsstrahlung production, mean radiative energy loss, experimental correction factors, etc.

- Datapac-4 — This program accepts data from the library tape and processes, evaluates, and

expands these data for use in Etran-15. For example, Datapac-4 evaluates mean energy loss per unit path length, mean radiative energy loss of an electron, mean electron range, cumulative distribution of angular deflections resulting from multiple scattering, etc.

- Etran-15 — This program accepts physical information from Datapac-4 and generates, by random sampling, large sets of electron and photon histories. These histories are analyzed to obtain information about radiation transmission and reflection, energy deposition, production of bremsstrahlung, etc.

An experimental study of electron transmission and bremsstrahlung production is being conducted at the LTV Research Center by Dr. David H. Rester, principal investigator. The purpose of the study is to measure secondary electron spectra, bremsstrahlung spectra, and cross sections for electron interactions in the primary energy range  $\leq 3$  MeV. Electron beams are provided by a Van de Graff accelerator. A schematic diagram of the experiment is shown in Figure 1. Figures 2 through 5 are transmission spectra histograms that illustrate results of computations by Etran-15. Figure 6 shows the total penetration spectra constructed from non-normal incidence data for  $\pi$  incident electrons distributed in intensity and varying as the cosine of the angle of incidence. The source of electrons for the comparisons in Figure 6 was a 1.0-MeV beam; comparisons are made for targets corresponding to 0.4 and 0.56 of the range at 1.0 MeV.

Studies of electron shielding are being performed by Gulf General Atomic, Inc. Dr. J. A. Lonergan is the principal investigator for this program. The purpose of the experiments and studies performed under this contract is to measure accurately secondary electron spectra, bremsstrahlung spectra, and electron reaction cross sections in the primary energy range of 1 to 10 MeV. As shown in the schematic diagram of the experimental equipment (Fig. 7),



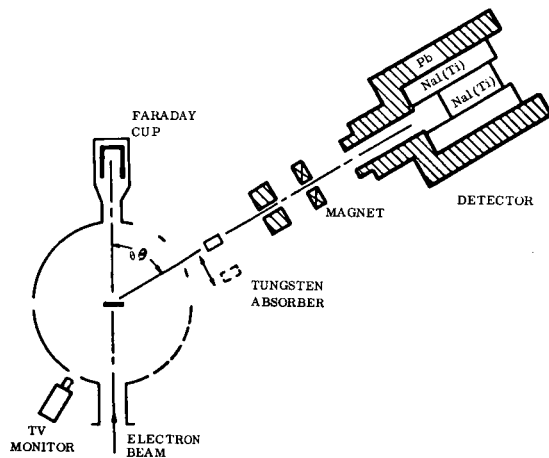


Figure 1. Schematic of experimental arrangement.

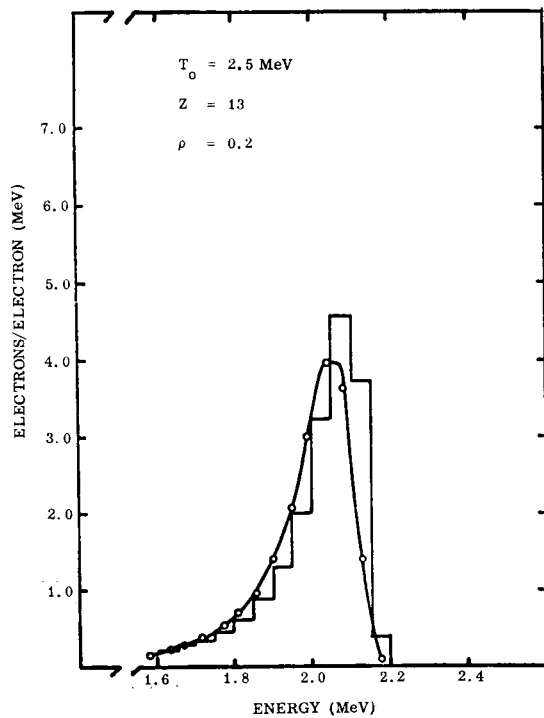


Figure 2. Comparison of computed and experimental transmission spectra for an aluminum target of thickness  $\rho = 0.2$  for an incident kinetic energy of 2.5 MeV.

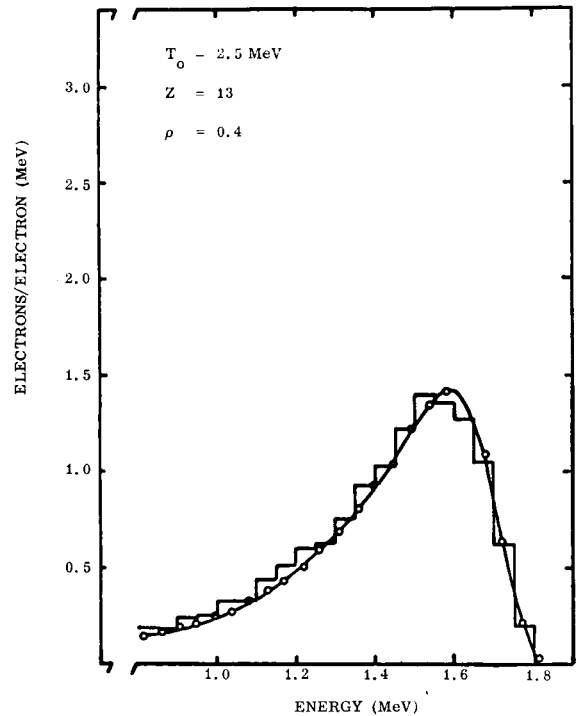


Figure 3. Comparison of computed and experimental transmission spectra for an aluminum target of thickness  $\rho = 0.4$  for an incident kinetic energy of 2.5 MeV.

the primary electron beam is supplied by a linear accelerator. Figures 8, 9, and 10 illustrate results of experiments performed under this contract.

A contract to experimentally determine the distribution in energy and angle of photons produced in coincidence with electrons inelastically scattered into a fixed direction is being performed by the Physics Department of Texas Christian University. The principal investigators are Dr. L. L. Baggerly and Dr. C. A. Quarles. This experiment is still in progress and data are still being taken. The resultant data will be shown in reduced differential cross sections as functions of photon angles.

## In-House Research

Computations using Dr. Martin J. Berger's procedure and theoretical computations of electron bremsstrahlung cross sections have been performed in-house. Dr. Berger's methods have been applied to the computation of electron secondary spectra.

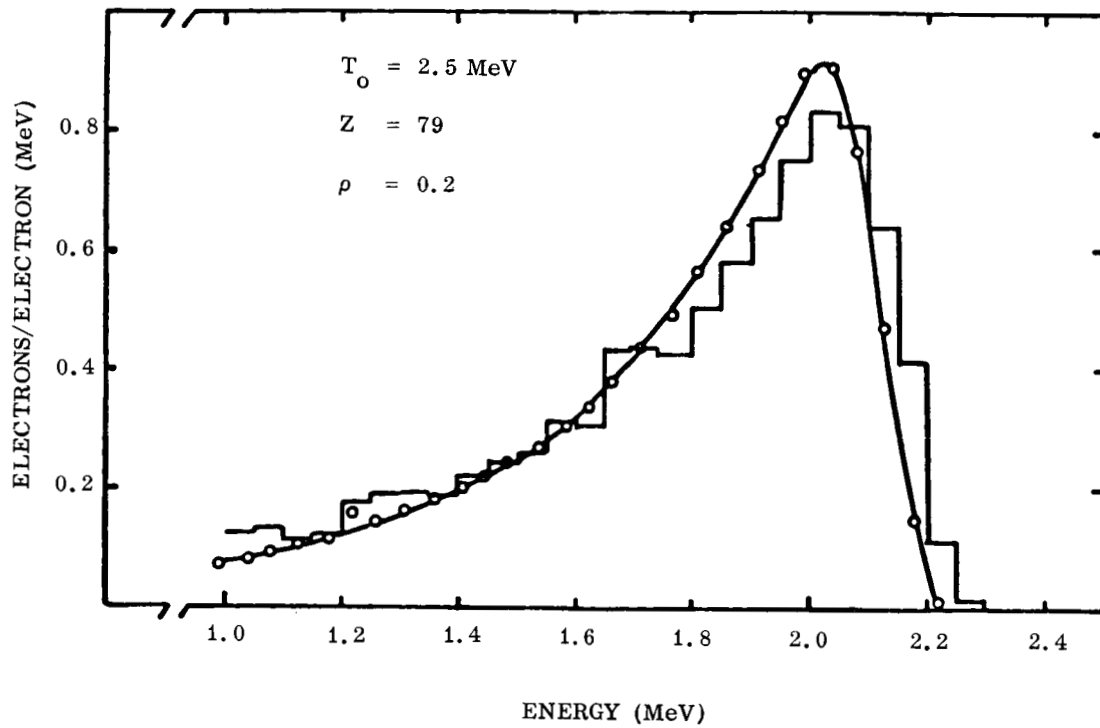


Figure 4. Comparison of computed and experimental transmission spectra for a gold target of thickness  $\rho = 0.2$  for an incident kinetic energy of 2.5 MeV.

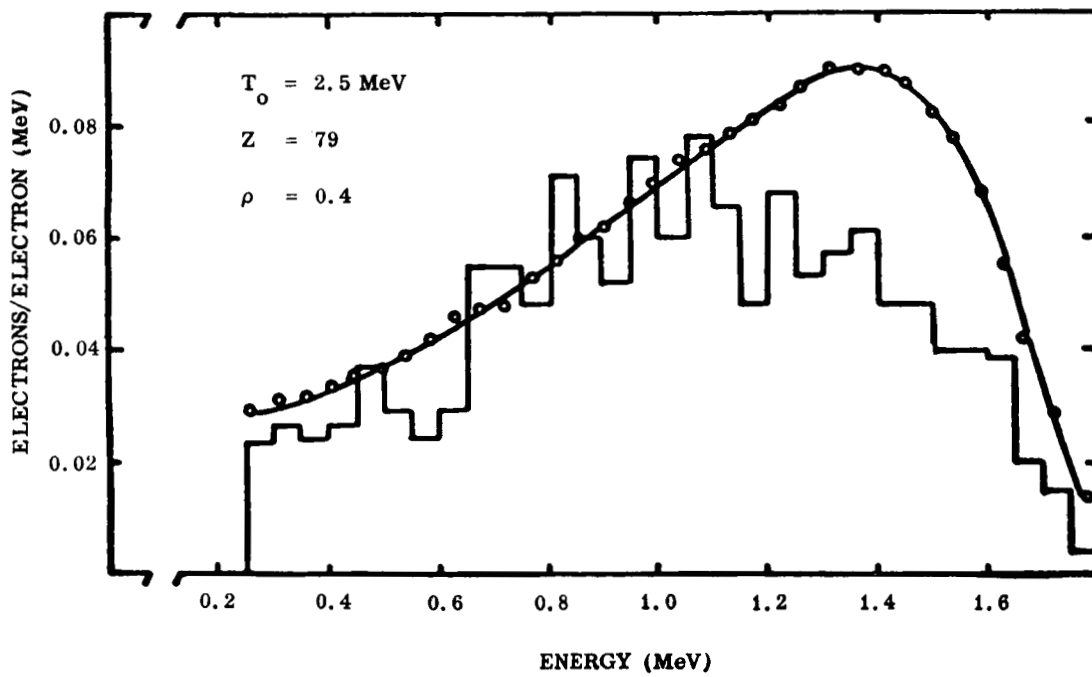


Figure 5. Comparison of computed spectrum for a gold target of thickness  $\rho = 0.4$  to an experimental spectrum for a gold target of thickness  $\rho = 0.39$  for an incident kinetic energy of 2.5 MeV.

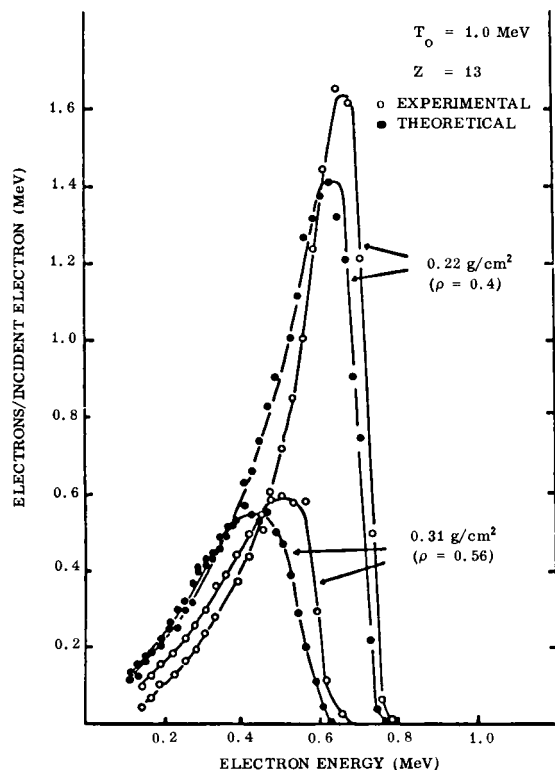


Figure 6. Comparison of Monte Carlo calculated and experimentally derived transmitted energy distribution for aluminum targets.

The theoretical computation of electron bremsstrahlung cross sections is also being performed in-house. This work was prompted by a desire to remove errors from the Bethe-Heitler approximation. This computation utilizes the methods of quantum electrodynamics. The cross sections are computed for the reaction of unpolarized electrons with the screened nucleus of the atom under consideration. The Bethe-Heitler approximation is not assumed. Hence, the method requires very complicated numerical procedures. The success obtained in performing these numerical procedures is shown in Figures 11 through 13. The extension of this method to higher energies is being studied. Another in-house project is the adapting of analytical methods developed by Gulf General Atomic, Inc., as a part of their Electron Shielding Studies contract, to numerical procedures for electron transport computations.

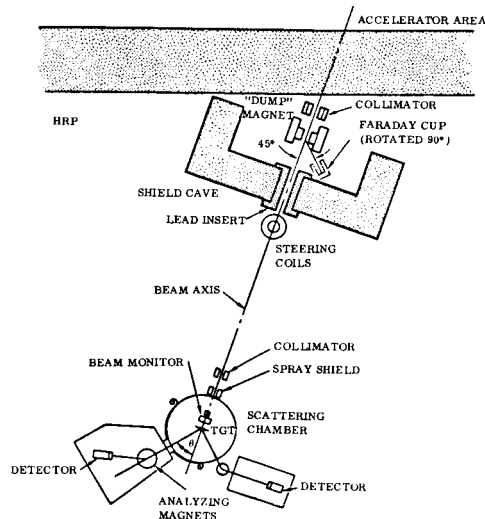


Figure 7. Schematic diagram of experimental equipment.

## RELATIVITY — ANALYSIS AND PROPOSED EXPERIMENTS

Two relativity experiments are in what might be called an active state relative to the Marshall Space Flight Center, the Stanford zero-g gyro experiment and the gravitational red shift experiment.

The Stanford experiment is still in the laboratory development stage; no time has been spent analyzing this experiment. Figure 14 shows the scheme of the experiment. The gyroscopes are in polar orbit. Gyroscope 1 has its axis of spin in the plane of the orbit and measures spin-orbit interaction. Gyroscope 2 has its axis of spin perpendicular to the plane of the orbit and measures spin-spin interaction. The effects are separated by the polar orbit and their expected magnitudes are shown on the figure.

In connection with the gravitational red shift, so-called error analyses are being carried out for various orbits. By using the hydrogen maser clock

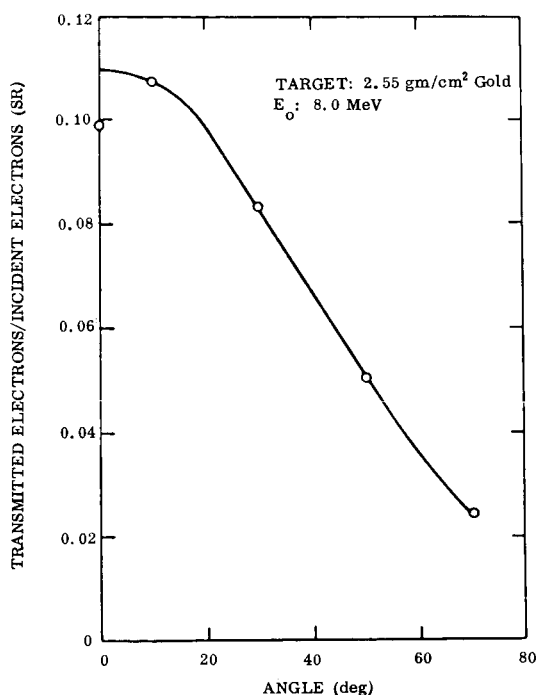


Figure 8. Angular distribution of electrons emitted from a 2.515 gm/cm<sup>2</sup> thick gold target bombarded by 8.0 MeV electrons.

experiment, the theory of the shift in the earth's gravitational field can be shown in simplest terms as follows:

It is an observational fact that spectral lines emitted by atoms on massive bodies are shifted toward the red end of the spectrum when compared with corresponding lines emitted on a less massive body; i.e., emitted in a field of lower gravitation. This statement is equivalent to the statement that the frequency of the signal emitted by a clock in a field of high gravitation will be reduced in comparison with the frequency of the signal emitted by an identical clock in a field of lower gravitational intensity. The reason for this effect is seen in the relations

$$E = h\nu$$

and

$$E = mc^2 ;$$

i.e., with each frequency there is an associated mass. Moving this mass in the gravitational field requires energy supplied by the emitted radiation. This is equivalent to a loss in frequency of the signal. This effect is derivable from changes in the gravitational field potential function according to the equation

$$\frac{\nu_1 \nu_2}{\nu_2} = \frac{\phi_2 \phi_1}{C^2} ; \quad \frac{\Delta \nu}{\Delta} = \frac{\Delta \phi}{C^2} ,$$

where

$\nu_1$  = frequency associated with gravitational potential function value  $\phi_1$

$\nu_2$  = frequency associated with gravitational potential value  $\phi_2$

In particular, let  $\phi_{\text{satellite}}$  be the value of the gravitational potential function at a satellite in synchronous orbit at a distance  $r$  from the center of the earth. Let  $\phi_e$  be the gravitational field at the earth's surface. If the time dilatation or second order Doppler effect resulting from the satellite's motion is added to the effect of the change in gravitation, then, in obvious notation:

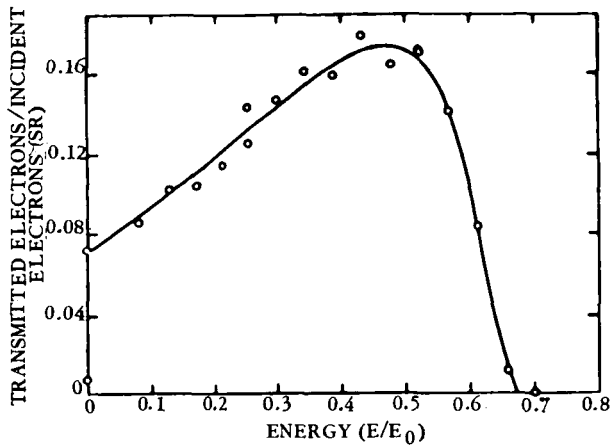
$$\begin{aligned} \frac{\nu_{\text{satellite}} - \nu_{\text{earth}}}{\nu_{\text{earth}}} &= \frac{\phi_{\text{earth}} - \phi_{\text{satellite}}}{C^2} \\ &= 6.94 \times 10^{-10} \left( 1 - \frac{3}{2} \frac{R_o}{r} \right) \\ &= \frac{GM}{C^2 R_o} \left( 1 - \frac{3}{2} \frac{R_o}{r} \right) . \end{aligned}$$

The second order Doppler term contributes

$$\frac{\Delta \nu}{\nu_{\text{Dopp}}} = \frac{1}{2} \frac{GM}{C^2 R_o} \frac{R_o}{r}$$

to the frequency shift.

The theory of the hydrogen maser clock is indicated in Figures 15 and 16. In a practical experiment, the frequency of the signal submitted by a hydrogen maser clock in orbit would be compared with that of an identical hydrogen maser clock at an earth station. In an actual physical situation the



Tabulation of Smoothed Data	
$E/E_0$	Transmitted Electrons/Incident Electron (SR)
0.05	0.0824
0.10	0.0944
0.15	0.1072
0.20	0.1192
0.25	0.1312
0.30	0.1440
0.35	0.1576
0.40	0.1660
0.45	0.1744
0.475	0.1760
0.50	0.1728
0.55	0.1584
0.60	0.1040
0.65	0.0224
0.675	0.0

## Notes:

1. Energy spread of incident electron beam = 1% FWHM.
2. Data measured using a magnetic spectrometer having a resolution of 5.1%.

Target: Gold

Thickness:  $2.51 \text{ gm/cm}^2 = 0.5 \text{ R}$ Incident Energy:  $E_0 = 8.0$ 

Angle of Incidence: Normal

Observed Emission Angle:  $\theta = 30^\circ$ Average Energy Transmitted:  $\bar{E} = 0.35$ Most Probable Energy Transmitted:  $E_{mp} = 0.47$ 

Absolute Error: 11%

Figure 9. Secondary electron spectra for data shown.

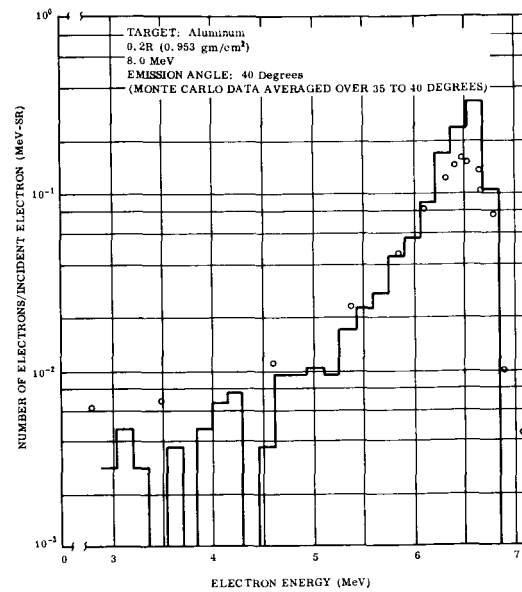


Figure 10. Spectra of electrons emitted for an aluminum target.

clock signals would be mixed with Doppler effects, transmission media effects, effects resulting from the nonspherical shape of the earth and moon, and possible sun gravitational effects. The gravitational shift effect must be separated from these other effects by a careful analysis. These analyses are being performed. One program for elliptical orbit is now in the Computation Laboratory of Marshall Space Flight Center waiting to be run.

## PLASMA SHIELDING AGAINST SPACE RADIATIONS

This review will be confined to the concepts and research originated and carried out by the staff of the Avco-Everett Research Laboratory.

The basic concept of plasma shielding against space radiations is shown in Figure 17. The torus-shaped space vehicle is encircled by superconducting coils, in which a current circulates to generate a magnetic field encircling the torus. The four-coil superconducting magnet system shown is merely a suggestion. The charge ejection system utilizes the inductive mechanism associated with the turning on of the magnet to transport electrons away from the

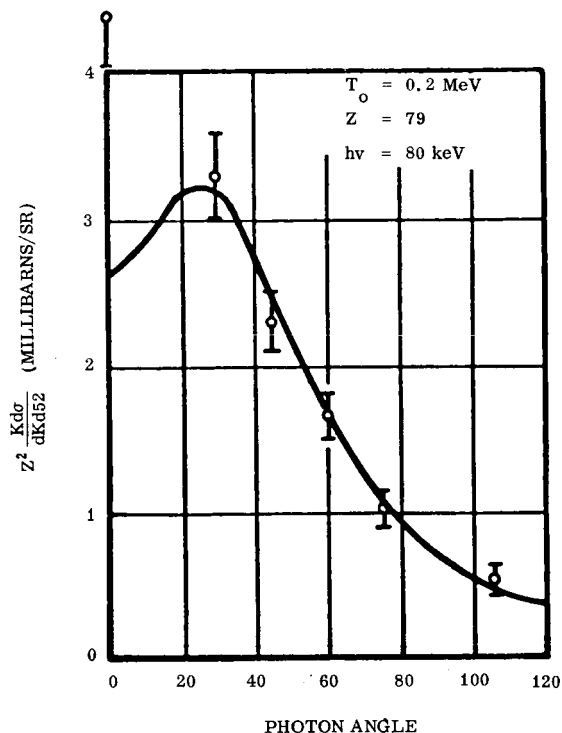


Figure 11. Bremsstrahlung cross sections as a function of photon angle [ $Z = 79$  (gold),  $T_o = 0.2$  MeV, photon energy = 80 keV].

vehicle. Ejection from the vehicle must be accomplished at a velocity greater than  $E/B$  velocity, or about 300 keV. The hull of the space vehicle is maintained at a positive electrical potential as shown in Figure 18. In the figure, the electric and magnetic field lines can be seen to be mutually perpendicular. All the electric field lines start on the surface of the vehicle and end on electrons in the cloud. This effect guarantees that the charge on the vehicle and the cloud will be equal and opposite. The arrangement is similar to a capacitor; the electric field is important only between the "plates." The "plates" attract each other, but are kept apart by the magnetic field. This potential is controlled so as to repel protons, as indicated. Electrons are injected into the magnetic

field to form an electrically neutral gross configuration so far as space electrons are concerned. Hence, the basic concept is that protons are repelled but electrons are not attracted.

A glance at this concept will cause one to think of plasma instabilities; such instabilities are the main concern of Avco-Everett. Even scaled down space experiments are prohibitively expensive, and supporting probes would destroy the plasma field. Two ideas are being considered. In one method the scaled space vehicle is dropped in a vacuum. This is, obviously, difficult and has not been attempted. The other procedure is to study plasma stabilities by setting up the plasma inside a toroidal vessel, as in Figure 19. The inside of the vessel is maintained at a high vacuum, electrons are introduced into the torus from a filament in the slot and compressed by a rising magnetic field, and a potential depression is created along the circular axis of the device. The resulting plasma cloud is studied. To date results have been encouraging.

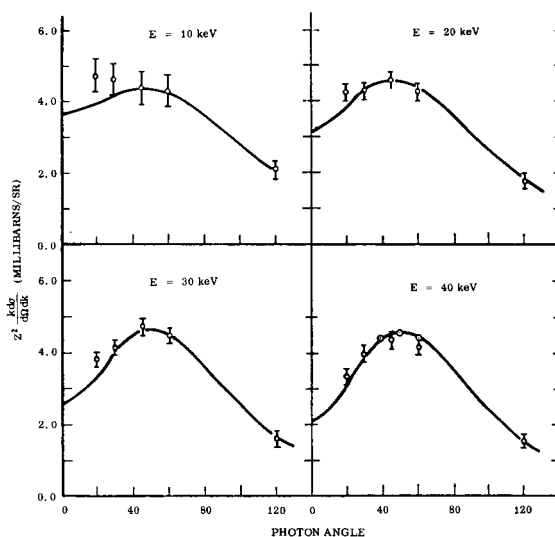


Figure 12. Bremsstrahlung cross sections as a function of photon angle [ $Z = 79$  (gold),  $T_o = 50$  keV, photon energies = 10 keV, 20 keV, 30 keV, and 40 keV].

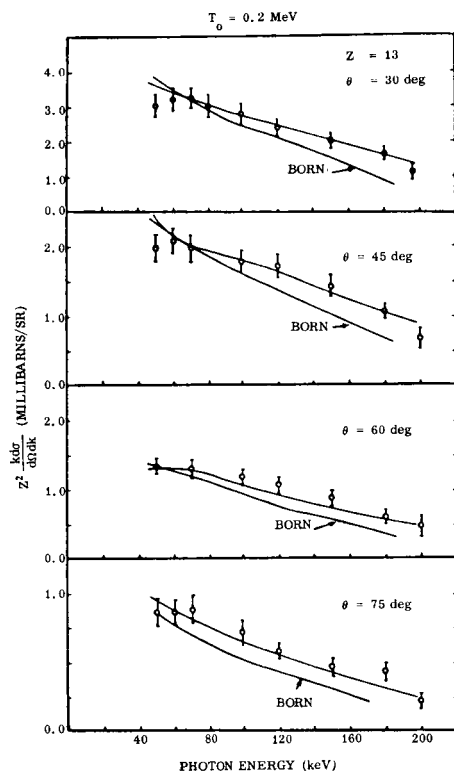


Figure 13. Electron bremsstrahlung cross sections (circles with error bars show experimental values; solid curves show theoretical values; curves labelled "Born" show theoretical values calculated by born approximation).

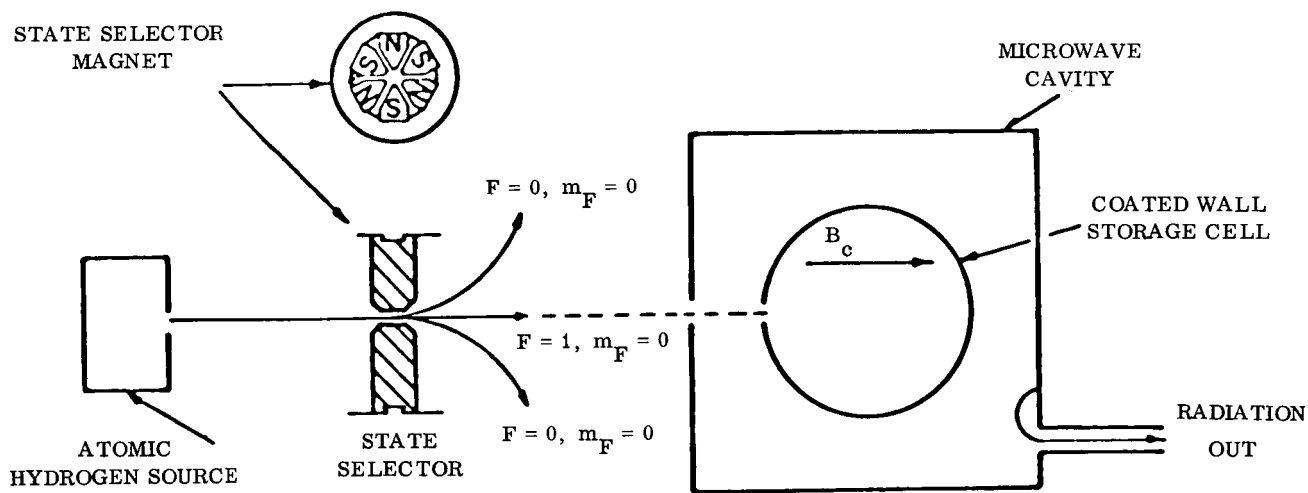


Figure 15. The atomic hydrogen maser (elements illustrated are contained within a vacuum enclosure; magnetic shields and means to create the small steady field,  $B_c$ , are not shown).

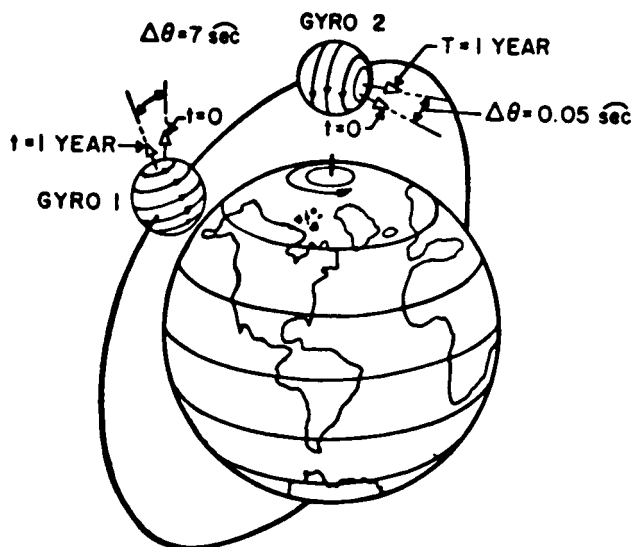


Figure 14. Relativistic precessions of gyroscopes in an 804.7-km (500-mile) polar orbit.

## HYDROGEN

$$L = 0, S = \frac{1}{2}, I = \frac{1}{2}$$

$$\Delta W = 9.4 \times 10^{-10} \text{ erg} = 5.9 \times 10^{-6} \text{ eV}$$

$$\nu_o = \frac{\Delta W}{h} = 1,420.4057518 \text{ Mcps}$$

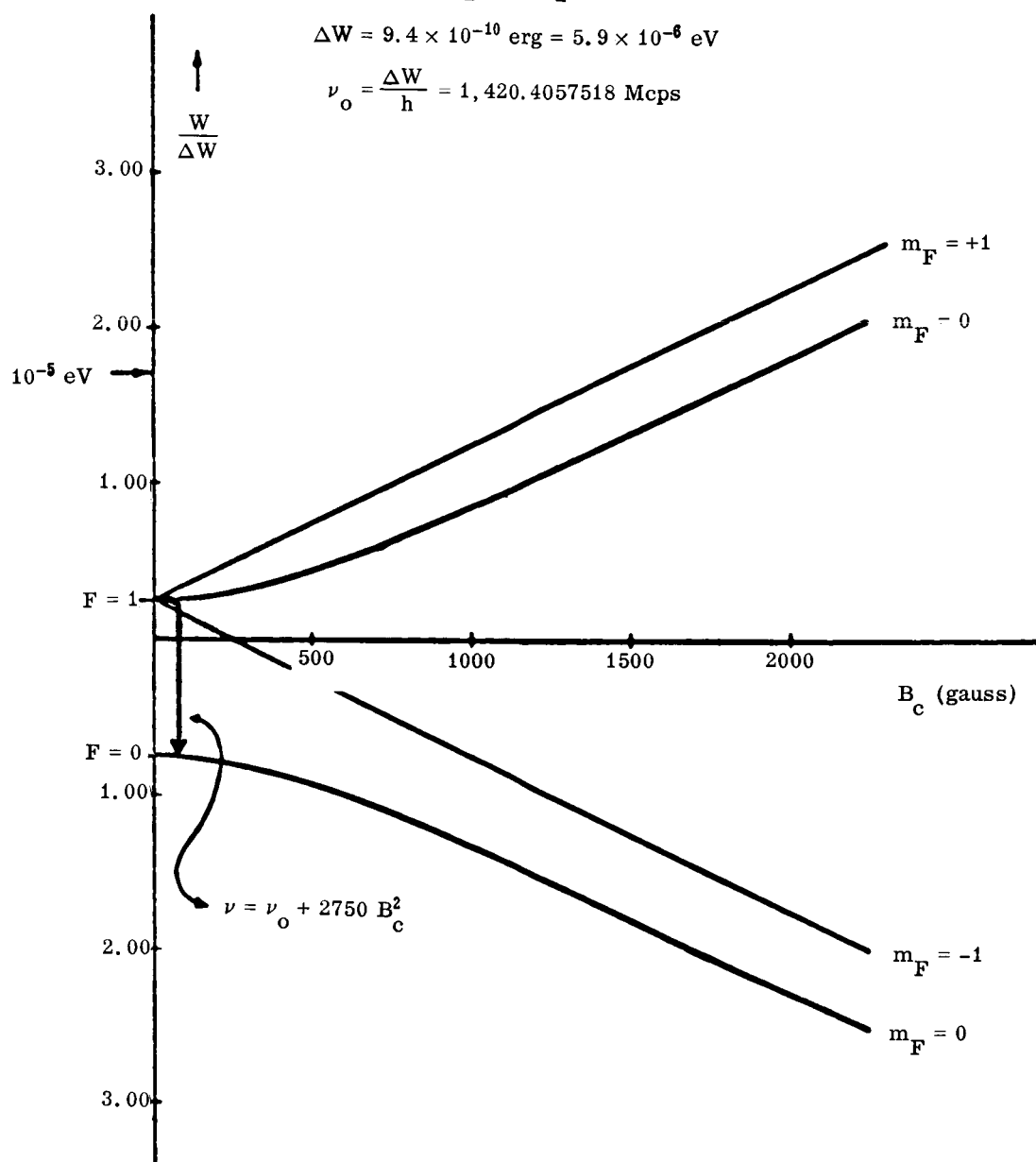


Figure 16. Zeeman energy diagram for atomic hydrogen in the ground electronic state (heavy arrow indicates the transition used in stable atomic oscillators).



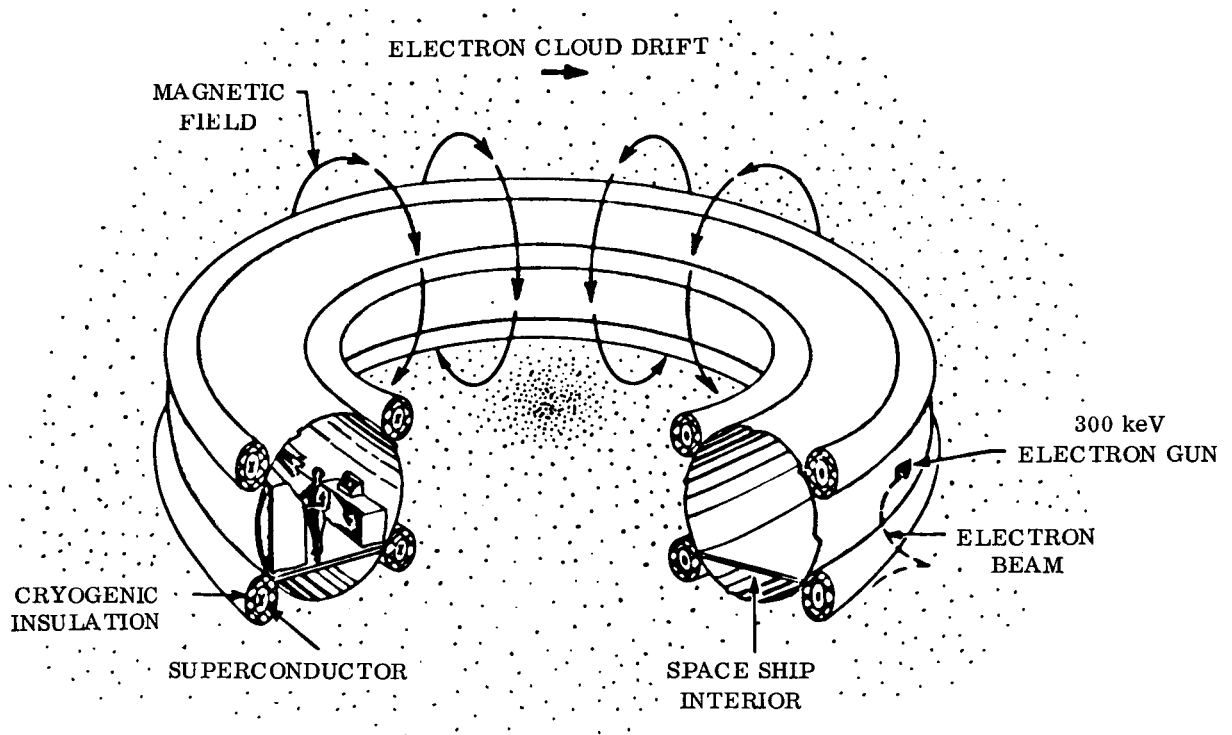


Figure 17. Schematic diagram of a space vehicle using a plasma radiation shield.

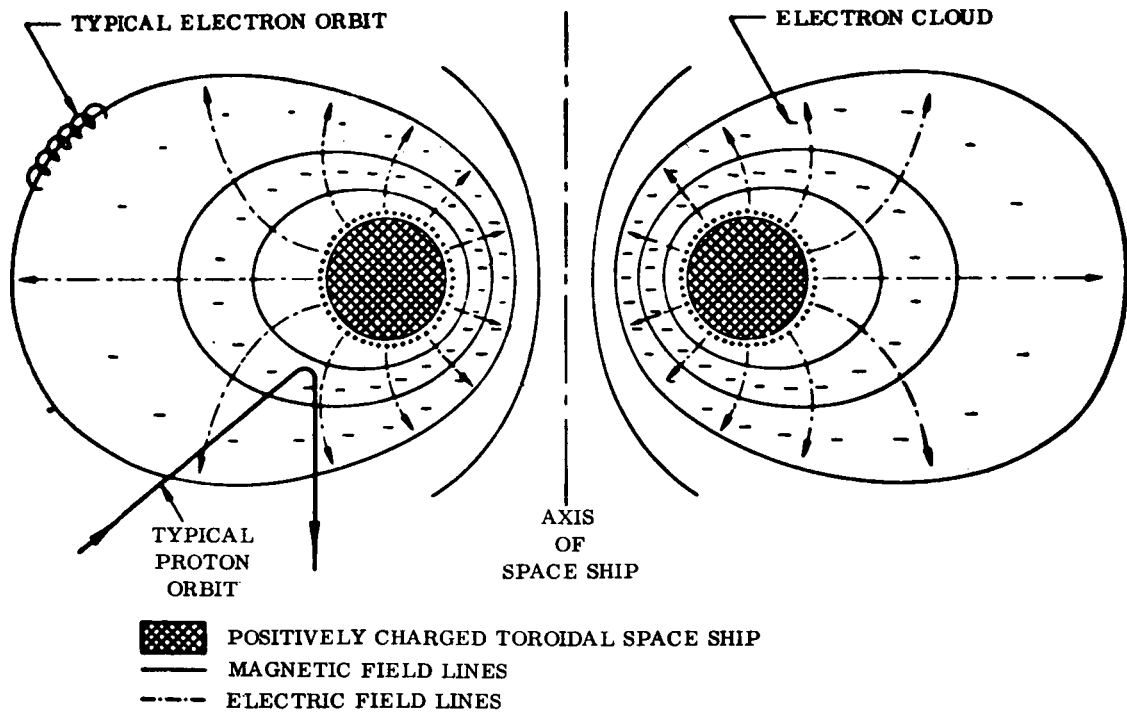


Figure 18. Section view of plasma radiation shield.

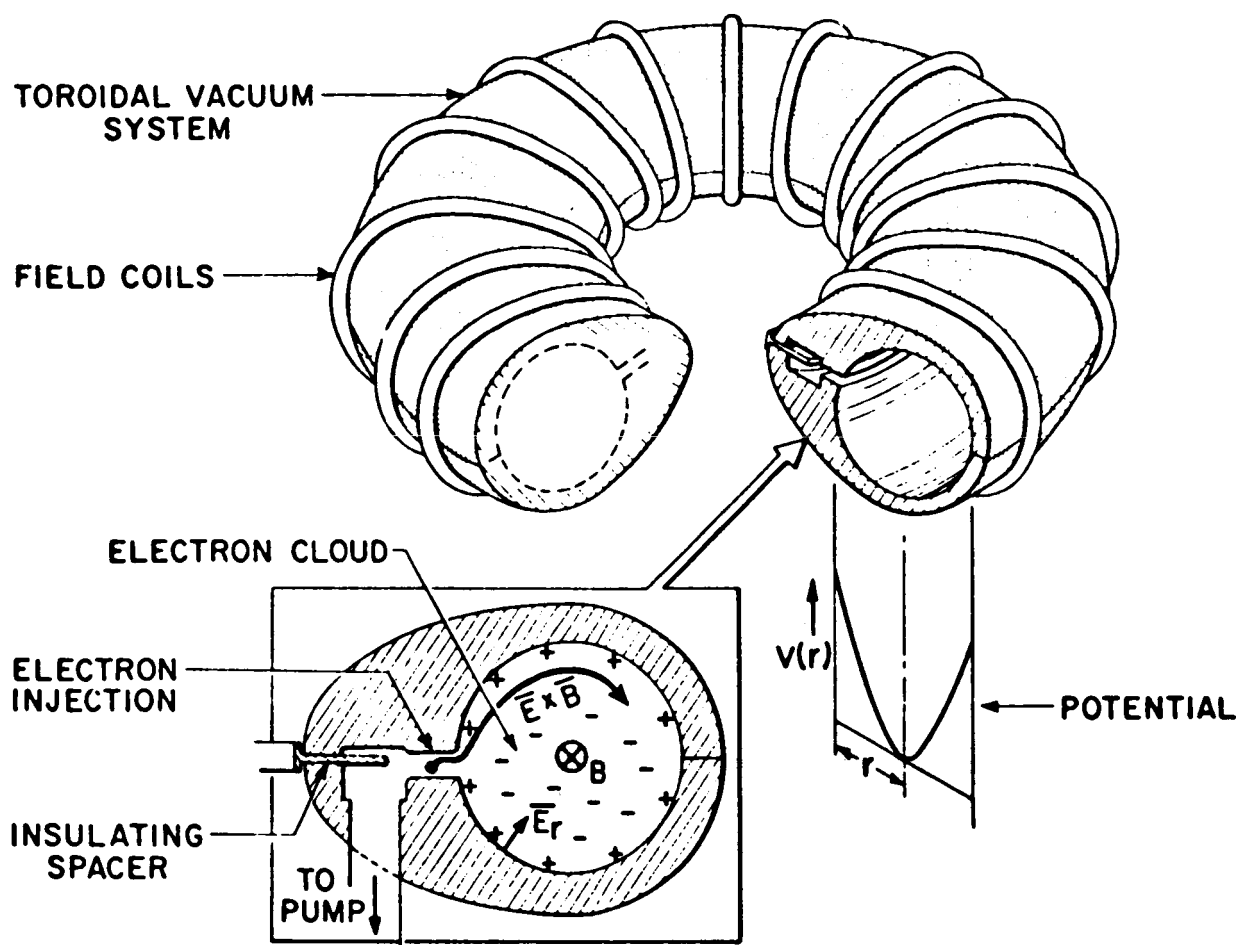


Figure 19. Schematic of toroidal electron plasma experiment.

## BIBLIOGRAPHY

Backscattering of 1 MeV Electrons from Silicone. Nuclear Instruments and Methods, vol. 41, 1966.

Berger, M. J.; and Seltzer, S. M.: Electron and Photon Transport Programs. National Bureau of Standards Report 9836, 1968.

Berger, M. J.; and Seltzer, S. M.: Electron and Photon Transport Programs. National Bureau of Standards Report 9837, 1968.

Berger, M. J.; and Seltzer, S. M.: Penetration of Electrons and Associated Bremsstrahlung Through Aluminum Targets. Proceedings of Special Sessions on Protection Against Space Radiation, American Nuclear Society, NASA SP-169, 1968.

Berger, M. J.; and Seltzer, S. M.: Results of Some Recent Transport Calculations for Electrons and Bremsstrahlung. Proceedings of Second Symposium on Protection Against Radiation in Space, NASA SP-71, 1965.

## BIBLIOGRAPHY (Concluded)

Bremsstrahlung Cross Section Measurements at Incident Electron Energy of 1.0, 1.7, and 2.5 MeV. Phys. Rev., vol. 161, 1967.

Calculation of Energy and Charge Deposition in a Medium Bombarded by 20 MeV Electrons. Journal of New York Academy of Science, (In Press).

GACD-7080, Monthly and Quarterly Reports. Gulf General Atomic, Inc.

GA-8486, Final Report. Gulf General Atomic, Inc.

Jupiter, C. P.; Lonergan, J. A.; and Merkel, G.: An Experimental Study of the Transport of Electrons Through Thick Targets. Trans. ANS, vol. 10, no. 1, June 1967.

Jupiter, C. P.; and Merkel, G.: Measurement of Thick Aluminum Target Bremsstrahlung Spectra Produced with 10 MeV Electrons. Bull. Am. Phys. Soc., series II, vol. 11, no. 5, 1966.

Response of Silicone Transmission Detectors to Monoenergetic Electrons. IEEE Transactions in Nuclear Science, NS-15, vol. 3, no. 359, 1968.

Response of Silicone Detectors to Monoenergetic Electrons in the 0.15 and 5.0 MeV Range. Nuclear Instruments and Methods, (In Press).

Rester, D. H.; and Rainwater, W. J.: Coulomb Scattering in Aluminum Without Atomic Excitation for 1.0 MeV Electrons. Phys. Rev., vol. 138, 1965.

Rester, D. H.; and Rainwater, W. J.: Measurement of Transmission Spectra of 1 MeV Electron with Normal Incidence on Aluminum Slab. J. Appl. Phys., vol. 37, 1966.

Rester, D. H.: Bremsstrahlung Cross Section Measurements on Be at Incident Electron Energies of 1 and 2 MeV. Nuclear Physics, vol. A-118, no. 129, 1968.

Rester, D. H.: Coulomb Scattering in Aluminum Without Atomic Excitation. Phys. Rev., vol. 140, 1965.

Rester, D. H.; Dance, W. E.; et al.: Bremsstrahlung Production in Thick Aluminum and Iron Targets by 0.5 and 21.8 MeV Electrons. J. Appl. Phys., vol. 39, 1968.

# SUPERCONDUCTING MAGNETS FOR ACTIVE SHIELDING

By

Eugene W. Urban

Because active space radiation shields will require rather high magnetic fields over large volumes and because superconducting magnets are the only feasible source of such fields, a research program is being conducted to explore and solve the problems that would restrict such applications. This report covers the probable requirements for shield magnets and the current research, both contractual and in-house, to advance the state-of-the-art of large, high field superconducting magnets for space application.

Superconductors are materials, most of which are metals, that lose all their dc electrical resistance when cooled to a sufficiently low temperature. The temperature at which they transform from the normal to the superconducting state is called the transition or critical temperature and is a characteristic value for each different superconductor. Transition temperatures range from a few millidegrees to a maximum known value of 20.2°K. Most technologically important superconductors have transition temperatures in the range from 5 to 18°K.

Type II superconductors remain superconducting in the presence of high magnetic fields and while carrying a large electric current. It is this property that allows the construction of very large, high field superconducting magnets which have an operating power loss of virtually zero.

When the active shielding concepts were first advanced (1960-1964), it was clear that only superconducting magnets could provide the high magnetic fields and low power consumption that would be needed in a space application. A broad research program was initiated to study not only the characteristics and feasibility of the active shielding techniques, but also the problems of high field superconductivity that affected the construction of large volume, high field, efficient superconducting magnet systems for space application.

The characteristics of superconducting magnet systems, how they would be applied to a flyable

space shield, the requirements of a shielding magnet system, and current and future research to contribute to the solution of some of the technological problems of superconducting magnets are summarized as follows.

Table 1 shows some of the applications of the two classes of superconductors. The type I

TABLE 1. APPLICATIONS OF SUPERCONDUCTIVITY

● <u>TYPE I SUPERCONDUCTORS</u>
QUANTUM ELECTRONIC DEVICES; SENSITIVE MEASURING INSTRUMENTS
COMPUTER MEMORY ELEMENTS
GYROSCOPES
DC ELECTRICAL POWER TRANSMISSION
● <u>TYPE II SUPERCONDUCTORS</u>
HIGH FIELD MAGNETS
PASSENGER TRAIN LEVITATION
LARGE ROTATING ELECTRICAL MACHINERY
AC ELECTRICAL POWER TRANSMISSION

materials are generally those that have low transition temperatures and remain superconducting only in relatively low magnetic fields. They have many very promising applications including quantum electronic measuring devices with extremely high sensitivity, computer memory elements, magnetically levitated gyroscopes, and dc electrical power transmission lines.

The type II superconductors are of primary interest to us. In addition to their uses in fixed magnets, they have potential application in rotating machinery such as motors and generators, as repulsion magnets in high speed passenger train levitation systems, and for ac electrical power transmission lines.

The major characteristics of superconducting magnets and their relation to a complete operating

system are shown in Table 2. First, and most important, when fully energized and operating in a steady-state mode, superconducting magnets have virtually no power loss. No power is dissipated in the magnet, and no power is required to maintain the magnetic field, in contrast to a normal conductor magnet with Joule heating losses that requires a continuous power input and continuous extraction of the same power in the form of heat by a cooling system. Thus, the operating power of a superconducting magnet is small. Several large, ground-based superconductor systems are currently being planned or constructed. Although initial construction costs are greater than for a similar conventional magnet system, operating costs are much lower.

A very low temperature environment is required for the magnet; typical operating temperatures are 4 to 10°K. An efficient thermal enclosure, as well as a primary low temperature refrigerator, must be provided for initial cool-down and to remove heat that leaks into the cryogenic environment or is generated locally as discussed below. Refrigeration near 0°K is inherently an inefficient process, and a continuous electrical power source for the refrigerator is needed.

During magnet startup or shutdown and in the event of certain types of disturbances, electrical power is dissipated in the superconductor. To minimize these losses and to ensure that they do not lead to catastrophic collapse of the magnetic field with rapid and perhaps damaging energy dissipation, stabilized conductors are used. These

conductors generally are a composite consisting of a relatively small amount of superconductor, in the form of a thin strip or finely divided wires, imbedded in a large amount of normal, high conductivity conductor such as pure copper or aluminum. The presence of this stabilizer greatly increases the mass of the conductor and lowers its current density resulting in a heavier and more voluminous magnet winding.

Finally, large magnetic fields imply very high magnetic forces (proportional to the product of the local field and its gradient), and strong, heavy structures are required to hold the magnet together.

To illustrate the past development and current status of superconducting magnet technology, Figure 1 shows a plot of peak central magnetic field versus bore diameter of several superconducting magnets. Of most interest are the commercial, off-the-shelf, small bore laboratory magnets (typified by the RCA and GE points), the large bore and large field magnets (Lewis Research Center, Stanford Linear Accelerator Magnet (SLAC), AVCO, and RCA), and the very large bore, medium field bubble chamber magnets (Brookhaven and Argonne) that lie in the region indicating field-volume combinations of possible use for active space radiation shield systems. Some details of three of these magnets are listed in Table 3, including the mass breakdown of the SLAC magnet that illustrates the large fraction of non-superconducting material present.

TABLE 2. CHARACTERISTICS OF SUPERCONDUCTING MAGNET SYSTEMS

MAGNET CHARACTERISTIC	SYSTEM CHARACTERISTIC
1. Quiet, Persistent Operation; Negligible Steady-State Power Loss	Much Smaller Operating Power Than for Conventional Magnets; Lower Operating Costs (Fixed Installation)
2. Very Low Temperature Operation	Cryogenic Refrigerator and its Electrical Power Source; Efficient Thermal Enclosure
3. Instabilities in Transient Operation (Startup, Shutdown, or External Disturbance)	Stabilized Conductors; Increased Mass and Lower Current Density
4. Large Magnetic Forces	Heavy Support Structure

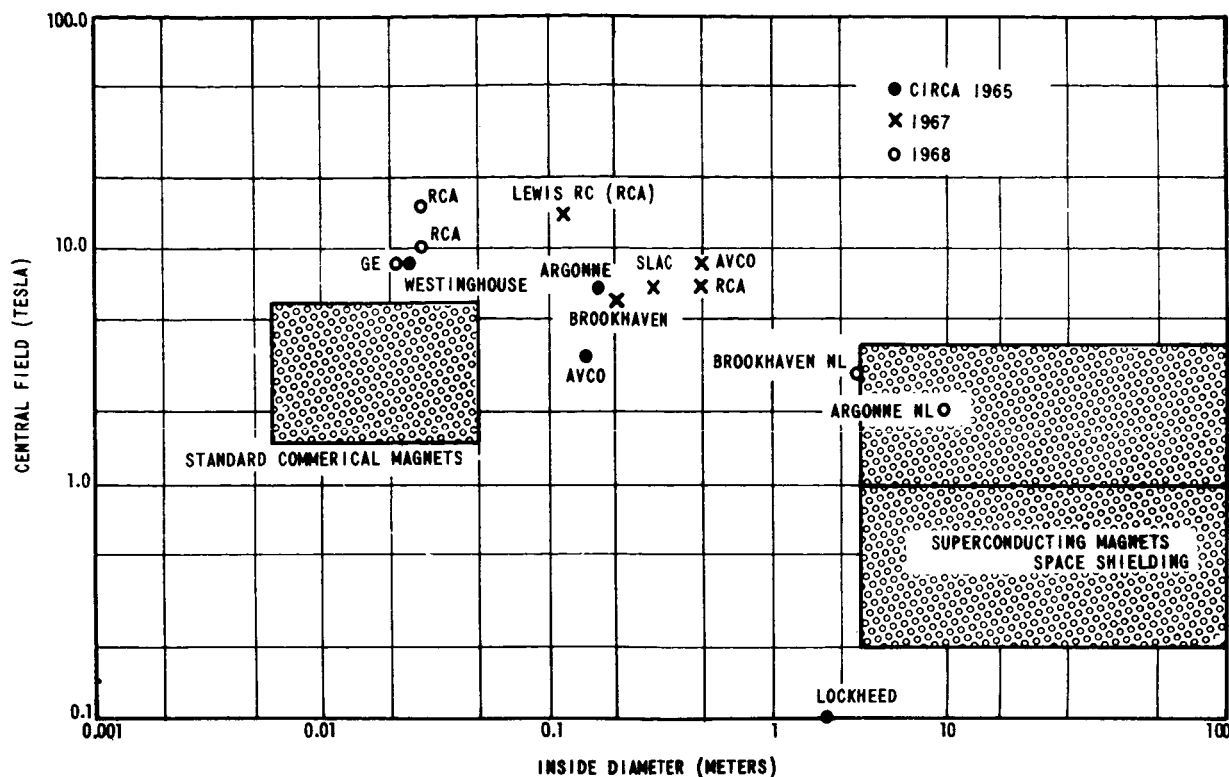


Figure 1. Superconducting magnet technology.

TABLE 3. THREE EXCEPTIONAL SUPER-CONDUCTING MAGNETS

● LEWIS RESEARCH CENTER MAGNET (LARGEST FIELD) (CONSTRUCTED BY RCA)	
CENTRAL FIELD	14.0 TESLA (140 KILOGAUSS)
BORE DIAMETER	15 CM.
LENGTH	35 CM.
MASS OF MAGNET	455 KILOGRAMS
STORED ENERGY	2 MEGAJOULES
● ARGONNE NATIONAL LABORATORY (LARGEST DIAMETER AND STORED ENERGY)	
CENTRAL FIELD	2.0 TESLA (20 KILOGAUSS)
BORE DIAMETER	4.8 METERS
LENGTH	3.0 METERS
MASS OF COMPOSITE (CONDUCTOR)	45,350 KILOGRAMS (50 TONS)
STORED ENERGY	80 MEGAJOULES
● STANFORD LINEAR ACCELERATOR MAGNET (SLAC)	
CENTRAL FIELD	7.0 TESLA (70 KILOGAUSS)
BORE DIAMETER	30 CM.
LENGTH	66 CM.
MASS OF MAGNET	1,600 KILOGRAMS
STORED ENERGY	4.8 MEGAJOULES
MASS BREAKDOWN:	
SUPERCONDUCTOR	200 KG 12.5%
COPPER STABILIZER	840 KG 52.5%
STRUCTURE	560 KG 35.0%
	1,600 KG

Table 4 presents the characteristics that would be required for a flyable shield system and the research necessary to satisfy these requirements. Shielding studies have indicated that moderately high fields of about 4 tesla would be required for a magnetic shield and approximately 0.2 tesla would be adequate for a plasma shield system. These field strengths are well within the current state-of-the-art, as are the magnet sizes that would be required to provide shielded volumes for several men. In addition, the ability to construct the reasonably complex coil configurations that would be needed in some shielding systems have been well demonstrated by the successful operation of saddle-shaped magnet windings.

The system requirement deserving the greatest attention is that of low overall system mass. Within this area, improved composite conductors and higher operating temperatures would make the most significant contributions; these two subjects are receiving the bulk of our attention. The thermal engineering problems of refrigeration and thermal-enclosure design improvement are not being pursued in this program.

TABLE 4. DESIRABLE CHARACTERISTICS OF A SHIELDING MAGNET SYSTEM

CHARACTERISTIC	R & D NEEDED
1. Modest Fields (0.2 - 4.0 tesla)	Current State-of-Art
2. Large Volumes (> 30 m <sup>3</sup> Shielded)	Current State-of-Art
3. Low Power Drain; Light System Weight	<sup>a</sup> Higher Operating Temperature (Higher Transition Temperature, $T_c$ ) <sup>a</sup> Lighter, Stable Composite Conductors with High Current Density  More Efficient Cryogenic Refrigerators  More Efficient Thermal-Structural Enclosures
4. Special Geometries	Current State-of-Art

<sup>a</sup> Current Research is Concentrated in these Areas.

Achievement of significantly increased operating temperature implies the availability of materials with significantly increased transition temperatures, a subject of great interest to all who work with superconductors. Refrigerator efficiencies increase rapidly as the operating temperature increases. For example, the power required to extract 1 W at 4.2°K (liquid helium) is seven times greater than that required to extract 1 W at 20°K (liquid hydrogen) and 60 times greater than that required at 77°K (liquid nitrogen). The mass of the refrigerator and its electrical power demands will decrease dramatically with increasing operating temperatures. Also, the smaller the temperature difference is between the cryogenic container and the external environment, for example, a manned cabin, the smaller the tendency is for heat to leak into the low temperature region and the lighter the thermal insulation system can be. Both of these considerations demonstrate the great value of a higher temperature superconductor. Because many space vehicles have liquid hydrogen on board for propulsion, it would be very desirable to operate superconductors at or above 20°K, rather than the usual 4 to 15°K, and this in turn implies the need for a material with a transition at 25 to 30°K.

RCA, under contract NAS8-21384, is currently conducting an excellent research study of the transition temperature in Nb<sub>3</sub>Sn and related compounds. A simple, but very accurate, band model of Nb<sub>3</sub>Sn,

which has been developed, has led to the prediction that if the crystal structure of the material can be suitably and slightly modified, its transition temperature should rise from 18°K to 30 to 35°K. Study of the validity of this prediction is the major goal of this research at present.

Mass reduction of the magnet system can also be approached through optimization of the composite superconductor winding material. The term "stabilization" refers to the degree of insensitivity of a conductor to local disturbances or gross current or field changes. It is achieved for large magnet systems by the presence of a heavy normal metal stabilizer referred to above. Research is being conducted to provide a better understanding of the instability problem in type II materials and of the techniques for assuring adequate stability. Table 5 lists the titles and general goals of present research. Atomics International Division of North American Rockwell Corporation, under contract NAS8-21415, is concentrating on understanding flux motion and resulting heat generation in order to evaluate the possibilities of practical conductors with little or no normal cladding. The Oak Ridge National Laboratory, under Government Order H-29278A, is studying transient and steady-state stability of both commercial type and special-geometry composite and bare conductors in order to optimize the stability provided by the commonly used copper cladding. In relation to this aspect, there is considerable

TABLE 5. SUPERCONDUCTIVITY RESEARCH STUDIES

CONTRACTOR	SUBJECT	GOAL
RCA NAS8-21384	STUDY OF TRANSITION TEMPERATURES IN SUPERCONDUCTORS	INCREASED $T_c$ , INCREASED OPERATING TEMPERATURES
ATOMICS INTERNATIONAL NAS8-21415	STUDY OF INHERENTLY STABILIZED HIGH FIELD SUPERCONDUCTORS	CONDUCTORS NOT REQUIRING HEAVY STABILIZER CLADDING
OAK RIDGE NATIONAL LAB G.O. H-29278A	STUDY OF MAGNETIC FLUX FLOW AND SUPERCONDUCTOR STABILIZATION	OPTIMUM CURRENT DENSITY, COOLING PROPERTIES, FLUX FLOW CONTROL AND STABILIZATION
STANFORD RESEARCH INSTITUTE PENDING	RESEARCH ON FLUX PINNING MECHANISMS IN SUPERCONDUCTORS	UNDERSTANDING MAGNETIC vs. MATERIAL PROPERTIES OF SUPERCONDUCTORS
S&E-SSL-NP, MARSHALL SPACE FLIGHT CENTER	APPLICATIONS OF SUPERCONDUCTIVITY TO ACTIVE SPACE SHIELDING	UNDERSTANDING FLUX PINNING AND JUMPING MECHANISMS; TRANSITION TEMPERATURES; POSITRON ANNIHILATION STUDY OF FERMI SURFACE

interest in various government laboratories in the use of high purity aluminum cladding since it has excellent conductivity and mass density characteristics. A pending research study with the Stanford Research Institute will concentrate on relating the magnetic behavior of type II materials to their metallurgical properties. By utilization of a difficult but powerful powder pattern technique, the location of individual flux lines can be visualized and correlated with the material's structure.

In-house research at MSFC is conducted in the Superconductivity Laboratory of the Space Sciences Laboratory. The research is presently directed toward understanding how fields and currents are distributed and move in type II materials and toward studies of transition temperatures in superconductors, particularly type II.

When the current or field applied to a type II superconductor changes, magnetic flux tends to move in the material in discontinuous, rapid "flux jumps" that can, under some conditions, momentarily drive the sample into the normal state. The dynamics of flux motion are only partly understood and are important to the stability problem. A schematic of the sample holder of a flux jump experiment is shown in Figure 2. A hollow cylinder in the bore of a superconducting solenoid is outfitted with magnetic field probes and pickup coils to monitor flux motion during flux jumps. The

conditions for the onset of jumps and their propagation in the sample can be monitored in detail.

The relationship between ultrasonic measurements in materials and their transition temperatures

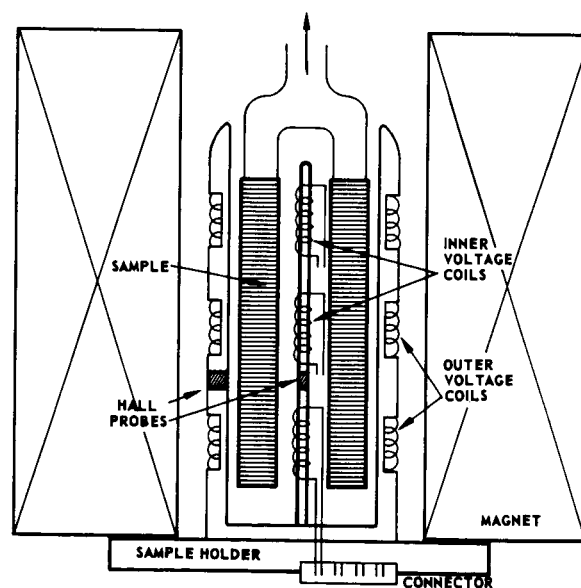


Figure 2. Schematic of a flux jump experiment holder.



is also being investigated. Striking correlations are seen to exist, but pertinent and accurate ultrasonic data are reported only rarely in the literature.

Apparatus for making ultrasonic measurements in superconductors at cryogenic temperatures is being assembled.

# REACTOR RADIATION SHIELDING

By

Martin O. Burrell and Henry E. Stern

The primary effort in reactor radiation shielding research has been directed toward application to the nuclear rocket program. Work previously discussed in this report included a comparison and evaluation of various shield calculation methods; that is, point kernel, discrete ordinates or angular segmentation, and stochastic or Monte Carlo. Additional work has been performed in this area by Westinghouse Astronuclear Laboratory (WANL). Their effort was divided into three tasks, as follows:

## TASK I

- Evaluate Previous Work
- Review Available Methods
- Select Geometrical Models
- Select Promising Methods
- Evaluate Methods Versus Experiment

## TASK II

- Evaluate Most Promising Method
- Select Preliminary Design Method
- Select Final Design Method

## TASK III

- Program Preliminary Design Method
- Formulate and Program Final Design Method

As a result of this study, a program package was assembled for use on the Marshall Space Flight Center (MSFC) computing machines. Codes were included for relatively rough preliminary shield design and for more precise final design. The package comprised a point kernel code, one-dimensional and two-dimensional angular segmentation programs, a Monte Carlo code, various auxiliary data preparation and analysis codes, and libraries of required neutron and gamma-ray cross section information.

To obtain some checks of calculations against experiments, measured data from the NRX-A2 reactor at the National Reactor Development Station and the Preassembly Experiment (PAX) reactor at the Westinghouse Astronuclear Experimental Facility

(WANEF) at Waltz Mills, Pennsylvania, were used in comparison with calculated results. Two typical comparisons are shown in Figures 1 and 2.

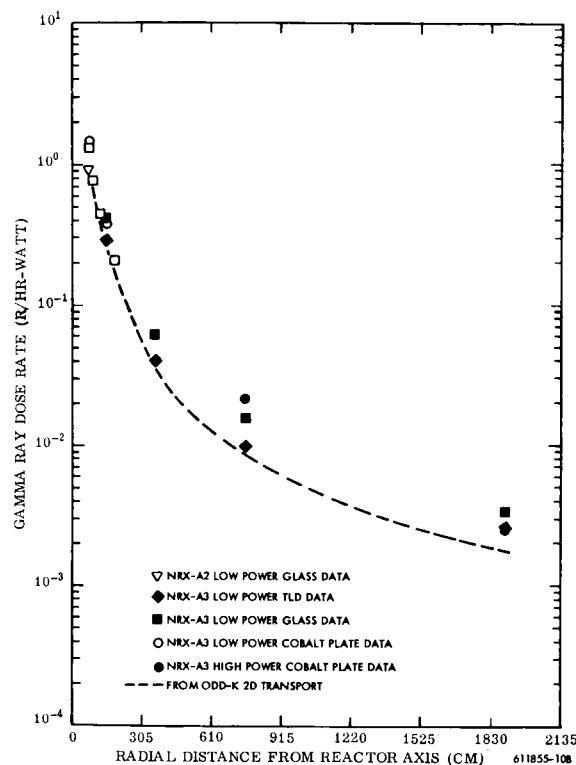


Figure 1. Gamma data comparison.

A summary of the work performed including a synopsis of the methods, the results of analyses and comparisons, and descriptions of all the programs considered is presented in Reference 1. To help familiarize MSFC personnel and other interested shielding people with the shielding codes developed, a 1-week seminar-workshop was held at MSFC in December 1967.

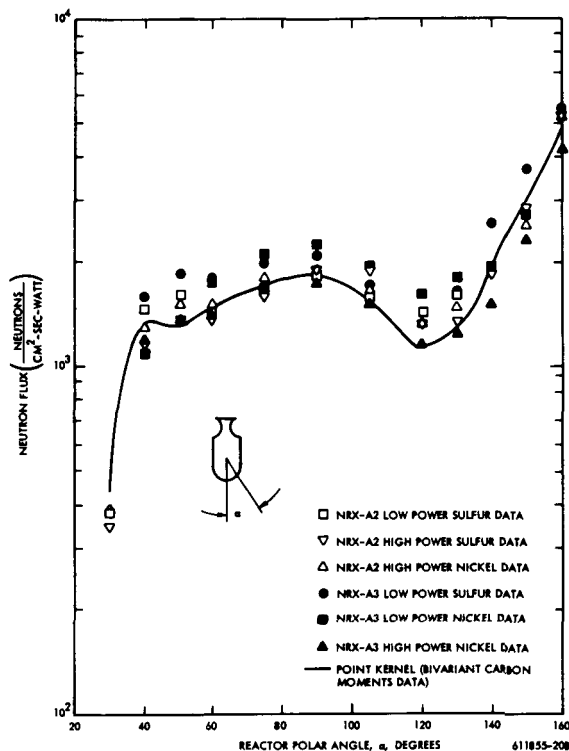


Figure 2. Neutron data comparison.

Since the implementation of this program package at MSFC, further development work has resulted in changes in some of the codes. The original WANL angular segmentation codes are being replaced by versions of the Oak Ridge ANISN and DOT codes. The Westinghouse FASTER Monte Carlo code has not been employed extensively. Instead, for stochastic calculations, an in-house effort (performed by support contract) has resulted in the CAVEAT program, a complete revision and extension of the general-purpose Monte Carlo code COHORT [2]. This new program has such features as time dependence, real atmosphere models for air transport, variable dimensioning, and for third-generation computing machines, a pass option that allows complete execution of a given problem from source particle generation to fluence calculation.

As a follow-on to the calculation methods development, limited radiation level measurements were performed at WANL in a simulated propellant tank mockup, and the results were evaluated using the program package. The tests were performed using

the PAX reactor, constructed to simulate the NRX-A6 reactor assembly. A Saturn IB lox tank was furnished to WANL by MSFC. It was cut down in length, modified for handling and to allow for insertion of instrumentation, and load-tested to satisfy safety requirements. Three shield material configurations were used in the experiments (Table 1); all contained boral for suppression of thermal neutrons.

TABLE 1. SHIELD CONFIGURATIONS

Shield Configuration Designation	Area Density (gm/cm²)	Description
4B	59.05	A bare PAX reactor with a mockup of a typical core support plate, plenum region, and pressure vessel on a NERVA type reactor.
7D	139.70	Configuration 4B with six BATH (Boron-Aluminum-Titanium-Hydride) shield modules interposed between the core support plate and the plenum-pressure vessel region.
11	213.93	A "thick" shield consisting of polyethylene, lead, and boral.

Since liquid hydrogen is costly, difficult to maintain, and hazardous, particularly around nuclear reactors, two densities of polyethylene were used in simulation. For mocking up photon transport properties, electron densities in the two materials were equated, resulting in a polyethylene density of 0.12 g/cm³; for neutron transport, hydrogen atom densities were equated, resulting in a polyethylene density of 0.48 g/cm³. In the actual experiments, densities of 0.14 g/cm³ and 0.59 g/cm³ were used for reasons of availability. To obtain some idea of the validity of using polyethylene to simulate hydrogen, consider the curves shown in Figures 3 and 4. In Figure 3, the gamma energy absorption coefficients of hydrogen and carbon and their ratio are plotted versus gamma energy. Throughout the range of interest, the ratio is quite constant, indicating the response of the two elements to be very similar. In Figure 4, absorbed neutron dose rate in rads is plotted against neutron energy for polyethylene and hydrogen. Again, the curves are almost parallel.

Instrumentation included a Hurst proportional counter for fast neutron dose; a boron-10 lined, compensated ion chamber for thermal neutron flux; a U-238 fast fission detector for fast neutron threshold flux; and a carbon wall, gamma-sensitive ionization chamber for gamma dose rate. In addition,

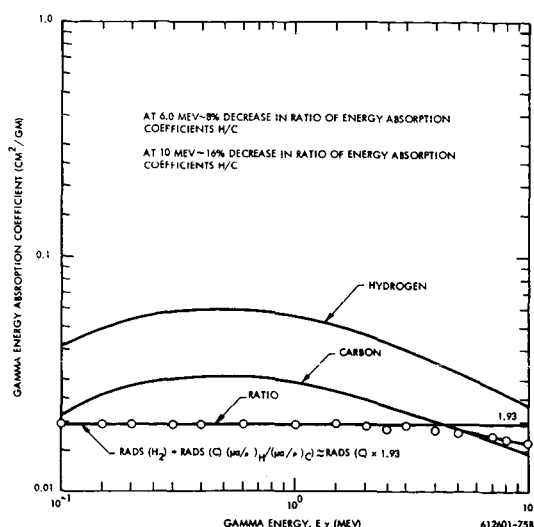


Figure 3. Gamma energy absorption coefficients.

bare and cadmium-covered gold foils, plutonium foils, sulfur pellets, phylatrons (wide-based p-i-n silicon diodes), and thermoluminescent dosimeters were employed to obtain further information concerning neutron energy spectra, fast neutron flux and dose, and gamma dose.

Horizontal and vertical traverses in the tank were effected through the insertion of several traverse tubes and the use of a specially designed motor-drive mechanism. The experimental setup is shown in Figure 5. Typical fast-neutron and gamma-ray comparisons are shown in Figures 6 and 7. In general, agreement between calculated and measured data is good. A detailed description of the experimental work and an analysis of the results are given in Reference 3.

A recent application of shield calculation methods consisted of a preliminary calculation of the dose above the propellant tank resulting from secondary gamma rays produced in the nozzle, nozzle skirt, and nozzle skirt extension for a typical reactor shield.

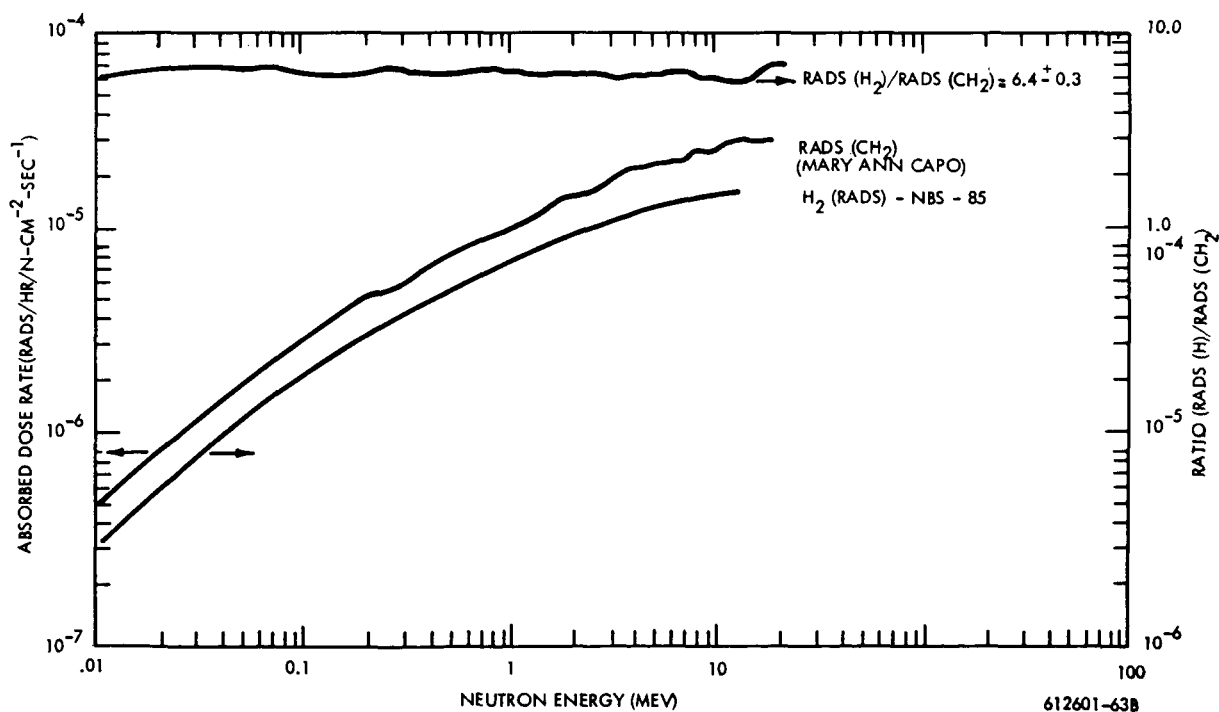


Figure 4. Neutron dose conversion factors.

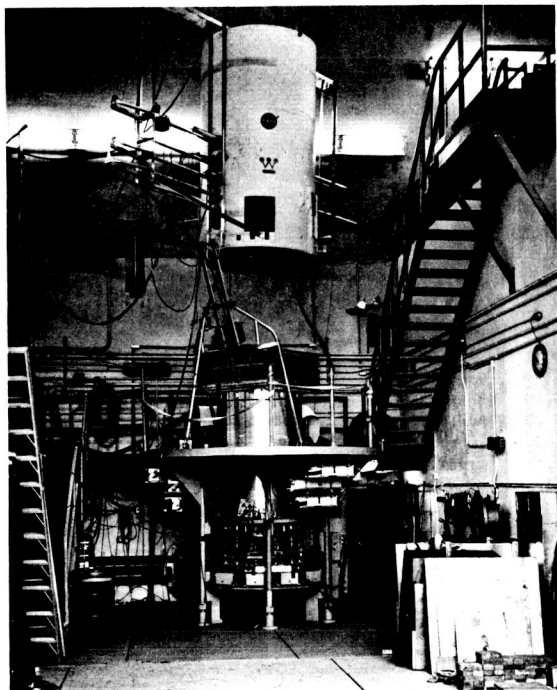


Figure 5. Experimental setup.

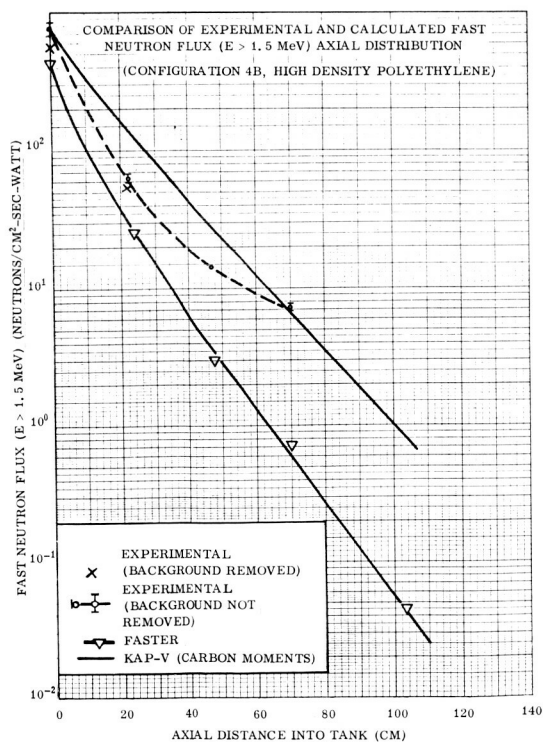


Figure 6. Fast neutron data comparison.

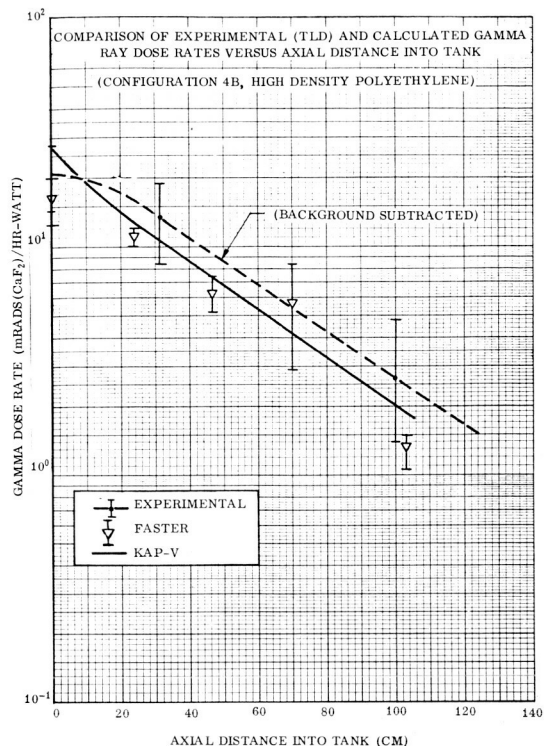


Figure 7. Gamma data comparison.

Starting with a reference geometry model, the DOT code, a two-dimensional discrete ordinates program was used, first to determine the neutron fluxes and resulting activation in the exhaust structure and then to calculate the transport of the gamma rays through the propellant tank. Figure 8 shows the geometric approximation of the exhaust structure used for the DOT code. Figure 9 shows preliminary results of secondary gamma dose rate as a function of radial distance from the axis of the tank for various levels of propellant in the tank.

Another application, the determination of neutron and proton dose rate fields near a SNAP-8 nuclear power system in an S-IVB orbital workshop configuration, is presented in Reference 4.

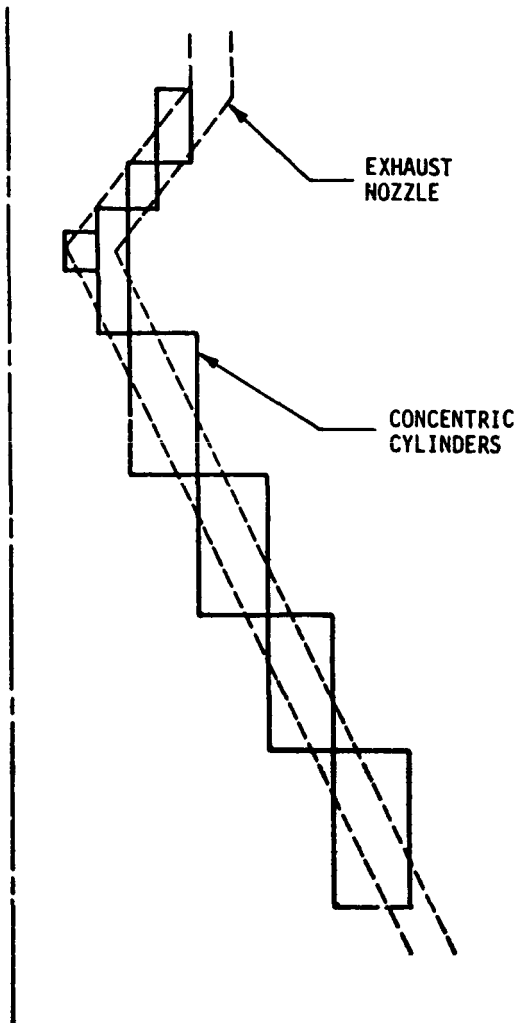


Figure 8. General approximation of exhaust nozzle with cylinders.

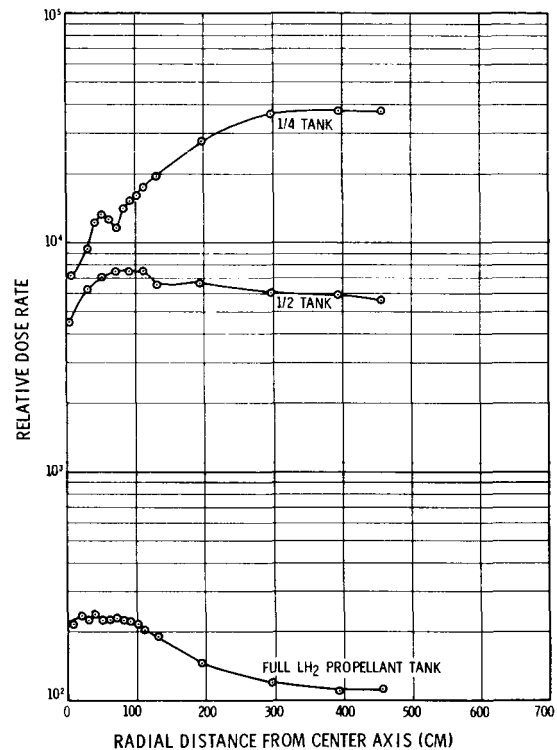


Figure 9. Secondary gamma dose rates at propellant tank top.

## REFERENCES

1. Synthesis of Calculational Methods for the Design and Analysis of Radiation Shields for Nuclear Rocket Systems. Final Progress Report, Vols. 1-9, Contract NAS8-20414, Westinghouse Astronuclear Laboratory, Pittsburgh, Pennsylvania, WANL-PR(LL)-010, June 1967.
2. Byrn, N. R.: CAVEAT A Revised Version of the General Purpose Monte Carlo Program, COHORT. Vol. II - User's Manual, Brown Engineering, Technical Note SE-290, August 1969.
3. Synthesis of Calculational Methods for the Design and Analysis of Radiation Shields for Nuclear Rocket Systems. Vol. 1, Radiation Measurements, and Vol. 2, Analysis of Radiation Measurements. Contract NAS8-20414, Westinghouse Astronuclear Laboratory, Pittsburgh, Pennsylvania, WANL-PR(LL)-022, Sept. 30, 1968.
4. Smith, T. W.: Radiation Levels for the SNAP-8 SIVB Orbital Workshop. Preliminary Results, Brown Engineering, RL-SSL-363, Dec. 1968.

# RADIATION INDUCED OUTGASSING

By

Raymond L. Gause

## SUMMARY

The radiation environment associated with the operation of a nuclear engine is an important factor in the design of nuclear-propelled space vehicles, since it can drastically affect the performance and reliability of vehicle materials and components. One area that is pertinent to the design of a nuclear stage and in which relatively little information concerning radiation effects has been obtained is that of radiation induced outgassing (the evolution of gas by polymers during irradiation). Because of the sparsity of data in this area, a program was initiated to generate quantitative gas yield data for various polymeric materials considered to be appropriate for application on a nuclear vehicle.

This paper briefly describes this program and presents the gas yield data that were obtained for 10 different polymers. The data, presented in terms of G-values (defined as the number of gas molecules formed by the absorption of 100 eV of energy), show that considerable quantities of gases are evolved by these materials and that radiation induced outgassing, if not considered in the design of a nuclear stage, could have a significant deleterious effect on vehicle performance and reliability.

## INTRODUCTION

A nuclear vehicle currently is being developed jointly by the National Aeronautics and Space Administration (NASA) and the Atomic Energy Commission (AEC). This engine, whose acronym is NERVA (Nuclear Engine for Rocket Vehicle Application), is being considered as the primary propulsion system for advanced space vehicles such as (1) the lunar ferry that would operate as a logistics vehicle between earth orbit and lunar orbit and (2) the Deep space stage for the proposed grand tour of the outer planets and the manned Mars mission. To design a vehicle to accept this engine and reliably perform an assigned mission, it is mandatory that a complete

assessment be made of the vehicle environment and the effects that this environment will have on materials and systems performance. Since such an assessment was made for the chemically powered stages of the Saturn V launch system, much non-nuclear environmental effects information is available that can be directly applied to the design of a nuclear stage. However, the additional effects resulting from the radiation environment produced by the operation of the nuclear engine must also be considered. It is known that nuclear radiation can drastically alter the properties of materials. For this reason, it is vitally necessary that the effects of radiation on potential stage materials be considered early in stage design.

In general, the effects of radiation on metals and polymers have been studied for many years, and considerable data are available in the literature [1-4]. However, the majority of previous radiation effects programs have been concerned with either (1) neutron induced radioactivity or (2) alterations in electrical, mechanical, thermal, or optical properties. One area that is pertinent to the design of a nuclear stage for which relatively little data have been obtained is that of radiation induced outgassing (the evolution of gas by polymers during irradiation). Because of the sparsity of data in this area, a program was initiated to generate quantitative gas yield data for various polymeric materials considered to be appropriate for application on a nuclear vehicle.

## RADIATION INDUCED OUTGASSING

During operation, a nuclear engine generates two primary types of radiation, neutron and gamma. When polymeric materials are irradiated with high intensity gamma rays, gases are evolved [5]. This process is known as radiation induced outgassing and depends to a considerable degree on the chemical structure of the polymer. In order to discuss the mechanism of radiation induced outgassing, it is necessary to briefly consider the basic interactions that can occur when gamma photons interact with

matter. Three basic types of interaction are possible, each depending on the energy of the photon. At low energies, photons interact with the bound electrons of an atom and are completely absorbed. Electrons are emitted with a kinetic energy equal to the initial energy of the photon less the binding energy required to remove the electron; this is known as the photoelectric process. For higher photon energies, Compton scattering of the gamma photons occurs.

The Compton interaction results when a photon is elastically scattered by an orbital electron within the coulomb field of a nucleus. As illustrated in Figure 1, sufficient energy is transferred to the orbital electron to allow it to escape the coulomb field of the nucleus. Thus, after the interaction, there exists a Compton electron and a scattered photon with an energy less than the incident photon. For very high energy photons, interaction with matter occurs by the pair production process in which the photon is converted instantaneously into mass, producing an electron and a positron (a particle similar to the electron but with unit positive charge). Relative probabilities of photoelectric absorption, Compton scattering, and pair production depend on photon energy as shown in Figure 2. The energy range of the gamma photons emanating from a nuclear engine is approximately from 0.1 to 10 MeV. Figure 2

shows that Compton scattering is the predominant process for the absorption of gamma radiation in this energy range. Thus, polymeric materials located on a nuclear vehicle will absorb engine gamma radiation by this process.

Generally, the interaction of photons with polymeric materials can result in:

1. The cross-linking of molecular chains.
2. The destruction and disintegration of macromolecules with the formation of volatile products and of molecules of shorter lengths.
3. The change of the number and character of the double covalent bonds.
4. Oxidation and other reactions initiated by radiation under corresponding conditions.

These processes may, as a rule, proceed simultaneously during irradiation, but the correlation between their occurrences as governed by the chemical nature of the polymer, and also by the presence or absence of oxygen and other active reagents, determines the overall chemical effect

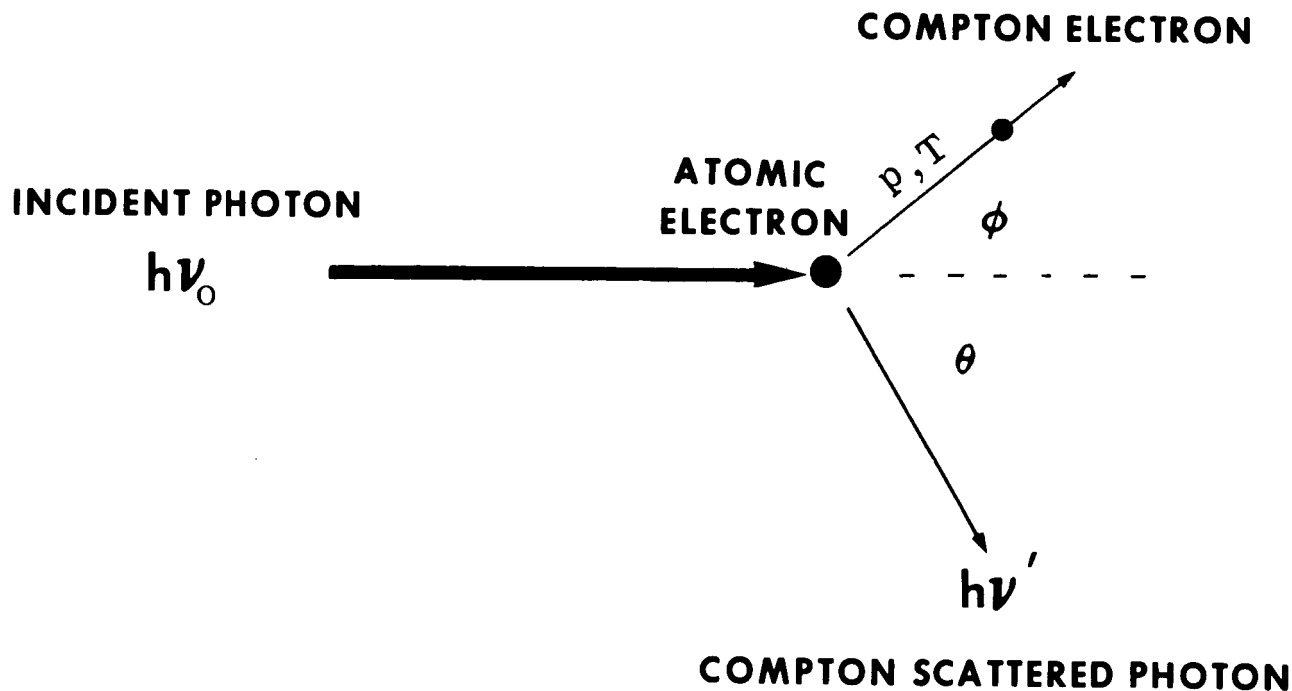


Figure 1. Compton scattering process.



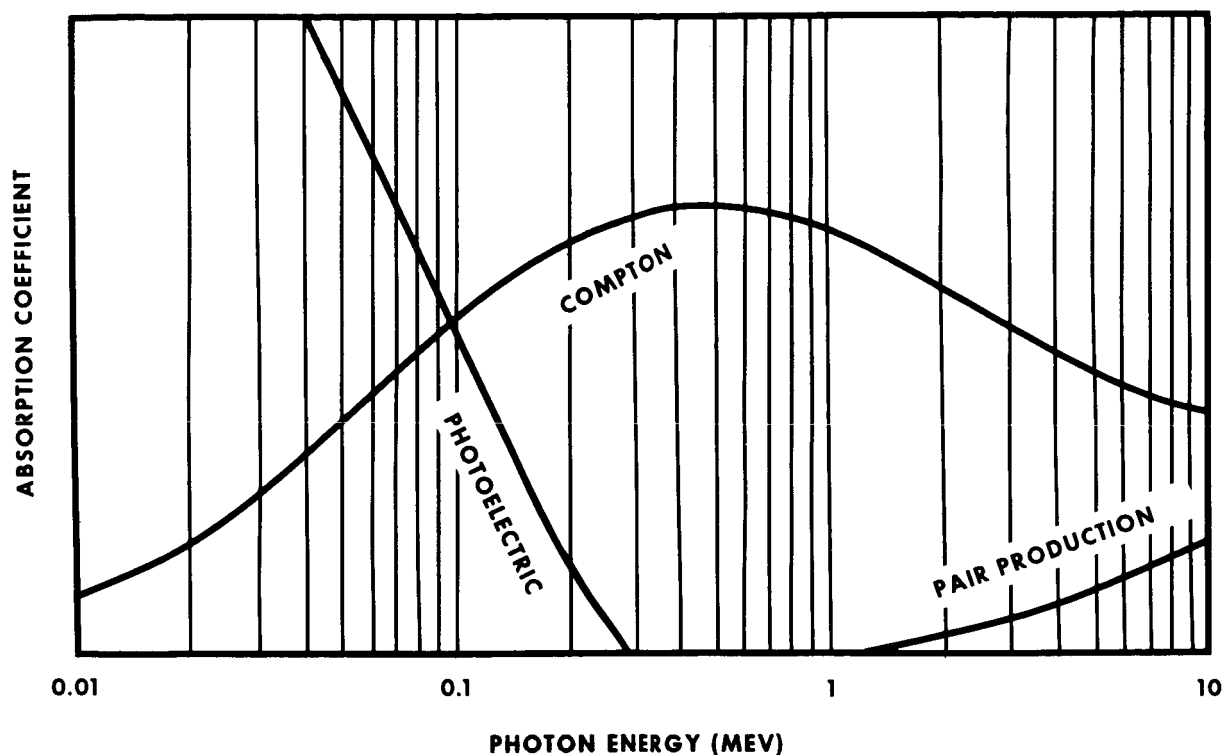


Figure 2. Absorption coefficient dependence on photon energy.

and the resultant change in polymer properties. To illustrate how these radiation chemistry processes are involved in the mechanism of gas formation by the absorption of gamma photons, consider the polymer polyethylene that is structurally and conceptually the simplest of the organic polymers.

Polyethylene is made by linking together molecules of ethylene monomer into a large molecule as shown in Figure 3a. When a gamma photon (indicated by the wavy arrow) is absorbed by this material, sufficient energy can be transferred to rupture the carbon-carbon or carbon-hydrogen covalent bonds. If the carbon-hydrogen bond is broken as shown in Figure 3b, a hydrogen atom is removed from the chain and the polymer molecule now contains a carbon atom that possesses an unpaired electron (indicated by the dot). This is the alkyl free radical. The free hydrogen atom is chemically unstable and will abstract a hydrogen atom from some other molecule, generating another alkyl radical and a hydrogen molecule. Of course, if many gamma photons are available for interaction, this

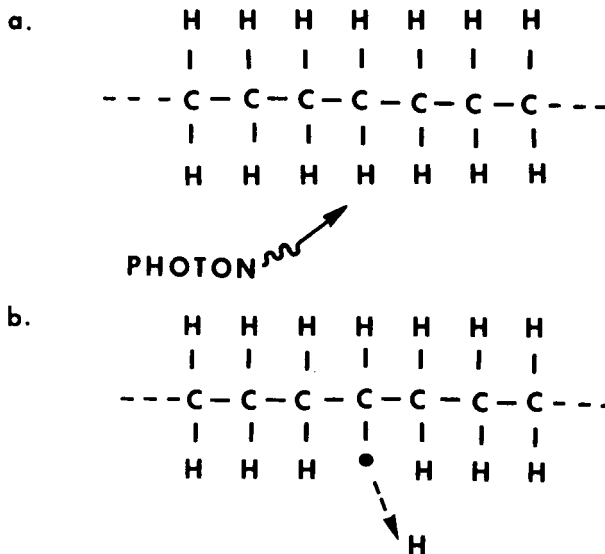


Figure 3. Radiation induced outgassing mechanism for polyethylene.

process can be repeated many times resulting in the formation of a significant quantity of hydrogen gas. Because the alkyl radicals are very reactive, they may react with other radicals to form cross-links or other products. In addition to the rupture of the carbon-hydrogen bond, the rupture of carbon-carbon bonds may occur simultaneously, which leads to the formation of two free radicals of a different type. These free radicals will recombine unless they are able to diffuse away from each other. If they do diffuse away, the molecule remains permanently broken and chain scission is said to have occurred. There are other processes that can occur but they will not be discussed since the purpose here is to illustrate in a simple fashion the mechanisms involved in the generation of gases by irradiated polymers. As can be seen from this discussion, hydrogen gas can be formed by the irradiation of polyethylene and other hydrogen-containing polymers in addition to other gaseous products that may be produced by free radical interactions.

## EXPERIMENTAL PROGRAM

The objective of the experimental program was to obtain quantitative gas yield data that could be used to determine the suitability of various selected polymers for use on a nuclear vehicle. Basically, the program involved (1) the design and fabrication of a vacuum chamber in which the materials could be irradiated, (2) the preparation of a computer program for the analysis of the experimental data, (3) the selection of test materials, (4) the preparation and irradiation of test specimens, (5) the collection and measurement of the composition and quantity of the evolved gases, and (6) the computer analysis of the experimental data.

## EXPERIMENTAL APPARATUS

The experimental equipment used in the program consisted of the vacuum irradiation chamber, a radiation source, a mass spectrometer, and a gas chromatograph. Figure 4 shows a specimen being inserted in the vacuum irradiation chamber that was designed for use with the 24 000 Curie Cobalt 60 source shown in Figure 5.

The gases that were collected in the gamma irradiation chamber were analyzed with either a

conventional mass spectrometer or a gas chromatograph, depending on which was more appropriate for a particular specimen.

## EXPERIMENTAL PROCEDURES

Prior to irradiation, the test specimens were characterized by measuring their weight, surface area, density, and chemical composition. A control experiment was made by irradiating an empty chamber to determine the type and quantity of any contaminating gases that were evolved from the vacuum seals of the chamber or de-adsorbed from the chamber walls. After the control data were obtained, a specimen was inserted into the chamber, and the chamber was evacuated. It was then irradiated for a prescribed time after which the chamber atmosphere was analyzed to determine the composition and quantity of the evolved gases.

## DATA ANALYSIS

The computer program for the analysis of the raw data obtained from the mass spectrometry and/or gas chromatography measurements was written in Fortran IV language for an IBM 1130 computer. To operate the program, a sequence of inputs is required. First the program requires the radiation flux at an initial time and date and the time and date of the initiation of the irradiation. With this information, the program corrects for the radioactive decay of the radioisotopic source. Next, the time duration of the irradiation is inputted, and the program computes the exposure level of the specimen in roentgens (R). The molecular weight, chemical composition, mass, and density of the specimen are introduced into the program, and the radiation dose absorbed by the specimen is computed in rads. From the gas temperature, gas pressure, chamber volume, and evolved gas concentration data, the molar concentrations of the evolved gases are computed. Finally, the program computes and prints out the gas yield data in terms of partial G-values for each of the evolved gases. The G-value is defined as the number of gas molecules that is evolved for every 100 eV of energy that is absorbed by the specimen. The total G-value for a material is obtained by summing the partial G-values that are calculated for the individual gases evolved from that material.

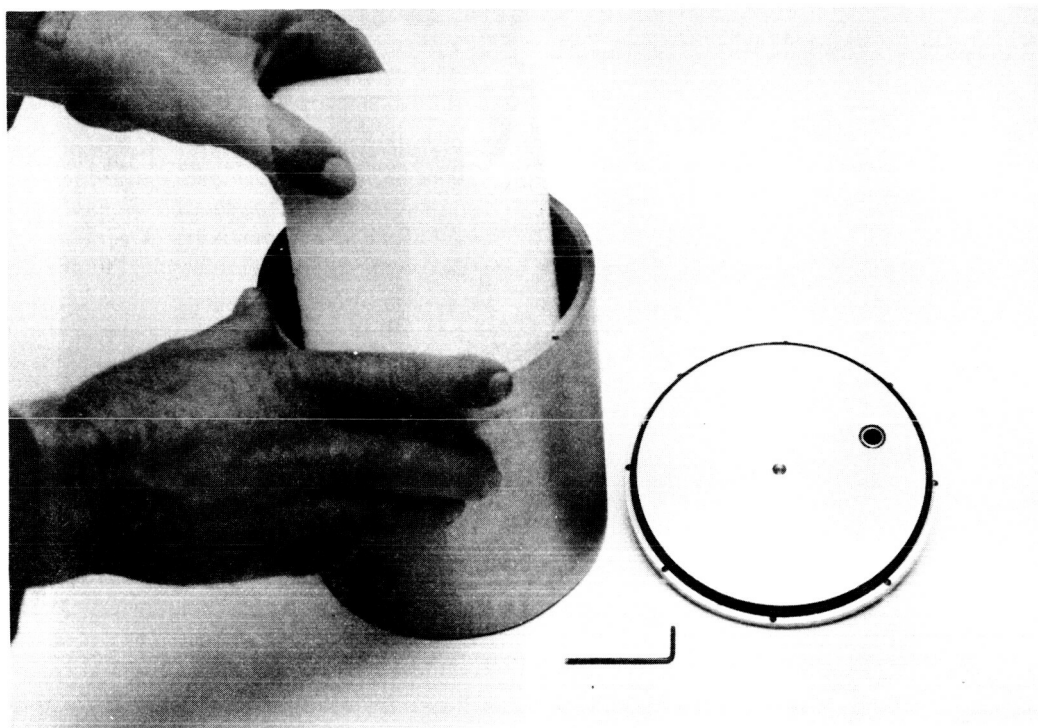


Figure 4. Vacuum irradiation chamber.



Figure 5. Gamma irradiation source.

## DISCUSSION OF EXPERIMENTAL RESULTS

The following 10 polymeric materials were evaluated in this initial program to determine the quantity and types of gases that are evolved during irradiation:

1. Polyethylene Terephthalate (Mylar)
2. Polyethylene
3. Polystyrene
4. Polypropylene
5. Polymethyl Methacrylate (Plexiglas)
6. Cellulose Acetate Butyrate
7. Ethyl Cellulose
8. Polycarbonate (Lexan)
9. Phenolic (Bakelite)
10. Cellulose Acetate

The partial G-values obtained for each of the gases generated by these materials are given in Table 1 and the integrated gas yields (total G-values) are shown in Table 2. An analysis of these data shows that the largest gas yield ( $G = 5.20$ ) was obtained from polyethylene  $\{C_2H_4\}_x$  and that 95 percent of

the gas evolved was hydrogen. The next highest G-value of 4.28 was obtained for polycarbonate  $\{C_{16}H_{14}O_3\}_x$  and cellulose acetate butyrate  $\{C_{14}H_{20}O_8\}_x$ . Both of these materials generated significant quantities of carbon dioxide and carbon monoxide but produced less hydrogen than polyethylene. The evolved gas from polycarbonate consisted of carbon dioxide (47 percent), carbon monoxide (51 percent), hydrogen (1.4 percent), and methane (0.6 percent). Ten gases were generated by the irradiation of cellulose acetate butyrate, but only four were produced in significant quantities. These were hydrogen (30 percent), carbon dioxide (25 percent), carbon monoxide (25 percent), and propane (12 percent). Polypropylene  $\{C_3H_6\}_x$

also evolved 10 different gases and had a G-value of 3.31. However, 98 percent of the gas generated was hydrogen. (Carbon dioxide and various hydrocarbons accounted for the remainder.) The G-value obtained for polymethyl methacrylate  $\{C_4H_6O_2\}_x$  was 2.01. The gases evolved from this polymer consisted of hydrogen (22 percent), carbon dioxide

(33 percent), carbon monoxide (37 percent), methane (6 percent) and ethane (2 percent). Ethyl cellulose  $\{C_{12}H_{22}O_5\}_x$  generates more gases than any of the other materials. However, of the 11 gases produced, only 5 were evolved in significant quantities; hydrogen (53 percent), carbon dioxide (10 percent), carbon monoxide (5 percent), ethane (6 percent), and acetaldehyde (17 percent). The G-value for ethyl cellulose was 1.92, which was only slightly greater than the 1.72 value that was obtained for phenolic  $\{C_7H_8O\}_x$ . The principal gas evolved by this polymer was hydrogen (98 percent).

Cellulose acetate  $\{C_{12}H_8O_8\}_x$  had a G-value of 0.64 and evolved principally hydrogen (30 percent), carbon monoxide (31 percent), and methane (14 percent). Polyethylene terephthalate  $\{C_{10}H_8O_4\}_x$  evolved principally hydrogen (12 percent) and carbon dioxide (87 percent) and had a G-value of 0.33. Polystyrene  $\{C_8H_8\}_x$  also evolved hydrogen (30 percent) and carbon dioxide (69 percent) but exhibited the lowest G-value (0.26) of any of the materials tested.

In summary, all 10 of the materials evaluated in this program evolved significant quantities of gases. The most prolific hydrogen producers were polyethylene, polypropylene, phenolic, cellulose acetate butyrate, and ethyl cellulose. Those polymers that generated large quantities of carbon dioxide and carbon monoxide were polycarbonate, cellulose acetate butyrate, and polymethyl methacrylate. Polyethylene, as expected, exhibited the largest gas yield whereas polyethylene terephthalate and polystyrene produced the least amount of gas.

## CONCLUSIONS AND RECOMMENDATIONS

It has been shown that polymers evolve gases when they are irradiated. Many miles of electrical insulation, thousands of square feet of thermal insulation, and several cubic feet of encapsulants in addition to large quantities of other polymeric materials will be used in the fabrication of a nuclear stage. Thus, the generation of copious quantities of assorted gases can be anticipated since all of these materials will be exposed to the radiation environment of the nuclear engine. If proper

TABLE 1. PARTIAL G-VALUES FOR SEVERAL POLYMERS

Partial G-Value															
Material	H <sub>2</sub>	CO <sub>2</sub>	CO	CH <sub>4</sub>	C <sub>2</sub> H <sub>6</sub>	C <sub>2</sub> H <sub>4</sub>	C <sub>3</sub> H <sub>6</sub>	C <sub>3</sub> H <sub>8</sub>	C <sub>4</sub> H <sub>10</sub>	C <sub>5</sub> H <sub>10</sub>	C <sub>5</sub> H <sub>14</sub>	Ethyl Alcohol	Acetaldehyde	Acetone	Methanol
Polyethylene Terephthalate (Mylar)	0.0402	0.289		0.0011											
Polyethylene	4.930			0.0079	0.120	0.023	0.0027	0.0095	0.088	0.0013	0.014				
Polystyrene	0.077	0.182		0.0014											
Polypropylene	3.239	0.008		0.046	0.0021	0.0011	0.0015	0.0019	0.0037	0.0011	0.0011				
Polymethyl Methacrylate (Plexiglas)	0.449	0.6728	0.7476	0.1389	0.0039										
Cellulose Acetate Butyrate	1.294	1.063	1.063	0.153		0.025		0.513			0.0027	0.0250	0.1279		0.0086
Ethyl Cellulose	1.017	0.203	0.0872	0.0390	0.1188	0.059		0.0046				0.0272	0.3341	0.0018	0.0242
Polycarbonate	0.058	2.023	2.196	0.0055											
Phenolic (Bakelite)	1.680	0.034		0.0066											0.0044
Cellulose Acetate	0.195	0.039	0.200	0.0882	0.037			0.0063				0.0045	0.0124	0.0121	0.0405

TABLE 2. RADIATION INDUCED GAS YIELD (G)  
FROM SEVERAL POLYMERS

Polymer	G-Value
Polyethylene	5.20
Polycarbonate (Lexan)	4.28
Cellulose Acetate Butyrate	4.28
Polypropylene	3.31
Polymethyl Methacrylate (Plexiglas)	2.01
Ethyl Cellulose	1.92
Phenolic (Bakelite)	1.72
Cellulose Acetate	0.64
Polyethylene Terephthalate (Mylar)	0.33
Polystyrene	0.26

consideration is not given to the outgassing characteristics of these materials during materials selection and vehicle design, vehicle performance could be deleteriously, if not catastrophically, affected.

As a practical example of how radiation induced outgassing can have a catastrophic effect, consider the liquid hydrogen cryogenic dewar shown in Figure 6. The dewar was insulated on two sides with 5.08 cm (2 in.) of corkboard insulation. The other two sides and the top and bottom were insulated with 5.08 cm (2 in.) of a spray-on type of polyurethane foam. The entire dewar was covered with a vapor barrier to prevent cryopumping of atmospheric gases. Unfortunately, in this case, the vapor barrier served another function: it prevented any radiation induced gaseous products from escaping. The dewar containing several hundred gallons of liquid hydrogen was subjected to neutron and gamma radiation from a 3-MW nuclear reactor for several hours. After being irradiated to a gamma dose of approximately  $10^{10}$  ergs-gm<sup>-1</sup>(C), a detonation occurred resulting in the damage shown in Figure 7.

Figure 6. Liquid hydrogen dewar  
before irradiation.

Subsequent investigation showed that the detonation was initiated in the corkboard as a result of radiation induced outgassing [6]. Since corkboard is largely cellulose, hydrogen gas was evolved during the irradiation. The vapor barrier prevented the hydrogen from escaping, thereby allowing the hydrogen concentration to steadily increase. The corkboard, being a very porous material, had a considerable quantity of air in it that was entrapped when the vapor barrier was applied. The detonation resulted when the mixture of radiation induced hydrogen and entrapped air reached the critical value.

It is obvious that problems like the one described above must be discovered in the laboratory and not on an operational nuclear stage. For this reason, it is strongly recommended that radiation induced outgassing be included as one of the materials selection and design criteria for the nuclear stage.

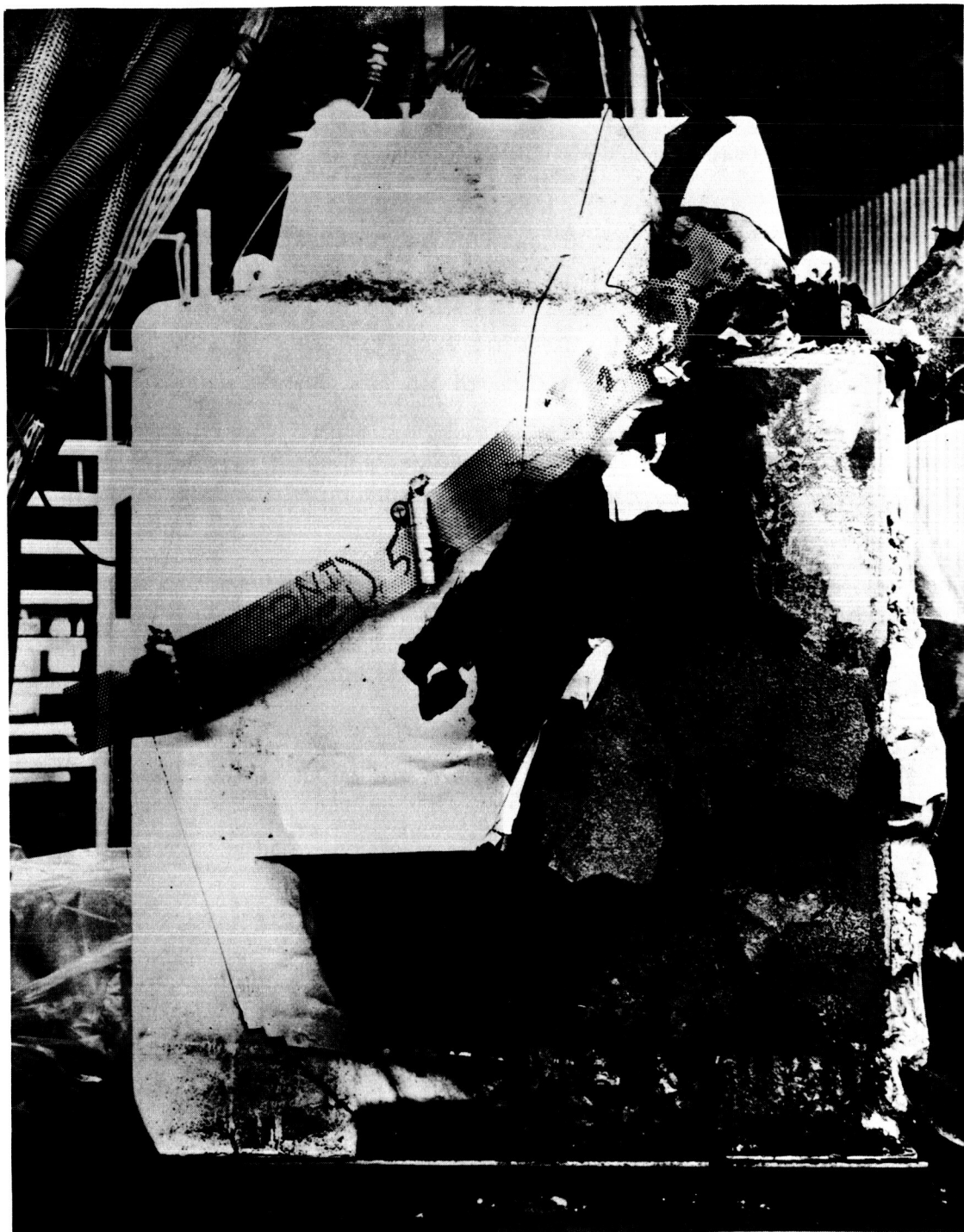


Figure 7. Liquid hydrogen dewar after irradiation to  $1 \times 10^{10}$  ergs-gm<sup>-1</sup>(C) .

## REFERENCES

1. The Effects of Nuclear Radiation on Elastomeric and Plastic Components and Materials. Radiation Effects Information Center, Report No. 21, Sept. 1961.
2. The Effect of Nuclear Radiation on Structural Metals. Radiation Effects Information Center, Report No. 20, Sept. 1961.
3. The Effect of Nuclear Radiation on Electronic Components. Radiation Effects Information Center, Report No. 18, Sept. 1961.
4. McKannan, E. C. ; and Gause, R. L. : Effects of Nuclear Radiation and Cryogenic Temperatures on Nonmetallic Engineering Materials. J. Spacecraft Rockets, vol. 2, no. 4, July 1965.
5. Nikitina, T.S. ; et al. : Effect of Ionizing Radiation on Polymers. State Scientific Publishing House for Chemical Literature, Moscow, 1959.
6. Evaluation of Cryogenic Insulation Material and Composites for Use in Nuclear Radiation Environments. General Dynamics Corporation Report FZK-347.



# COSMIC RAY RESEARCH AND NUCLEAR INSTRUMENTATION DEVELOPMENT

By

T. A. Parnell

## SUMMARY

The experimental cosmic ray research group of the Radiation Physics Branch of Space Sciences Laboratory is pursuing research programs concerning the earth's trapped radiation belts and the galactic cosmic radiation. One of the objectives of these programs is to measure characteristics of the particle populations to illuminate questions involving the origins and temporal stability of the trapped radiation belts and the problems in astrophysics related to the origin and transport of galactic cosmic rays. Detailed knowledge of the particle populations is also needed for estimating the radiation dose received by the spacecraft, occupants, and experiments on extended space flights, such as the Apollo Applications Payload (AAP) missions.

This group supports other research activities within the Space Sciences Laboratory with specialized nuclear instrumentation and also designs nuclear radiation measuring equipment to be used as operational equipment on spacecraft.

## INTRODUCTION

In recent years, the trapped radiation belts of the earth have been mapped out rather well, and many interesting features of the particle population and temporal behavior of these belts have been observed [1]. However, a coherent model of the magnetosphere is not yet possible, and the injection, acceleration mechanisms, and stability lifetimes of the particles in the trapped radiation belts are still a mystery, and much research remains to be done. Also, in some regions, data on high energy particles that will cause appreciable radiation effects on long duration spacecraft are not available.

Similarly, although the particle identities and energy spectra of galactic cosmic rays are known

rather well up to a few billion electron volts [2], and the all-particle energy spectrum is less well known up to about  $10^{20}$  eV, the origin, life history, and transport of the galactic cosmic rays are still subjects of speculation. Measurements of detailed properties of the cosmic radiation that are designed to answer specific questions such as the age of the flux, possible origins, path length through interstellar gas, etc. are vital to an understanding of the astrophysical processes that originated the cosmic ray flux. The energy density of the galactic cosmic rays (about  $1 \text{ eV/cm}^3$  in the galaxy), their extreme energy range (up to  $10^{20}$  eV), and their mean energy per particle (about  $10^{10}$  eV) make it clear that experiments on the galactic cosmic ray flux are an important part of observational astrophysics.

The interest of the cosmic ray group of the Space Sciences Laboratory in these problems will be illustrated by a discussion of three current projects. The first, a proton spectrometer that is being developed as an operational instrument for the AAP program will also produce scientific data bearing on the questions above. The proportional counter project to be described below is being developed principally for use in observing the galactic cosmic radiation, but other uses of the counters are being considered. The large air shower experiment is for observation of high energy primary cosmic rays having energies greater than  $10^{14}$  eV.

## RESEARCH PROGRAM OF THE COSMIC RAY GROUP

### Proton Spectrometer for the AAP Workshop

For manned space stations a circular earth orbit of 400- to 450-km altitude and at approximately 35-degree inclination is most economical and yields a spacecraft lifetime of approximately 2 years. Therefore, this orbit is chosen for several manned launches in the future, including the AAP workshop.

One disadvantage of this orbit is that it intersects a low region of the inner Van Allen belt over the South Atlantic Anomaly (Fig. 1). In this area

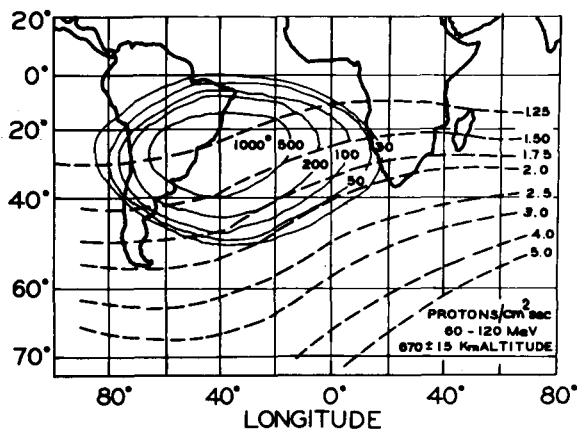


Figure 1. Contours of proton flux over the South Atlantic at 670 km. (The dotted lines are L lines at 670 km in the McIlwain Coordinates.)

the radiation approaches the earth to about 250 km [3]. The spacecrafts in this orbit are exposed to Van Allen radiation up to 20 percent of the 92-minute orbit duration. The accumulated dose on the outside of the spacecraft in this orbit may reach 1000 rads and may reach 5 to 50 rads on the inside for a typical 56-day mission of the AAP program [4].

The purpose of the proton spectrometer is to measure the flux of energetic protons and electrons on the outside of the spacecraft and, in particular, to measure the particle spectrum of those protons that are energetic enough to penetrate the structure of the AAP workshop and cause radiation damage (especially to photographic materials) on the inside during a long-term mission. A measurement of the primary particle flux on the outside of the spacecraft is necessary to be able to calculate the radiation dose received at any arbitrary point in the spacecraft. A dosimeter measurement on the inside would not give sufficient information for this purpose.

The measurement of the electron and proton spectrum will facilitate the calculation of future spacecraft shielding structures and enable more precise background subtraction from film materials extensively used on the AAP missions. The information will also be of scientific importance in determining particle injection and loss mechanisms for the trapped radiation.

The prime emphasis is to measure protons above 100 MeV since data are relatively scarce [5] at this energy and are not available for energies above 170 MeV [6]. The measurement has been extended down to 18.5 MeV, because only the lower energy particles are likely to exhibit time variations in the trapped radiation that can be studied during the lifetime of the dry workshop. The instrument measures the proton spectrum from 18.5 to 400 MeV and also measures the electron spectrum from 1.2 to 10 MeV.

The proton spectrometer is a  $dE/dx$ -E telescope composed of four detectors (Fig. 2) and an electronic analyzing system. Two of those ( $D_1$  and  $D_2$ ) are fully depleted Si-surface barrier detectors (300 mm<sup>2</sup> and 500 mm<sup>2</sup> thick) and are used as  $dE/dx$  detectors; they also define the instrument's energy-independent, geometric factor of 0.4 cm<sup>2</sup> steradian. A cone-shaped CsI (Na) crystal of 14.2 g/cm<sup>2</sup> acts as a total E detector up to 105 MeV; higher energy protons suffer an energy loss in this crystal which determines their energy if the energy deposit in the  $dE/dx$  detectors is simultaneously analyzed. All three detectors are surrounded by a plastic guard detector,  $D_4$ ; both scintillators are viewed by RCA 7151N photomultipliers.

The detector system will measure protons up to 400 MeV and electrons up to approximately 10 MeV. The lower threshold is defined by the counting rate, and is set to 18.5 MeV for protons or 1.2 MeV for electrons. No particle is counted unless it deposits more than 235 keV in  $D_1$  and  $D_2$ , establishing a coincidence of 40 nsec resolving time ( $D_1 D_2 \bar{D}_4$ ). A triple coincidence is required for particles of higher energy that enter  $D_3$  and deposit more than 1.8 MeV there. The coincidence resolving time,  $D_1 D_2 D_3 \bar{D}_4$ , is 250 nsec. Zero crossover timing is used throughout the instrument to establish the short coincidence widths necessary to accurately count protons in this environment.

The energy analysis for protons is done by a delay line-gated, 2-MHz, 8-bit, analog-to-digital converter (ADC). The available telemetry restricts readout to 8 digital channels. Therefore, the ADC pulse train is fed into a diode decoding matrix that divides the 256 ADC pulses into 8 groups. The width of the channels increases logarithmically with particle energy for better statistical accuracy of the higher channels. The decoding matrix is gated by the threshold discriminator of the  $dE/dx$  detector,  $D_2$ , which permits discrimination between particles stopped in the CsI crystal and those penetrating completely

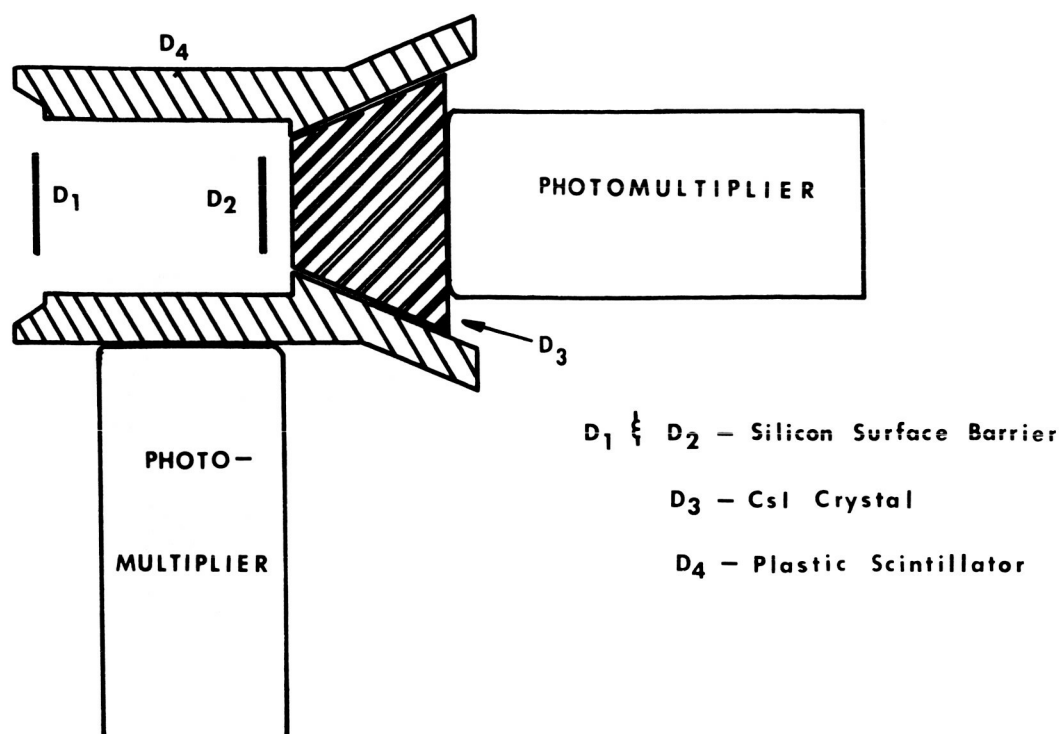


Figure 2. Cross section of the detector system of the proton spectrometer.

(protons above 105 MeV). The data are stored in 10-bit binary accumulators.

The electron energy is determined by single channel analyzers of 1- $\mu$ sec pulse-pair resolution. The electron events are stored in three binary accumulators.

The instrument has a closed-loop, digital, inflight calibration system [7] that utilizes an  $\text{AM}^{241}$  alpha source grown into the CsI crystal and automatically adjusts a programmable, multidynode Cockcroft Walton generator [7] supplying the photomultiplier tube.

The electronic analyzing system has been designed in modular form with the power supplies, preamps and amplifiers, analog section, control section, and digital storage units in separate modules. This allows flexibility in adapting the instrument and its components to other uses.

The instrument has been calibrated for protons at the Harvard Cyclotron and exhibits an energy resolution of 6 percent at 150 MeV.

Figure 3 is a picture of the complete proton spectrometer which weighs less than 10 lb and consumes less than 3 W of raw power in the flight configuration.

## Large Area Proportional Counter Development

The high energy primary cosmic rays are known to consist mostly of the nuclei of the elements, with an energy spectrum that extends to  $10^{20}$  eV per particle. In recent years, rather detailed information has been collected on the energy spectrum and relative abundances of the nuclear species present in the primary cosmic rays up to energies of a few billion electron volts [8]. However, the present evidence is insufficient to determine the origin, acceleration mechanisms, lifetime, and path length through interstellar matter of the cosmic rays.

For measurements of the specific ionization  $\left(\frac{dE}{dx}\right)$  of energetic charged particles, a detector of low specific mass is often desirable. For a particular example of this requirement, consider

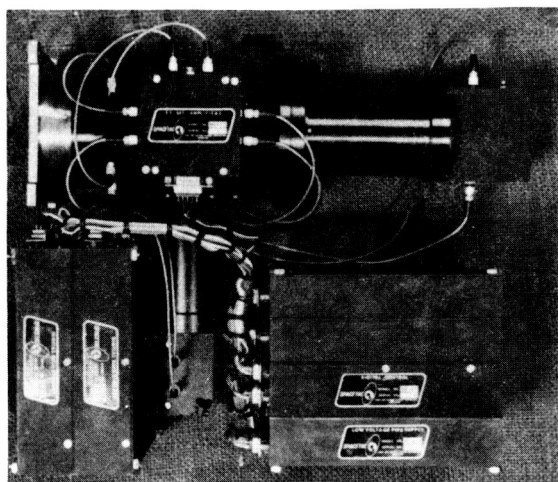


Figure 3. Prototype proton spectrometer with electronic analyzing circuits.

the high energy cosmic ray experiment of Goddard Space Flight Center (GSFC), which consists of a complex  $\frac{dE}{dx}$  detector system (charge identification section) to measure the charge of the cosmic ray and an ionization calorimeter to measure its energy. The GSFC experiment is shown schematically in Figure 4.

The GSFC experiment is designed to measure the energy spectrum and relative abundances of the nuclei and electrons from  $10$  to  $10^5$  GeV. At these energies, the  $\frac{dE}{dx}$  detector system furnishes a measure of the charge of the particles and unambiguously identifies the charge of the nuclear component of cosmic rays up to approximately  $Z = 26$ .

To accomplish this resolution, the  $\frac{dE}{dx}$  detector system consists of two sheets of plastic scintillator, a CsI crystal mosaic, a lucite Cerenkov counter, and three spark chambers. This system of detectors has a specific mass of approximately  $4 \text{ gm/cm}^2$  (equivalent to a layer of water 4-cm thick). This amount of matter poses a problem for measurements of nuclear abundances above  $Z = 26$ , where the nuclear interaction length becomes less than  $4 \text{ gm/cm}^2$  and nuclear interactions would occur predominantly in the  $\frac{dE}{dx}$  detector, destroying the charge measurement.

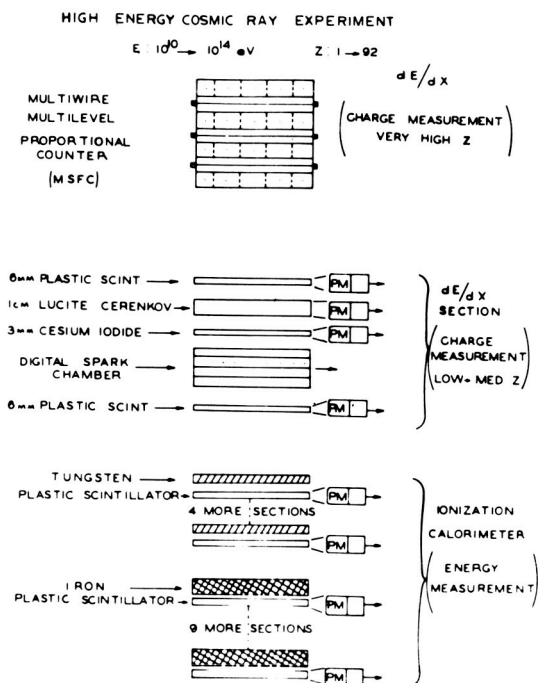


Figure 4. Schematic of the detector system used by GSFC to detect and identify high energy cosmic rays. (The proportional counter at the top is being developed at MSFC.)

The measurement of the abundance of very heavy nuclei would be very interesting from the astrophysical standpoint. Since the heavy nuclei are more subject to destruction by interactions with interstellar gas and photons than the lighter elements, their abundance furnishes important information relative to age and path length of the flux. The abundances of superheavy nuclei would also be important in determining the origin of the cosmic rays in either rapid or slow processes of nuclear synthesis.

Within the Space Sciences Laboratory, the development of some large area proportional counters to measure specific ionization of primary cosmic rays has been undertaken. The objective of this work is to produce a counter or set of counters that present a specific mass of less than  $1 \text{ gm/cm}^2$  to the particle flux in order to identify the charge of the primary cosmic rays from  $Z = 26$  to  $92$  with a resolution of  $Z \pm 3$ . The counter is also being designed to give the trajectory of the particle within a few millimeters. Figure 4 shows how this counter will be used in series with the GSFC experiment on a high altitude balloon flight for preliminary calibrations.

The requirements of making  $\frac{dE}{dx}$  measurements over a wide range of particle types and energies and making position measurements can be handled in separate counter sections.

For the transit position measurement, a method that has been investigated by others has been pursued [9]. Parallel anode wires (1 mil in diameter) are spaced 2 mm apart between parallel ground sheets (aluminum laminated on mylar). Using an argon-methane mixture for the proportional gas, with an anode potential of about 1800 V, the counter produces a pulse on a particular anode wire when a relativistic proton is near the wire. Two such counter arrays with anode wires at 90 degrees will allow X-Y measurement on the position of the particles to within about  $\pm 2$  mm. Each anode wire has a preamplifier and feeds a flip-flop for digital storage.

The  $\frac{dE}{dx}$  measurement is more difficult since linearity, wide dynamic range, and uniform sensitivity over a large area are required. Work on this problem has involved investigating the electric fields of many electrode configurations, studying the ionization cascade and fluctuations in energy deposit, making theoretical estimates of the charge resolution for particular counter geometries, and computer model studies (Monte Carlo calculations) of the anticipated response of particular counters.

A configuration that has been investigated consists of a stack of independent proportional counters through which the particle passes in series. Ideally, each counter makes an independent measurement as the particle passes through. Then the pulse heights from the various counters are combined by some method (such as averaging) to get better pulse height resolution. It has been shown by statistical considerations and calculations that this method produces better resolution than would be produced by a single counter of depth equal to the stack of independent proportional counters.

The inherent resolution of a  $\frac{dE}{dx}$  counter can be calculated from the work of Vavilov. Figure 5 shows a theoretical calculation of the resolution of an ideal proportional counter 2 inches thick using argon-methane at 1-atm pressure. The curves are the Vavilov distributions for 100-GeV praseodymium and cesium nuclei. Figure 6 shows the result of a Monte Carlo calculation in which it is assumed that there are 10 such counters in series taking 10

independent measurements of  $\frac{dE}{dx}$ , and these 10 pulse amplitudes are simply averaged. The dotted lines thus represent the pulse height distribution of the "instrument" consisting of 10 independent proportional counters. A look at the abscissa shows that the resolution has been improved from ambiguously identifying the Z number only within  $\pm 6$  for the single counter to  $Z \pm 3$  for the instrument.

The experimental work has consisted of constructing proportional counters of proposed geometries and determining the performance of the counters using particles from isotope sources, cosmic ray mu-mesons, and protons from the NASA Langley Cyclotron. A balloon flight program to determine the proportional counter performance, and also to make measurements on the primary cosmic ray flux, is planned in the near future.

## Cosmic Ray Air Shower Studies

The only useful method of gaining knowledge about primary cosmic rays and nuclear interactions above  $10^{15}$  eV is by detecting and measuring parameters of large cosmic ray air showers. Typically, the primary cosmic ray particle interacts with a nitrogen or oxygen nucleus in the atmosphere at around 90 000 feet producing secondary particles that contribute to a cascade which eventually produces a "shower" of particles on the ground if the primary energy is above  $10^{14}$  eV.

The traditional method of studying cosmic ray air showers is by observing simultaneous signals from arrays of Geiger tubes or scintillation counters spread over large areas on the ground. This method has provided an approximate energy spectrum of the primaries between  $10^{14}$  and  $10^{20}$  eV [10], and has advanced some nebulous and sometimes conflicting clues concerning the nature of the primary particles, spatial distributions, and interaction cross sections. Ground level shower detector arrays have been increased in effective area to about 250 square miles in an attempt to measure the energy spectrum of the primary cosmic rays above  $10^{18}$  eV.

Recently, several new techniques for detecting the air showers have been proposed to extend the effective counting area and perhaps provide more precise information about shower cascades. These include observation of radio pulses, Cerenkov light, and scintillation light produced in the atmosphere

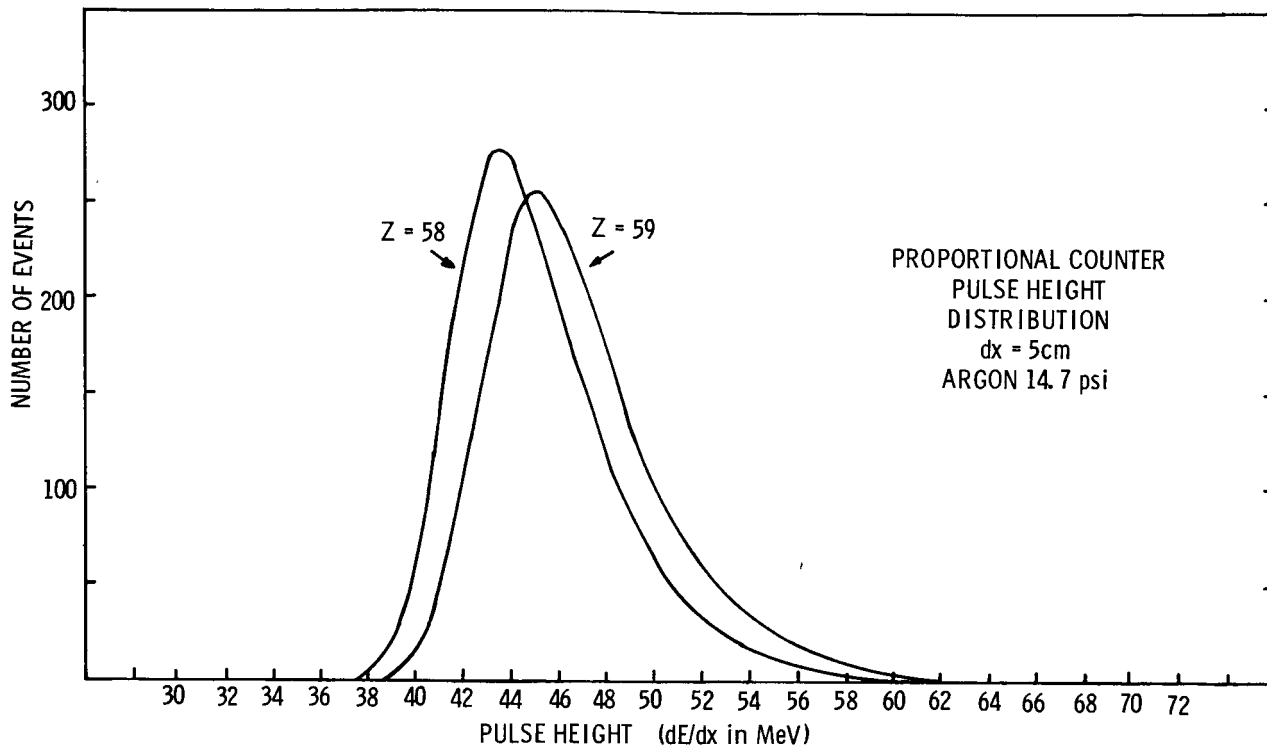


Figure 5. Theoretical pulse height distributions from an ideal proportional counter 5 cm thick for nuclei of  $Z = 58$  and  $Z = 59$  at 100 GeV total energy per particle.

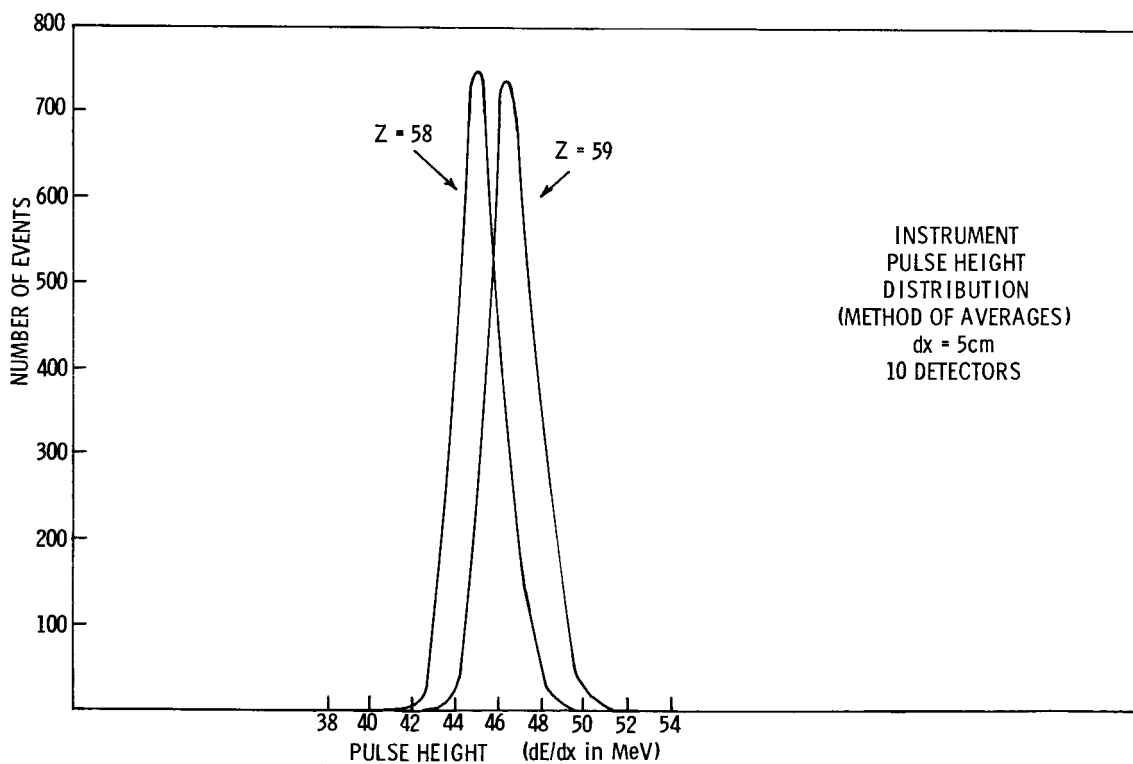


Figure 6. Results of Monte Carlo calculations considering that 10 000 identical particles of  $Z = 58$  and  $Z = 59$  penetrated a 10-layer proportional counter; the pulses from the 10 layers were averaged for each event.

by the large air showers. Cerenkov light has been detected from air showers, but since it is closely collimated with the shower axis, does not extend the effective counting area for a single detector. Radio pulses have also been detected [11], but according to several reporting groups, the radio pulse strength is not closely correlated with the size of the shower as measured by other techniques. A group at Cornell University is attempting to utilize the scintillation light from the atmosphere to detect air showers as far away as 20 miles from the ground-based detector.

At MSFC a small experiment has been initiated to measure the characteristics of the occasional radio pulses associated with some of the large air showers. The goal of the work is to explain the production mechanism of the radio pulses and to determine if the radio signal will provide a useful independent method of determining some of the large air shower characteristics.

Figure 7 shows a schematic of the present experimental arrangement. The system consists of four scintillation detectors, each  $0.4 \text{ m}^2$ , on a 120-m radius circle. The random pulses produced in the detectors by cosmic rays are transmitted via coaxial cables to a central four-fold coincidence circuit. A coincidence signal indicates the arrival of a shower caused by a primary cosmic ray of  $E > 10^{15} \text{ eV}$ . When this occurs (about seven times per hour), an oscilloscope trace is triggered. Displayed on the oscilloscope trace is the output of a radio receiver. The bandwidth of the receiver plus antenna is approximately 5 Mc at a 50-Mc center frequency.

Bandwidth limited (fast rise) radio pulses are observed to occur within 40 nsec of approximately 1 percent of the air showers detected by the scintillation array. These radio pulses are distinguished by the coincidence timing and by pulse shape from spurious noise.

Present efforts involve expanding the scintillator array to approximately 10 detectors for better statistics, and improving the radio receiver system

## COSMIC RAY AIR SHOWER EXPERIMENT

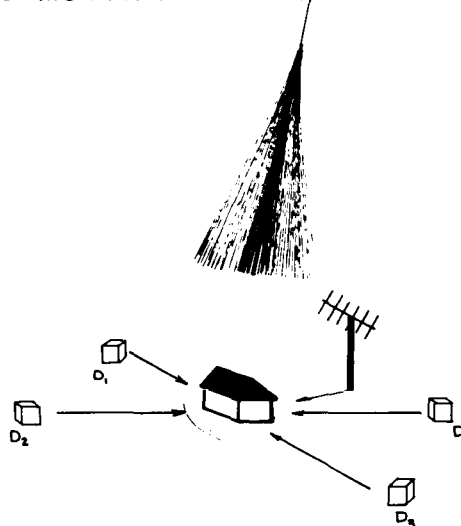


Figure 7. The cosmic ray air shower experimental arrangement. ( $D_1$  through  $D_4$  are plastic scintillators 100 m from the central station and are run in coincidence with the radio receiver to determine if a cosmic ray air shower produces a radio noise burst.)

to allow polarization measurements and multi-frequency measurements.

## CONCLUSIONS

Some of the areas of research that are of interest to the cosmic ray group of the Radiation Physics Branch of Space Sciences Laboratory have been discussed, and three specific research projects that are currently in progress have been presented. Also an attempt has been made to show how a comprehensive basic research program in a particular field (galactic cosmic radiation and trapped belt particles) can be of direct benefit to other projects at Marshall Space Flight Center. This is illustrated by our development of the proton spectrometer for the AAP Program.

## REFERENCES

1. Hess, W.: The Radiation Belt and Magnetosphere. Blaisdell, Waltham, Massachusetts, 1968.
2. Weber, W. R.; and Ormes, J. F.: Cerenkov-Scintillation Counter Measurements of Nuclei Heavier than Helium in the Primary Cosmic Radiation. *J. of Geophys. Res.*, vol. 72, no. 23, 1967.
3. Freden, S. C. and Paulicas, — — : Trapped Protons at Low Altitudes in the South Atlantic Anomaly. *J. Geophys. Res.*, vol 69, 1964, pp. 1259-1270.
4. Burrell, M. O. et al.: An Analysis of Energetic Space Radiation Dose Rates. NASA Technical Note D-4464, 1968.
5. Vette, J. I.: Models of the Trapped Radiation Environment. NASA SP-3024, vols. 1, 2, and 3 1966 and 1967.
6. Heckman, H. H.; and Nakano, G.: Low Altitude Trapped Protons During Solar Minimum Period 1962-1966. *J. Geophys. Res.*, vol. 74, no. 14, 1969.
7. Paper presented at the IEEE Symposium on Space Instrumentation, San Francisco, California, 1969.
8. Weber, W. R.: The Spectrum and Charge Composition of the Primary Cosmic Radiation. *Handbuch der Physik*, vol. 46, 1967, p. 173.
9. Amato, G.; Bondeir, R.; Charpak, G.; Rohn, D.; and Steiner, H.: Some Research on Time, Space and Energy Resolution With Multi-Wire Proportional Chambers. Paper presented at the Conference on Spark Chambers, Dubna U.S.S.R., April 1969.
10. Greisen, K.: Highlights in Air Shower Studies, 1965. *Proceedings of the International Conference on Cosmic Rays*, 1965, p. 609.
11. Jelley, J. V. et al.: Radio Pulses from Extensive Air Showers. *Il Nuovo Cimento*, vol. 46A, no. 4, 1966.



# PROTON SENSITIVITY OF FILMS USED IN APOLLO TELESCOPE MOUNT SATELLITE MISSIONS

By

Richard A. Potter

## SUMMARY

The mission of the Apollo Telescope Mount (ATM) satellite requires large amounts of photographic film that will be subjected to proton irradiation in the South Atlantic Anomaly of the Van Allen radiation belts. The films to be flown were exposed to 130, 90, and 50-MeV protons at the Harvard University Cyclotron and to 17.6 and 10-MeV protons at the Oak Ridge National Laboratory Cyclotron. The work was performed by groups from Kodak, Langley Research Center, Marshall Space Flight Center, and personnel of the cyclotron facilities. The tests yielded curves of dose versus density for film types proposed for ATM missions. The environment to which the spacecraft is to be subjected is fairly well known (within a factor of two), but the complex vehicle structure leads to an involved shielding problem. A computer study of this complex shielding problem is presently under way.

## INTRODUCTION

The ATM satellites use large amounts of photographic film in the acquisition and recording of data. The effect that trapped radiation would have on the candidate film types was first addressed in October 1966. A brief but comprehensive literature survey relating to the radiation tolerance of these films revealed that there was an insufficient amount of radiation effects data available. Three programs were initiated to solve this problem: (1) acquisition of the most accurate information possible concerning radiation environment, (2) the design of a proton-measuring device and acquisition of flight approval, and (3) acquisition of proton-sensitivity data for the candidate film types.

This discussion concerns a program to determine the proton sensitivity of the films, but it may be well to consider the environment to which the film is to be subjected. The ATM mission was designed for a

circular orbit with an altitude of between 330 and 407 km (180 and 220 n. mi.) and an inclination of between 30 and 35 degrees. Figure 1 is a plot of dose rate versus shield thickness for such an orbit. The graph clearly indicates that the film contained in a light-tight container will receive most of the radiation dose from protons. The orbit of the ATM is such that the bulk of this proton dose is obtained during the satellite's passage through the lower fringes of the Van Allen radiation belt. The radiation belts are not centered and symmetrical about

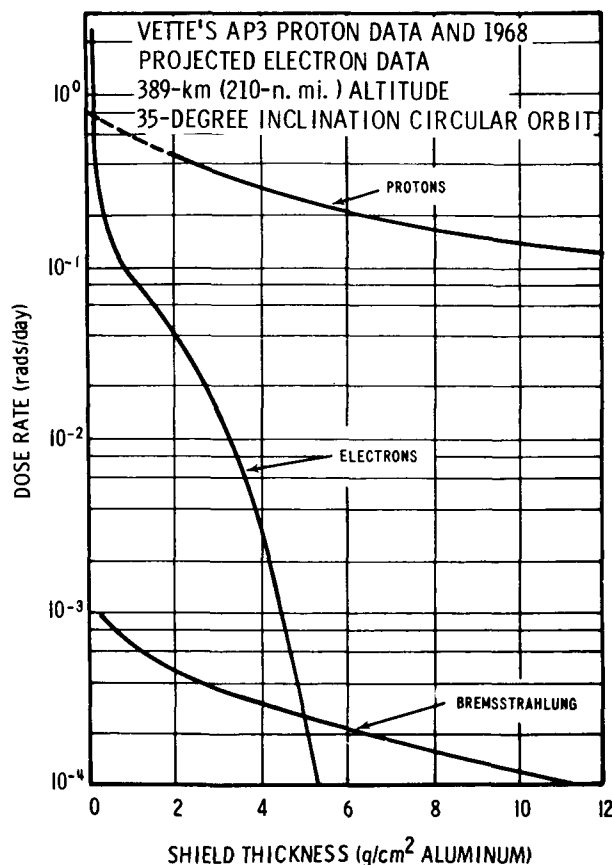


Figure 1. Plot of dose rate versus shield thickness.

the earth but are displaced and thereby dip into the atmosphere over the South Atlantic Ocean. This region is referred to as the South Atlantic Anomaly. Figure 2 is a map of the anomaly region with equi-flux lines. A satellite inclined at 30 degrees penetrates deeply into this high-flux region. Figure 3 indicates the effect of the anomaly region on a spacecraft with a 30-degree inclination. This plot of flux versus time shows the movement of the earth-fixed anomaly under the space-fixed satellite orbit causing the point of maximum inclination to pass in the region of the anomaly approximately every 30 hours. The plot indicates that the majority of the dose is received during these passes and that the background is insignificant.

The film proton response, or sensitivity problem, required answers as rapidly as possible to give the ATM planners and experimenters time to decide if changes in altitude, inclination, altitude control, or other mission-related parameters were required. To accelerate the program, the assistance of personnel at Langley Research Center and Eastman Kodak Company who had the experience and equipment from similar tests they had conducted was enlisted.

## FILM TEST PROCEDURES

Table 1 is a list of film types and their complete trade names. The list includes all candidate film types that were under consideration by the principal investigators. The film types range from a relatively fast, large-grained film, such as 103-0 UV, to the slow, fine-grained SO-375 film. The film was obtained in 35-mm strips and exposed, several strips to a stack. The stacks were placed in an aluminum, light-tight container with a thin aluminum window. The container was placed perpendicular to the proton beam, an exposure was made, and the container was moved perpendicular to the beam, etc. until several exposures of varying intensity were made.

Exposures to 130, 90, and 50-MeV protons were performed at the Harvard University Cyclotron Laboratory in May of 1967. The proton beam, which would normally be in the form of highly peaked Gaussian distribution, was spread to give a relatively flat distribution. A collimator with a hole of approximately 1.59 cm (0.625 in.) diameter was placed in the beam and a circular proton beam of uniform flux

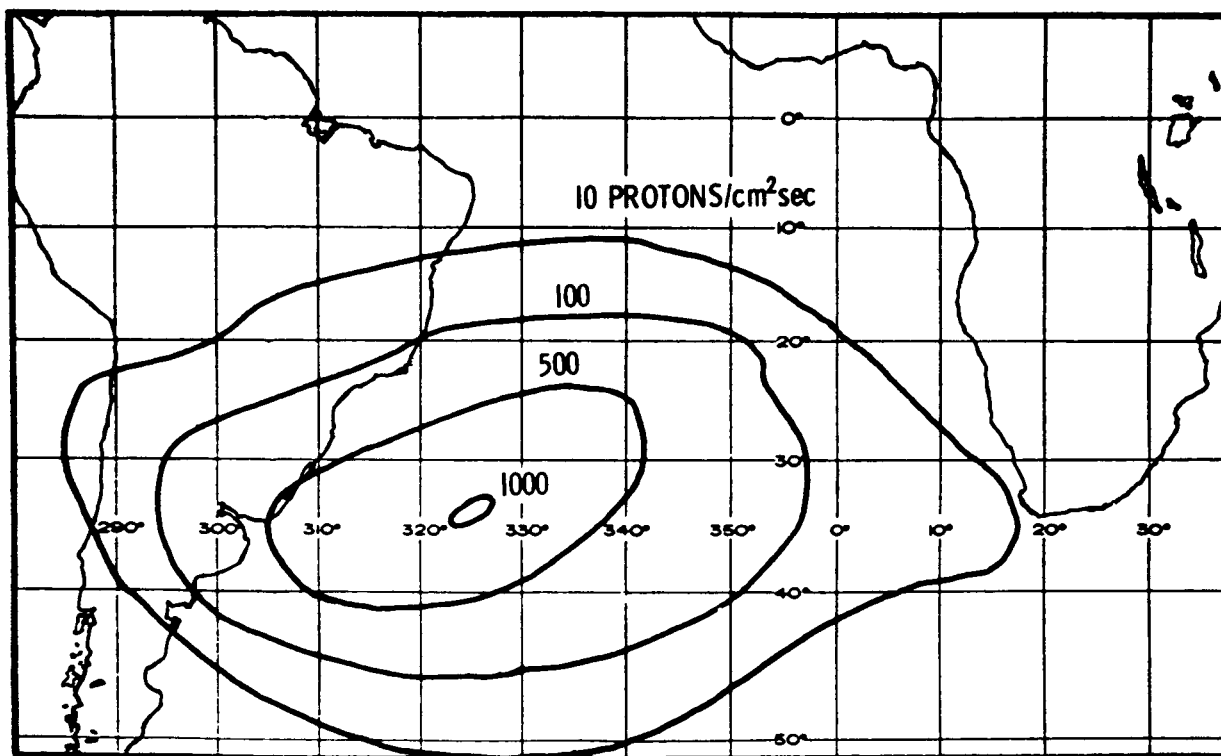


Figure 2. Map indicating the South Atlantic Anomaly (Vette's proton data AP1).

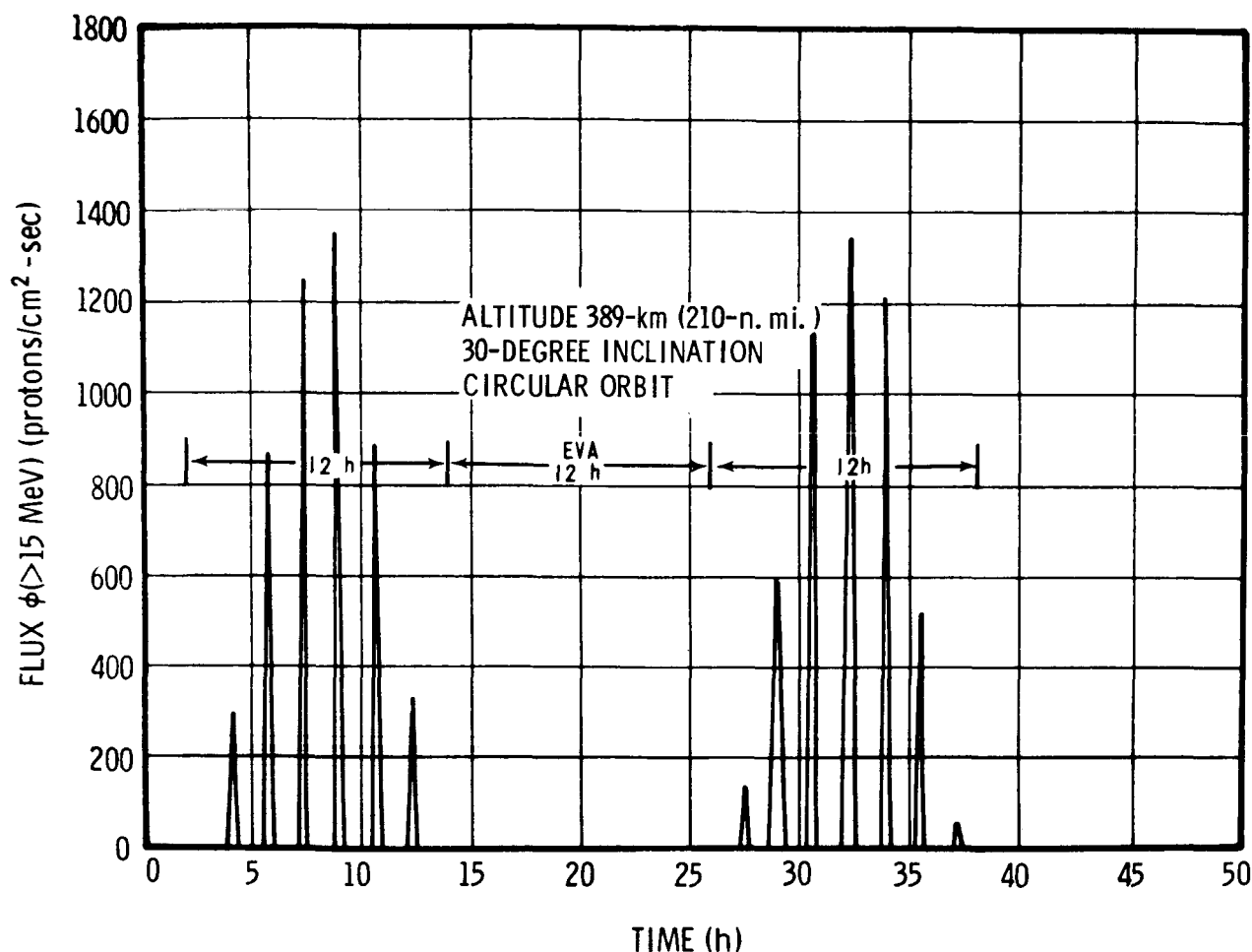


Figure 3. Flux versus time plot (spikes indicate passage through the South Atlantic Anomaly).

was thus obtained. The proton exposures were monitored by an ionization chamber placed in the proton beam upstream from the film. Before exposing the film, the ionization chamber was calibrated against a radiation-sensitive diode placed in the beam at the film exposure plane. The diode had previously been calibrated using a Faraday cup.

Exposures to 17.6 and 10-MeV protons were performed at Oak Ridge National Laboratory in June of 1967. The procedure was essentially the same as that used at the Harvard University Cyclotron Laboratory. The diameter of the proton beam was approximately 2.54 cm (1 in.). Again the beam was monitored by an ionization chamber located upstream from the film which was calibrated against a Faraday cup. During this period, strips of film were exposed to Cobalt-60 gamma rays in an effort to obtain a correlation between the effects of high-energy gamma rays as compared to protons of various energies.

The exposed films were divided into three groups, one being processed by Eastman Kodak, one by Al Brake of Sperry Rand who was associated with the Astrionics Laboratory of MSFC, and one by the MSFC photographic laboratory. This provided four important objectives: (1) extremely quick "ball park" data, (2) correlation between data, (3) the most accurate data, and (4) the possibility of film modifications to produce a less radiation-sensitive film.

## TEST RESULTS

The strips had at least six exposures for each of the five energy levels. The exposures were measured in rads, which is a unit of dose corresponding to the deposition of 100 ergs/g in the irradiated material. To specify the dose in silver halide (the photosensitive portion of the film) would require

TABLE 1. CANDIDATE FILM TYPES (Exposure Time and Temperature)

Film	Kodak Developer	Time (min.)	Temperature (° F)
Kodak High-Speed Panchromatic Film (Ester Gray Base), Type SO-166	D-19	12	75
Kodak No-Screen Medical X-Ray Film (One Emulsion Removed After Processing)	Rapid X-Ray	5	68
Kodak Spectroscopic Film Type 103-0	D-19	4	68
Kodak Spectroscopic Film Type 103-0, UV	D-19	4	68
Kodak Plus-X Aerial Film (Ester Thin Base), Type 3401	D-19	8	68
Kodak Panatomic-X Aerial Film (Ester Thin Base), Type 3400	D-19	8	68
Kodak Special Aerial Negative Film (Ester Thin Base), Type SO-206	D-19	8	68
Kodak Special Film Type 101-01	D-19(1:1) also DK-20	2 8	68
Kodak SC-7 Film	D-19B also DK-20	6 8	68
Kodak SC-5 Film	D-19B	2	68
Kodak SWR Film	D-19(1:1)	2	68
Kodak Special Solar Recording Film Type SO-375	D-19	8	68
Kodak Special High-Definition Aerial Film (Ester Gray Base), Type SO-243	D-19	8	68

the calculation of an effective atomic number for each film type investigated. It was decided to specify the dose as that which would be received by some standard material (in this case, air) had it been occupying the position of the film. With the known exposures, densities were measured and characteristic curves were drawn. Figure 4 is a typical characteristic curve that indicates the effect of the exposures. The shape of the response curves for the more sensitive films was found to be independent of the proton energy and is the same as for Cobalt-60 gamma rays and 80-kV X-rays. For equal

exposures in  $\text{rads}_{\text{air}}$ , it can be seen that the films are slightly more sensitive to Cobalt-60 gamma rays than 130-MeV protons. The sensitivity decreases as the proton energy decreases. For a constant fluence, that is, protons per unit area, the sensitivity increases as the proton energy decreases; that is, the effect per proton is greatest for the least energetic proton. For the least sensitive film types, the slope of the response curves for protons differs from those for gamma and X-rays; the slope increases with increasing energy.

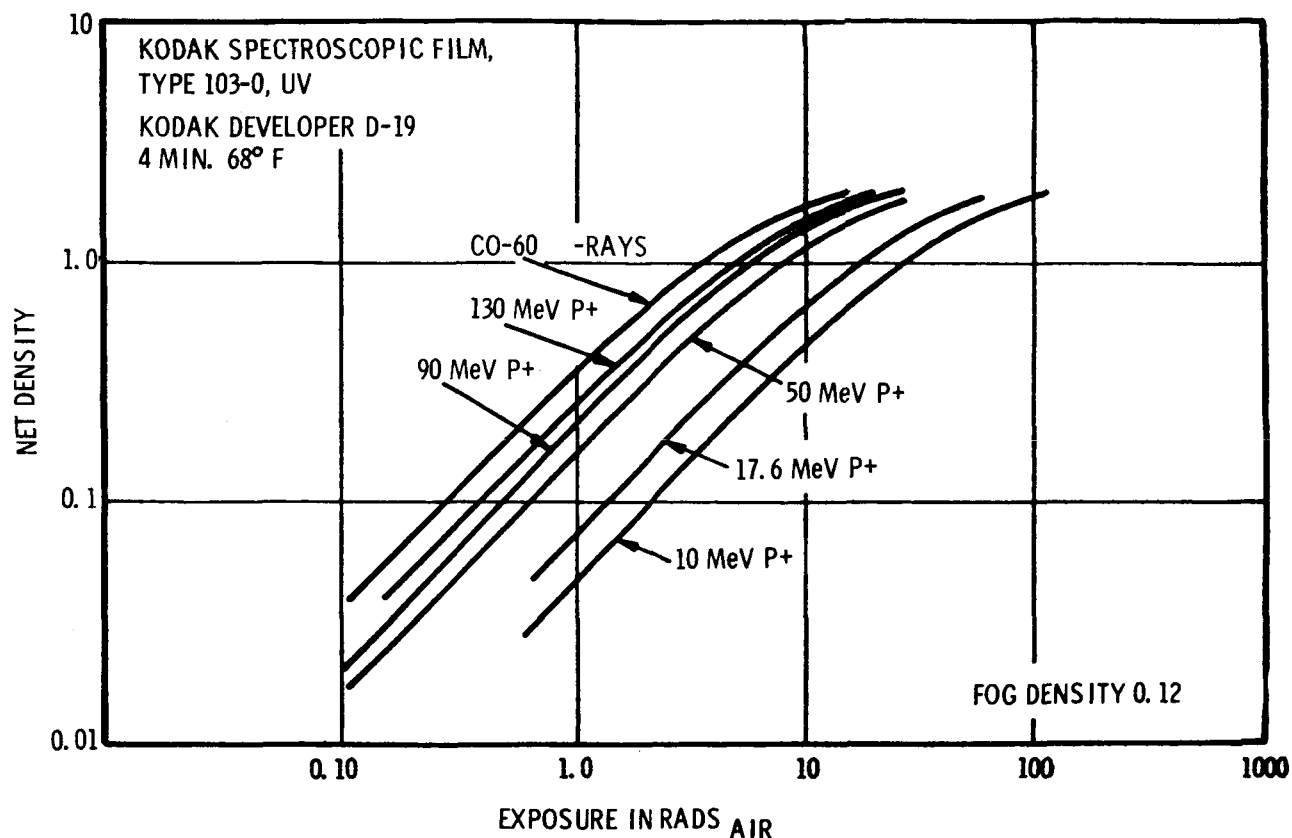


Figure 4. Curve of density versus exposure for Kodak spectroscopic film, type 103-0.

The characteristic curves of dose versus density were folded together with the radiation environment data to produce graphs of density versus time in orbit for various spherical shell-shield thicknesses. The data in Figures 5 through 7 are plotted for Kodak films 103-0, Panatomic-X, and SO-375. The three curves are representative of the types proposed for the ATM flight. Kodak 103-0 is the fastest, Panatomic-X is on the borderline, and SO-375 is the slowest tested. Figure 8 indicates the relative film speeds. The dose axis is directly related to time

in orbit. From curves of this type, it is expected that the investigator, using the film for a flight measurement, can decide the magnitude of the radiation problem.

The present work in this area is to analyze the dose that the film will receive in storage and deployed positions. This study involves the analysis of a complex shielding configuration of the space vehicle's structure and related flight equipment.

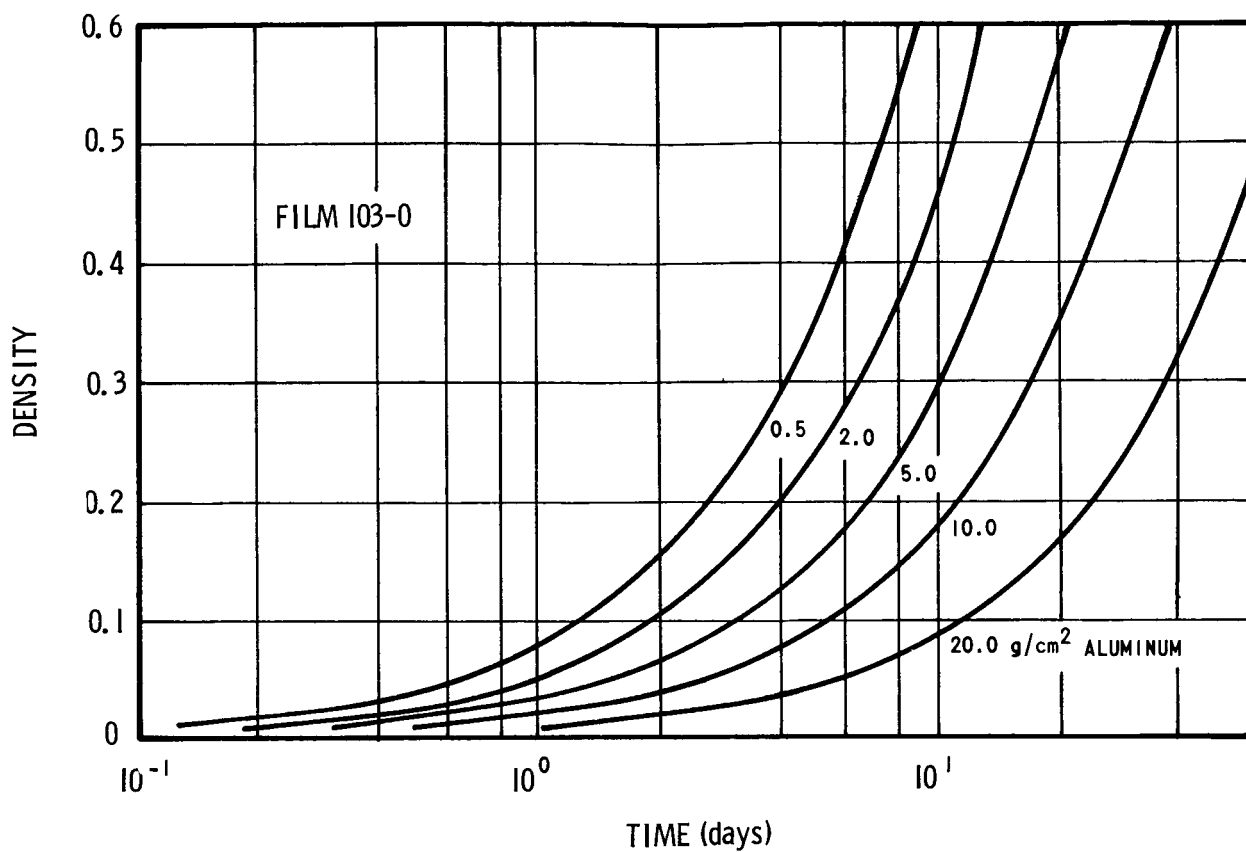


Figure 5. Curve of density versus time in orbit for Kodak 103-0 film  
[radiation calculations are based on a 389-km (210-n.mi.), 35-degree inclination orbit].

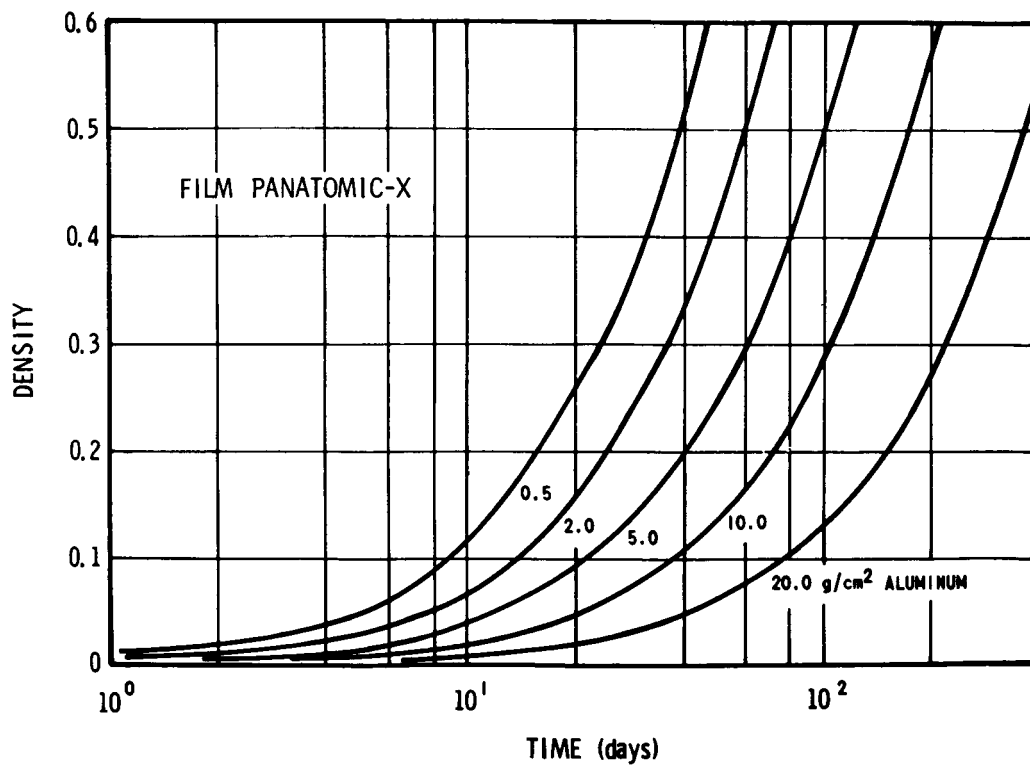


Figure 6. Density versus time in orbit for Panatomic-X film.

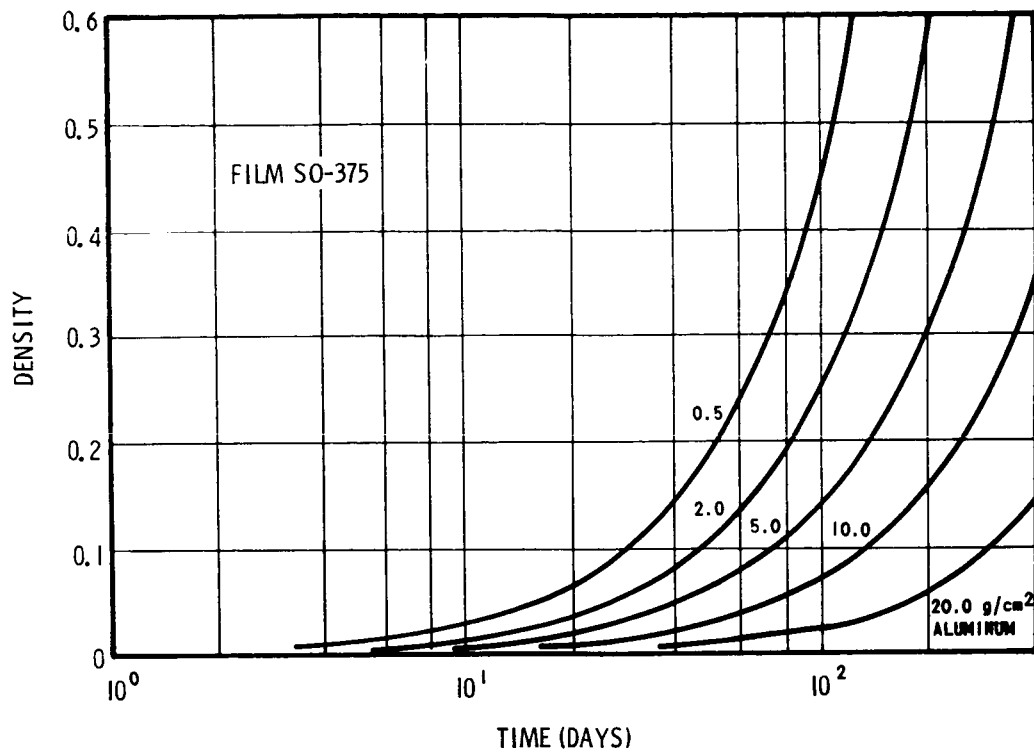


Figure 7. Density versus time in orbit for Kodak SO-375 film.

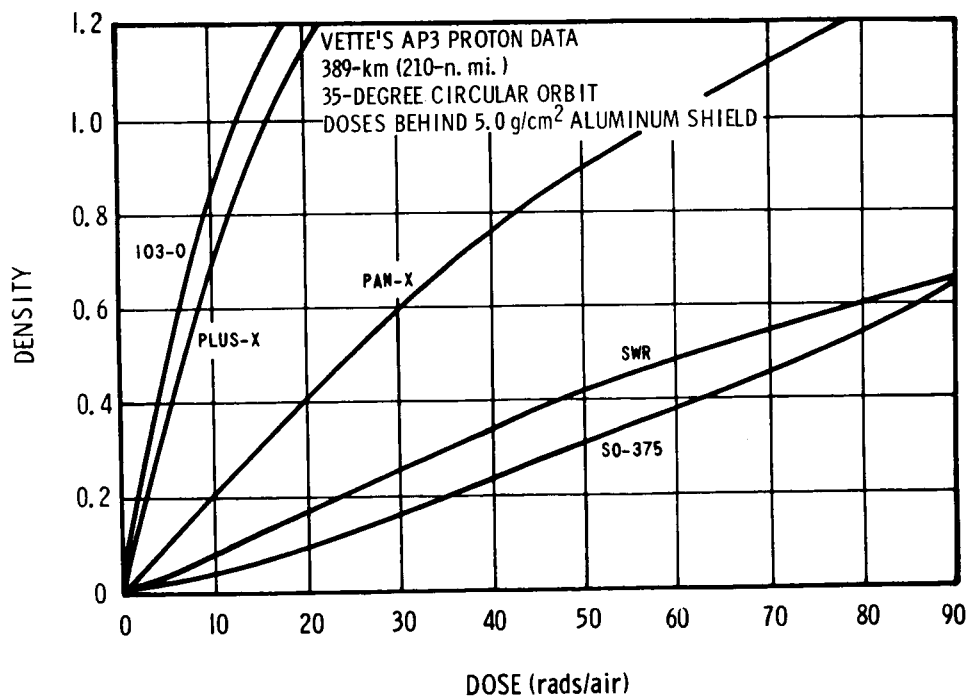


Figure 8. Density versus dose, indicating the relative speeds of the candidate film types tested.

# APPLICATIONS OF RADIATION PHYSICS RESEARCH

By

Martin O. Burrell

## SUMMARY

The applications of high-energy proton transport are discussed in this paper. As shown, this work may be utilized in many unrelated areas. The applications of the theoretical transport methods to real engineering problems are presented with emphasis on the necessity of treating such problems realistically.

## INTRODUCTION

Examples of the radiation physics research being conducted at MSFC and some of the applications will be discussed in this report. The first area concerns scientific investigation, and the second area concerns engineering requirements.

## OAK RIDGE NATIONAL LABORATORY STUDY

Approximately 7 years ago, Oak Ridge National Laboratory was awarded a study contract that was managed by the Office of Advanced Research and Technology. This study was basically the analysis and experimental verification of high-energy proton transport and attendant secondary particle production and transport. This work has led to some very sophisticated computer codes for which various applications have been found. Approximately 2 years ago, NASA transferred the theoretical portion of this contract to the Space Sciences Laboratory of Marshall Space Flight Center.

The amount of work and special studies carried out under this contract has been immense and elaborately detailed. However, only a few examples of the applications will be given here.

The first example is the estimation of the prompt photon spectrum that arises from the cosmic-ray bombardment of the moon [1]. Figure 1 depicts the neutron spectrum in a model lunar material. This spectrum is the source of the

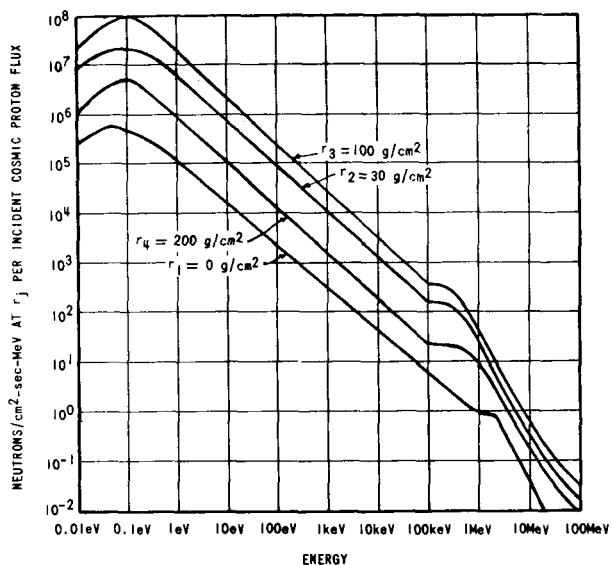


Figure 1. Estimated neutron spectra in moon because of cosmic-ray bombardment.

capture gammas shown in Figure 2. Note the large capture-gamma peaks in iron at 7.5 MeV and 6.0 MeV. One of the interesting capture-gamma lines to look for is the 2.3-MeV photons from neutron capture by hydrogen. This could be an indication of water present on the moon.

Calculations of the transport of solar neutrons in the earth's atmosphere have also been made [2].



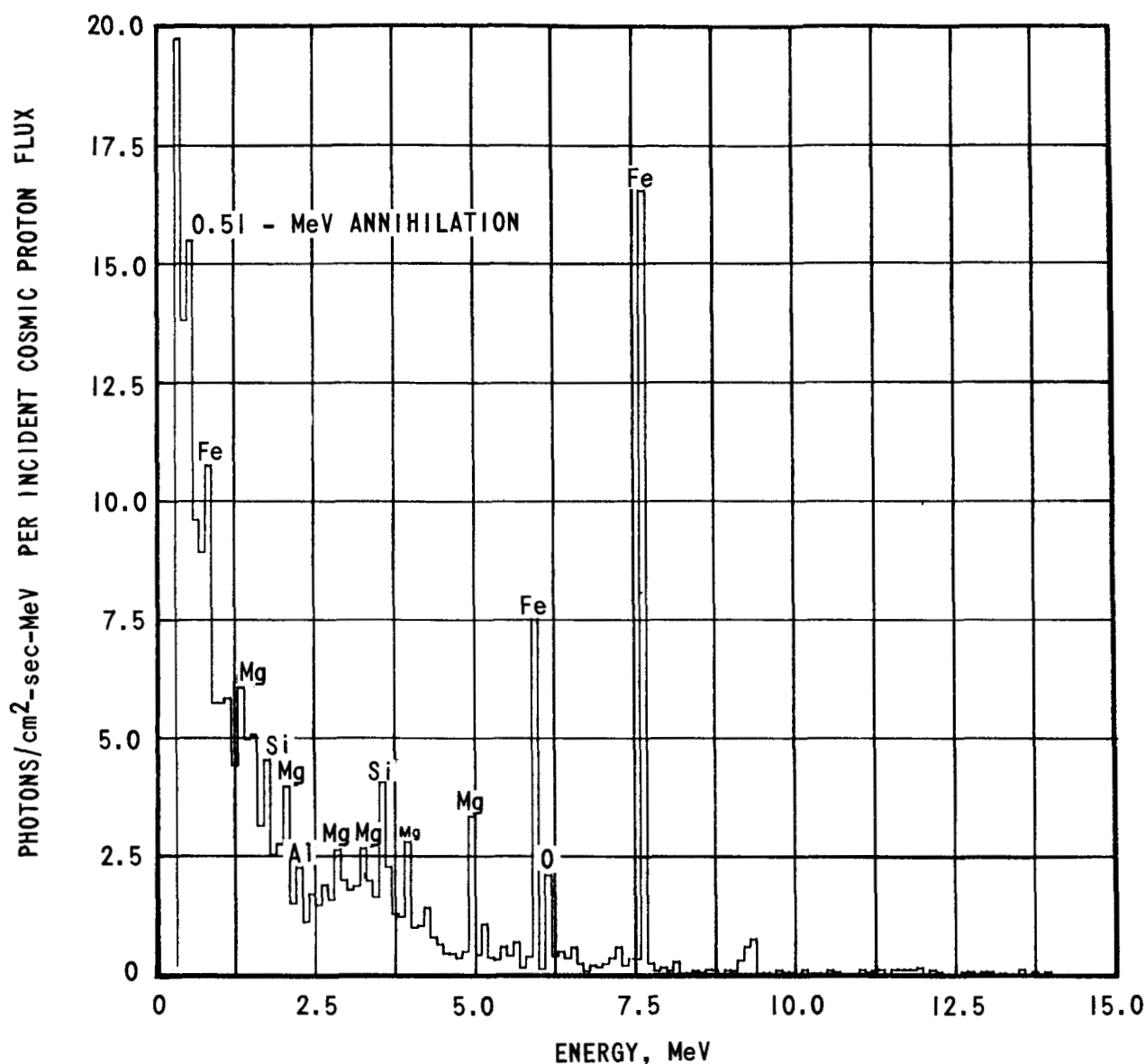


Figure 2. Photon leakage spectrum from lunar surface.

The 50 gm/cm<sup>2</sup> depth on Figure 3 represents an altitude of 70 000 feet. The source of the neutrons is from a large solar proton event, and the neutrons arrive at the earth only during the first hour of onset. The neutron spectrum at the sun is based on a theoretical calculation. Note that the cosmic ray neutron spectrum is below the solar neutron spectrum. Figure 4 is similar but at a height of 30 000 feet.

A study has been made of radiation hazards resulting from exposure of supersonic aircraft to solar protons [3]. This work is still being pursued

for Langley Research Center. Figure 5 depicts a typical set of curves from this study. The dose units are given per unit flux; to ascertain the order of magnitude for a large flare, multiply the curves by 10<sup>9</sup>. The doses shown are in depths of tissue for the various components of the radiation after passing through the indicated thickness of air and 1 gm/cm<sup>2</sup> of iron to simulate the aircraft.

The last application of this work that will be discussed is the calculation of the capture of negative pions and comparison with experiments

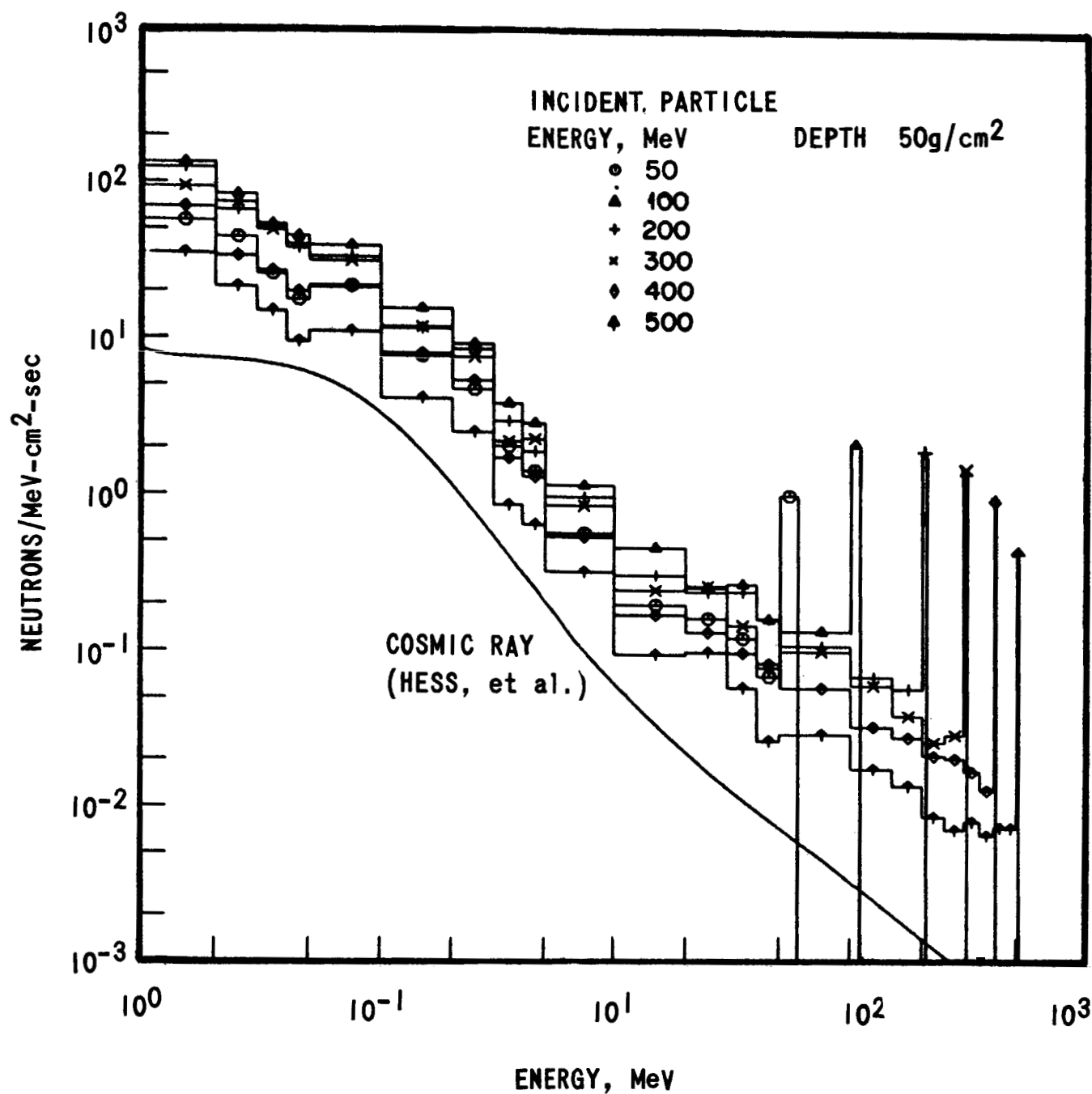


Figure 3. Neutron flux per unit energy versus energy at an atmospheric depth of 50 gm/cm<sup>2</sup>.

pertaining to cancer radiotherapy [4]. The capture of pions in human tissue leads to the release of a large amount of energy from secondary particles. This energy can be used to kill malignant tissue. Figure 6 shows very good comparisons between experimentation and the calculation of alpha particles released from pion capture in oxygen.

### COMPLEX GEOMETRY RESEARCH

Work dealing with the modification of the energetic space radiation as it penetrates the walls and components of a complex space vehicle was initiated

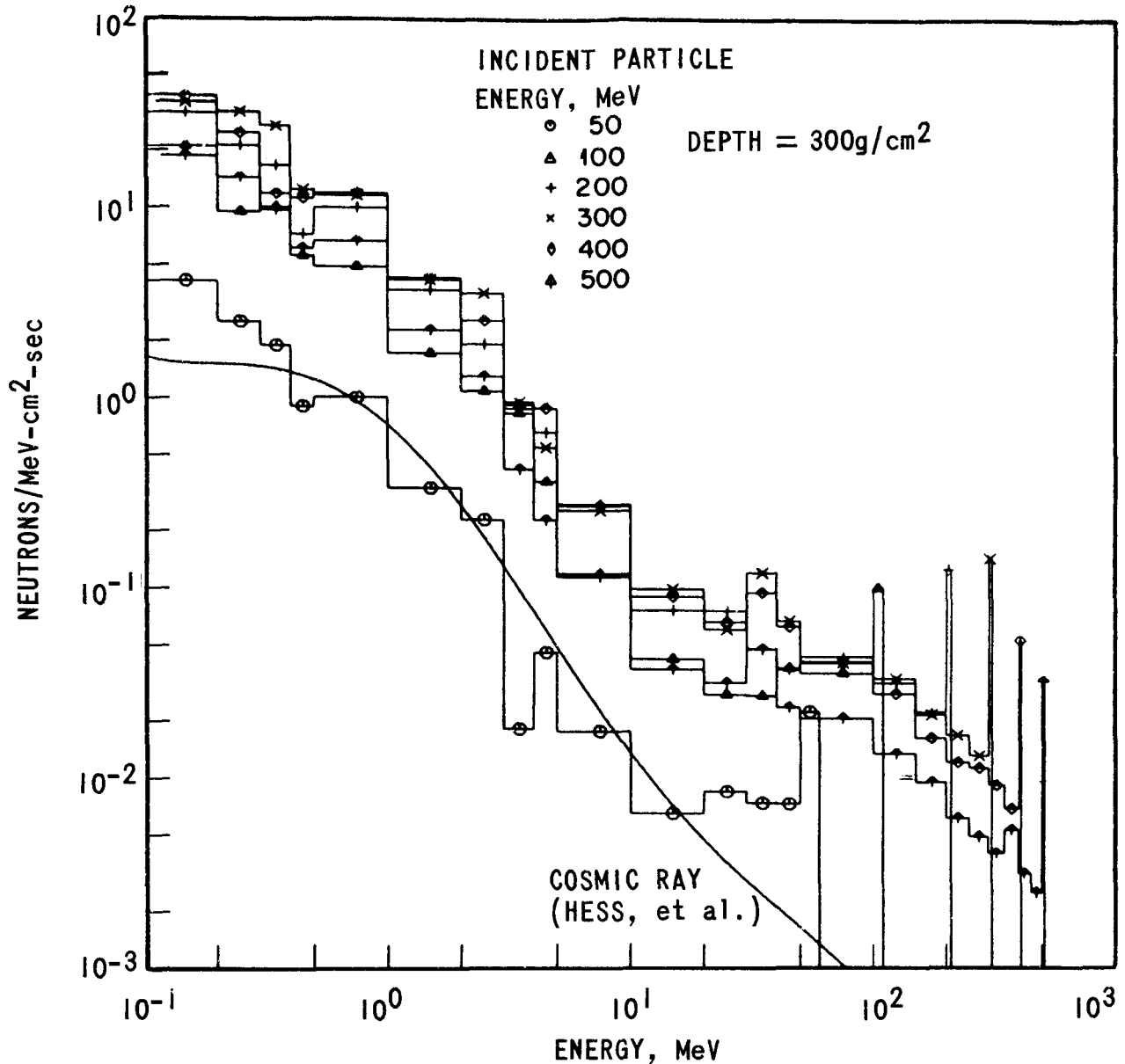


Figure 4. Neutron flux per unit energy versus energy at an atmospheric depth of 300 gm/cm<sup>2</sup>.

approximately 4 years ago in anticipation of Apollo applications. Similar work had been undertaken by the Manned Space Center in their analysis of the Command Module and the Lunar Module for the lunar mission. The Lockheed Georgia Company has played a prime role in the representation of various vehicles in mathematical models [5]. At present, NASA has a good mathematical model of the Apollo Telescope Mount, Command Module, and the Lunar Module. However, we intend to incorporate the Houston versions of the Lunar Module and Command Module into the present codes and complete the

workshop details as they become available. This work has been delayed because of a lack of funds available from the Apollo Applications Office.

To illustrate the importance of the work, it is necessary to point out that most of the basic research work in radiation transport is valid only for very simple geometrics such as simple slabs of material or spherical shells. The radiation dose rates are calculated at a point detector, usually at the center of a spherical shell or at the surface of a slab. Most parametric curves that we see in technical studies

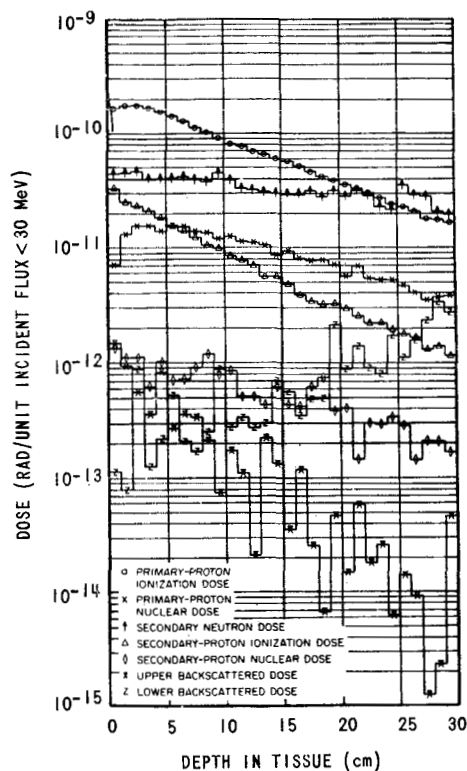


Figure 5. Rad dose versus depth in tissue for atmospheric depth of  $36 \text{ gm/cm}^2$  ( $\approx 75,000 \text{ ft}$ ).

are performed for this type of geometry. Great care must be exercised in the use of these curves for engineering design work because of the additional shielding provided by a complex geometry and the internal equipment plus the fact that the man or component that is exposed to the radiation provides additional self-shielding. The errors resulting from the above geometric relationships can lead to overestimation of the dose by a factor of 3 to 6. This may result in unnecessary weight penalties and/or limitations of a mission. The variations of dose inside a simple geometry are exemplified in Figure 7. Note that the bottom curve shows a dose variation of 4.5 between the ground level and the top of the cap.

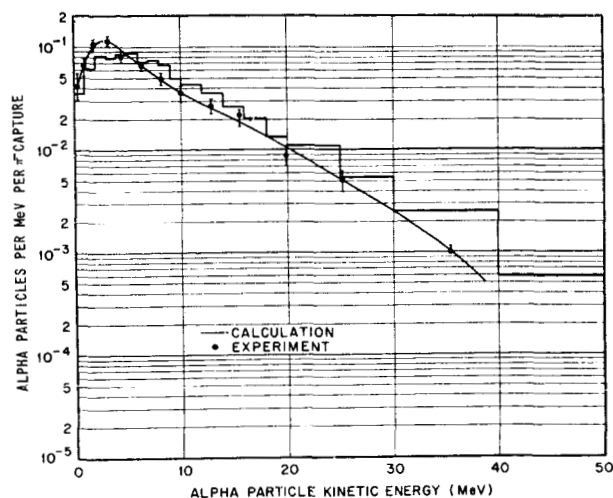


Figure 6. Alpha-particle emission spectra from  $\pi$ -capture in oxygen.

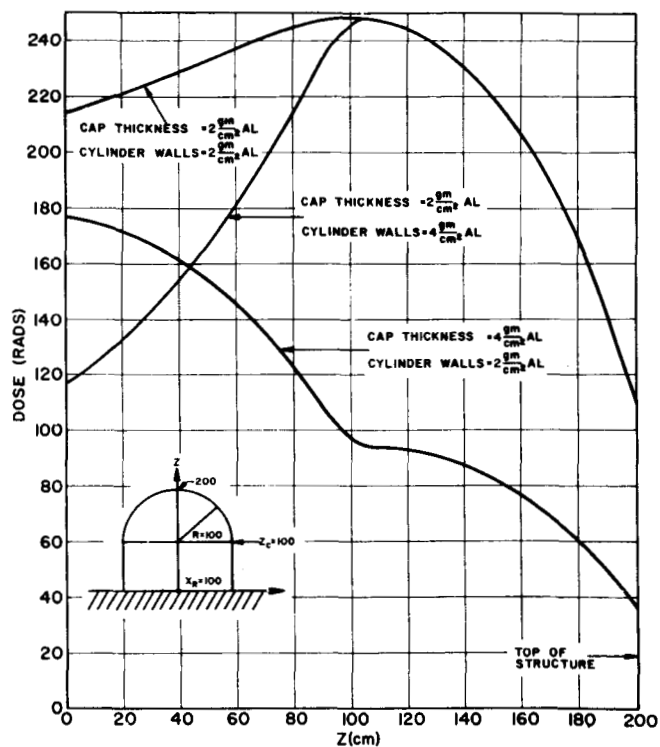


Figure 7. Centerline dose versus distance from base of cylinder with spherical cap.

The procedure used in a typical radiation analysis problem is shown in Figure 8. The difficulties involved in a realistic engineering problem are shown in Figure 9. The problem was to determine the

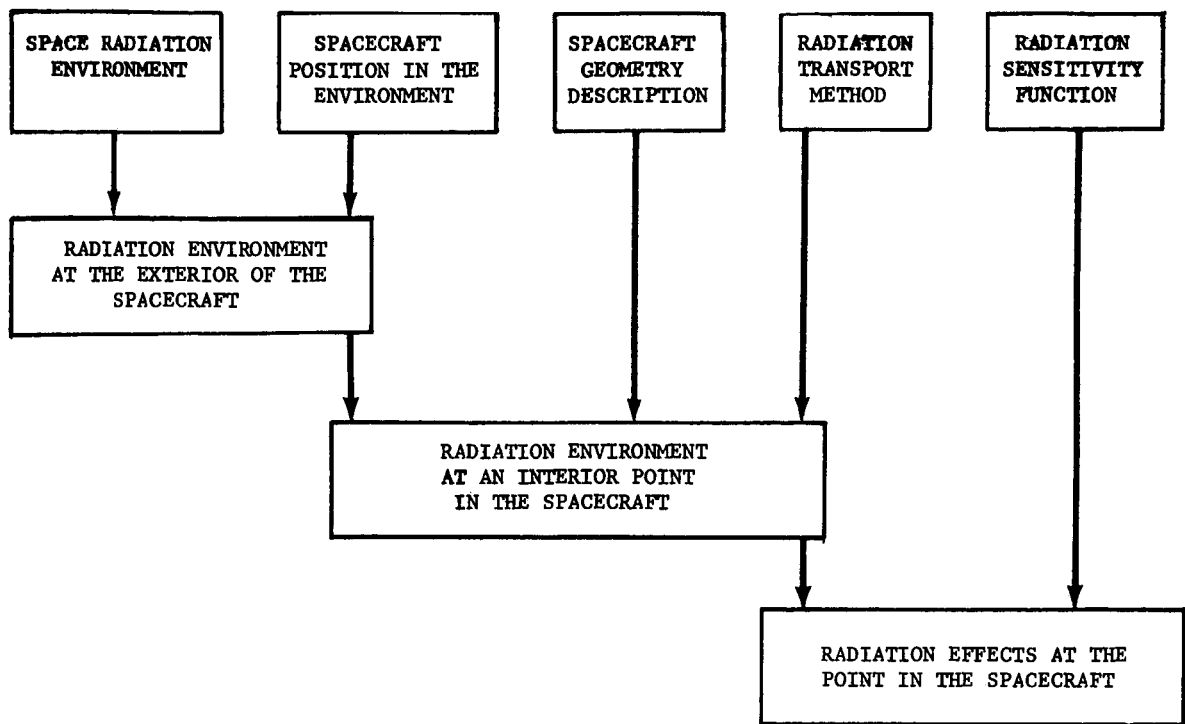


Figure 8. Flow chart of radiation analysis.

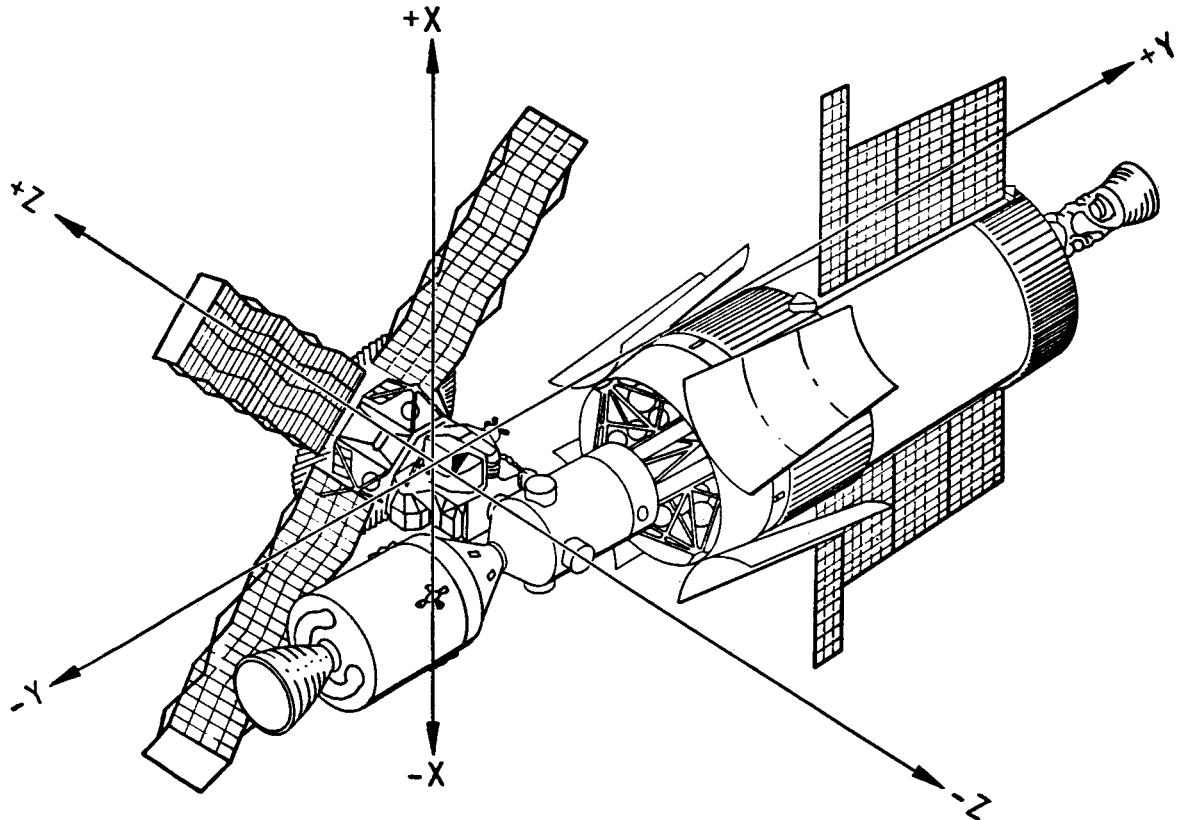


Figure 9. Conceptual drawing of Apollo systems.

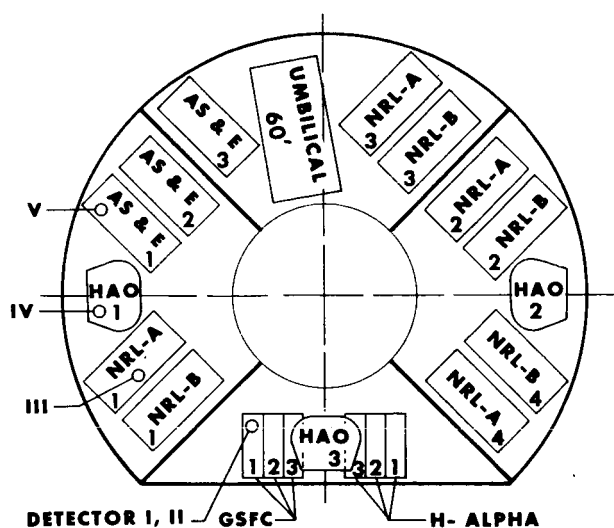


Figure 10. CPSM baseline stowage.

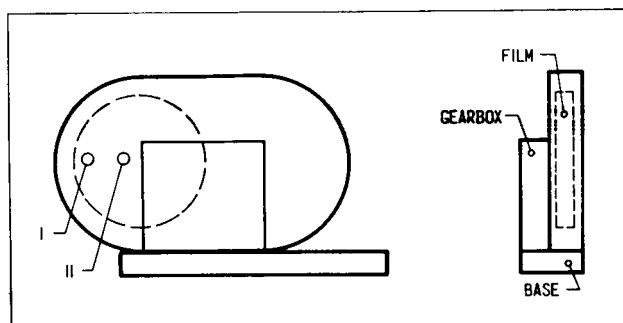


Figure 11. Goddard H-alpha camera and two detector points used in calculations.

radiation incident on film stored inside camera boxes in the Crew Provisions Service Module (CPSM), which was to be used later in the Apollo Telescope Mount (ATM) experiments. In Figure 9, the CPSM is located about 1.27 cm from the origin along the

-Z axis (between the Lunar Module and the Multiple Docking Adapter). Figure 10 shows the clustering of the various experimental packages in the CPSM. Figure 11 depicts the Goddard H-alpha camera and two detector points used in the calculations. Table 1 shows the results at locations I and II inside the camera. Note the differences between dose rates at the edge of the film and the inside point. The cumulative doses at the 14-day intervals also vary because of certain camera packages being moved to the Apollo Telescope Mount. It is believed that the foregoing problem depicts a typical situation in the analysis of radiation damage onboard a spacecraft. The problem will require an extensive amount of information and engineering preparation to arrive at meaningful answers.

TABLE 1. GSFC X-RAY TELESCOPE  
EXPERIMENT NUMBER S-056  
PANATOMIC -X FILM

## LOCATION 1

TIME (DAYS)	CUMULATIVE DOSE (RADS AIR)
14	1.05
28	2.22
42	3.81

LOCATION II

TIME (DAYS)	CUMULATIVE DOSE (RADS AIR)
14	0.82
28	1.73
42	2.99

## REFERENCES

1. Armstrong, T. W.; and Alsmiller, R. G., Jr.: An Estimate of the Prompt Photons Arising from Cosmic Ray Bombardment of the Moon. ORNL-4134, 1967.
2. Alsmiller, R. G., Jr.; and Boughner, R. T.: Solar Neutron Transport in the Earth's Atmosphere. ORNL-TM-2194, 1967.
3. Leimdorfer, M.; Alsmiller, R. G., Jr.; and Boughner, R. T.: Calculations of the Radiation Hazard Due to Exposure of Supersonic Aircraft to Solar-Flare Protons. Nuclear Science and Engineering, vol. 27, no. 2, 1967.

## REFERENCES (Concluded)

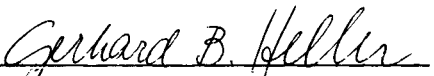
4. Guthrie, M. P.; Alsmiller, R. G., Jr.; and Bertini, H. W.: Calculations of the Capture of Negative Pions in Light Elements and Comparison with Experiments Pertaining to Cancer Radiotherapy. ORLN-TM-2371, 1968.
5. Hill, C. W.; et al: Data Compilation and Evaluation of Space Shielding Problems. Lockheed Report ER7777, vol. IV, NASA-11164, 1967.

## APPROVAL

RESEARCH ACHIEVEMENTS REVIEW  
VOLUME III REPORT NO. 7

The information in these reports has been reviewed for security classification. Review of any information concerning Department of Defense or Atomic Energy Commission programs has been made by the MSFC Security Classification Officer. These reports, in their entirety, have been determined to be unclassified.

These reports have also been reviewed and approved for technical accuracy.

  
GERHARD B. HELLER  
Director, Space Sciences Laboratory



## UNITS OF MEASURE

In a prepared statement presented on August 5, 1965, to the U. S. House of Representatives Science and Astronautics Committee (chaired by George P. Miller of California), the position of the National Aeronautics and Space Administration on Units of Measure was stated by Dr. Alfred J. Eggers, Deputy Associate Administrator, Office of Advanced Research and Technology:

"In January of this year NASA directed that the international system of units should be considered the preferred system of units, and should be employed by the research centers as the primary system in all reports and publications of a technical nature, except where such use would reduce the usefulness of the report to the primary recipients. During the conversion period the use of customary units in parentheses following the SI units is permissible, but the parenthetical usage of conventional units will be discontinued as soon as it is judged that the normal users of the reports would not be particularly inconvenienced by the exclusive use of SI units."

The International System of Units (SI Units) has been adopted by the U. S. National Bureau of Standards (see NBS Technical News Bulletin, Vol. 48, No. 4, April 1964).

The International System of Units is defined in NASA SP-7012, "The International System of Units, Physical Constants, and Conversion Factors," which is available from the U. S. Government Printing Office, Washington, D. C. 20402.

SI Units are used preferentially in this series of research reports in accordance with NASA policy and following the practice of the National Bureau of Standards.

## CALENDAR OF REVIEWS

### FIRST SERIES (VOLUME I)

REVIEW	DATE	RESEARCH AREA	REVIEW	DATE	RESEARCH AREA
1	2/25/65	RADIATION PHYSICS	12	9/16/65	AERODYNAMICS
2	2/25/65	THERMOPHYSICS	13	9/30/65	INSTRUMENTATION
3	3/25/65	CRYOGENIC TECHNOLOGY	14	9/30/65	POWER SYSTEMS
4 *	3/25/65	CHEMICAL PROPULSION	15	10/28/65	GUIDANCE CONCEPTS
5	4/29/65	ELECTRONICS	16	10/28/65	ASTRODYNAMICS
6	4/29/65	CONTROL SYSTEMS	17	1/27/66	ADVANCED TRACKING SYSTEMS
7	5/27/65	MATERIALS	18	1/27/66	COMMUNICATIONS SYSTEMS
8	5/27/65	MANUFACTURING	19	1/6/66	STRUCTURES
9	6/24/65	GROUND TESTING	20	1/6/66	MATHEMATICS AND COMPUTATION
10	6/24/65	QUALITY ASSURANCE AND CHECKOUT	21	2/24/66	ADVANCED PROPULSION
11	9/16/65	TERRESTRIAL AND SPACE ENVIRONMENT	22	2/24/66	LUNAR AND METEOROID PHYSICS

### SECOND SERIES (VOLUME II)

REVIEW	DATE	RESEARCH AREA	REVIEW	DATE	RESEARCH AREA
1	3/31/66	RADIATION PHYSICS	7	3/30/67	CRYOGENIC TECHNOLOGY
2	3/31/66	THERMOPHYSICS	8 **	5/25/67	COMPUTATION
3	5/26/66	ELECTRONICS	9	7/27/67	POWER SYSTEMS
4	7/28/66	MATERIALS	10	9/28/67	TERRESTRIAL AND SPACE ENVIRONMENT
5	9/29/66	QUALITY AND RELIABILITY ASSURANCE	11	11/30/67	MANUFACTURING
6	1/26/67	CHEMICAL PROPULSION	12	1/25/68	INSTRUMENTATION RESEARCH FOR GROUND TESTING

### THIRD SERIES (VOLUME III)

REVIEW	DATE	RESEARCH AREA	REVIEW	DATE	RESEARCH AREA
1	3/28/68	AIRBORNE INSTRUMENTATION AND DATA TRANSMISSION	6	1/30/69	THERMOPHYSICS
2	5/22/68	ASTRODYNAMICS GUIDANCE AND OPTIMIZATION	7	3/27/69	RADIATION PHYSICS
3	7/25/68	CONTROL SYSTEMS	8	6/26/69	METEOROID PHYSICS
4	9/26/68	AEROPHYSICS	9	9/25/69	COMPUTATION RESEARCH
5	11/21/68	COMMUNICATION AND TRACKING	10	12/18/69	MATERIALS RESEARCH FOR SHUTTLE AND SPACE STATION

\* Classified. Proceedings not published.

\*\* Proceedings summarized only.

Correspondence concerning the Research Achievements Review Series should be addressed to:  
Research Planning Office, S&E-R, Marshall Space Flight Center, Alabama 35812

MSFC-RSA, Ala